1988

# The Investigation of Platinum-Tellurium/Aluminum-Oxide and Platinum-Antimony/Aluminum-Oxide Bimetallic Reforming Catalysts.

Chi Hung Cheng
*Louisiana State University and Agricultural & Mechanical College*

## INFORMATION TO USERS

The most advanced technology has been used to photograph and reproduce this manuscript from the microfilm master. UMI films the text directly from the original or copy submitted. Thus, some thesis and dissertation copies are in typewriter face, while others may be from any type of computer printer.

The quality of this reproduction is dependent upon the quality of the copy submitted. Broken or indistinct print, colored or poor quality illustrations and photographs, print bleedthrough, substandard margins, and improper alignment can adversely affect reproduction.

In the unlikely event that the author did not send UMI a complete manuscript and there are missing pages, these will be noted. Also, if unauthorized copyright material had to be removed, a note will indicate the deletion.

Oversize materials (e.g., maps, drawings, charts) are reproduced by sectioning the original, beginning at the upper left-hand corner and continuing from left to right in equal sections with small overlaps. Each original is also photographed in one exposure and is included in reduced form at the back of the book. These are also available as one exposure on a standard 35mm slide or as a 17" x 23" black and white photographic print for an additional charge.

Photographs included in the original manuscript have been reproduced xerographically in this copy. Higher quality 6" x 9" black and white photographic prints are available for any photographs or illustrations appearing in this copy for an additional charge. Contact UMI directly to order.

U·M·I

University Microfilms International
A Bell & Howell Information Company
300 North Zeeb Road, Ann Arbor, MI 48106-1346 USA
313/761-4700 800/521-0600

Order Number 8917805

# The investigation of $PtTe/Al_2O_3$ and $PtSb/Al_2O_3$ bimetallic reforming catalysts

Cheng, Chi Hung, Ph.D.

The Louisiana State University and Agricultural and Mechanical Col., 1988

U·M·I
300 N. Zeeb Rd.
Ann Arbor, MI 48106

# The Investigation of $PtTe/Al_2O_3$ and $PtSb/Al_2O_3$ Bimetallic Reforming Catalysts

A Dissertation

Submitted to the Graduate Faculty of the
Louisiana State University and
Agricultural and Mechanical College
in partial fulfillment of the
requirements for the degree of
Doctor of Philosophy

in

The Department of Chemical Engineering

by
Chi Hung Cheng
B.S., Louisiana State University, 1983
December 1988

**Acknowledgments**

The author is pleased to acknowledge his indebtedness to Dr. Geoffrey. L. Price for his professional guidance and help throughout this work. The time Dr. Price devoted to reviewing this manuscript is especially appreciated.

The author is deeply indebted to Dr. Kerry. M. Dooley for his many valuable suggestions during the progress of this work.

The author would like to express his gratitude to the dissertation committee, Dr. K. M. Dooley, Dr. D. P. Harrison, Dr. A. B. Corripio in Chemical Engineering Department, and Dr. S. F. Watkins in Chemistry Department for their time spent developing constructive comments on this work.

The author wishes to thank Mr. Marcus Nauman in the Chemistry Department for $^{13}C$-NMR experiments.

The author also expresses his appreciation to the Exxon Foundation for financial support. The assistance of Drs. Kenneth Riley and Al Schweizer at Exxon Research and Development in Baton Rouge, Louisiana is especially appreciated.

Last, but not least, the author wishes to thank his parents and his three sisters for their encouragement

and understanding during his college education. Without them, the author's life would be empty and the work fruitless.

## Table of Contents

## List of Figures

## List of Tables

## Abstract

$PtTe/Al_2O_3$ and $PtSb/Al_2O_3$ bimetallics were characterized as possible reforming catalysts by kinetic studies, mechanistic investigations, and spectroscopic measurements. The results were compared with $Pt/Al_2O_3$ with the aim to understand the effects of tellurium and antimony on the platinum function.

Coimpregnated $PtTe/Al_2O_3$ and $PtSb/Al_2O_3$ catalysts exhibited an increase in selectivity for the isomerization of n-hexane. This enhancement in selectivity can be caused either by electronic effects, which increase the specific activities for isomerization, or by geometric effects, which reduce the rate of hydrocracking. The results of the kinetic experiments, along with FTIR spectroscopy of adsorbed carbon monoxide using the isotopic dilution method, suggest that electronic effects can be identified with Te/Pt alloying in catalysts of low (Te/Pt < 0.06) tellurium content, while geometric effects predominate in catalyst formulations more concentrated in the post-transition metal for both $PtTe/Al_2O_3$ and $PtSb/Al_2O_3$.

The cyclohexane dehydrogenation turnover frequencies were also enhanced at low Te/Pt ratio; in this respect the dehydrogenation and isomerization reactions are

similar. Direct six-member ring closure, rather than ring expansion by way of an adsorbed methylcyclopentane intermediate, accounted for most of the production of benzene.

The isomerization reactions of carbon-13 labeled 2-methylpentane were used to determine the relative contributions of cyclic and bond shift mechanisms. n-Hexane was formed primarily by a $C_5$ cyclic mechanism on the platinum surface, while 3-methylpentane was produced by both cyclic and bond shift mechanisms. Isomerization via bond shift increases when tellurium or antimony is added to $Pt/Al_2O_3$.

The reaction of benzene and deuterium at 110 and 250°C showed that carbon-hydrogen bond breaking/making is extremely fast. Since diffusion may affect the deuterium levels in the hydrocarbon molecules, no other firm conclusions may be drawn.

$PtTe/Al_2O_3$ catalysts were also prepared by vapor deposition of tellurium onto $Pt/Al_2O_3$. These catalysts exhibited selectivities which were influenced by the type of carrier gas used to deposit the tellurium. A carrier gas containing n-hexane improved the selectivity relative to hydrogen or helium carrier gases. The mechanism of this selectivity effect is unknown but possibly due to

**carbon incorporation into a Pt-Te alloy.**

# I. Introduction

The process of catalytic reforming has played an important role in the petroleum refining industry over the last two decades. In the process, petroleum feedstocks, which contain mostly straight chain paraffins and naphthenes, are converted to high-octane products, particularly aromatics and branched paraffins. The major reactions in catalytic reforming are (a) dehydrogenation of cycloalkanes to aromatics, (b) isomerization of straight chain paraffins to branched paraffins, (c) dehydrocyclization of paraffins to aromatics, (d) dehydroisomerization of naphthenes to aromatics, and (e) hydrocracking and hydrogenolysis reactions (carbon-carbon bond scissions) to give lower molecular weight alkanes. Figure I-1 gives examples of these major reactions in catalytic reforming of $C_6$ hydrocarbons. The gasoline quality of pure hydrocarbons expressed by their octane numbers are provided in Table I-1.

In 1949 [Haensel], the first bifunctional reforming catalyst, Pt supported on an acidic alumina, was introduced. This monometallic catalyst, though providing many benefits over the older chromia catalysts, has some shortcomings such as a high yield of gas products, and

(a) Dehydrogenation

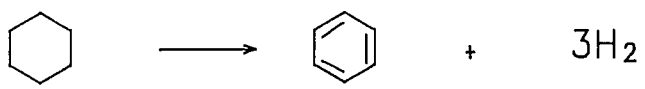


(b) Isomerization

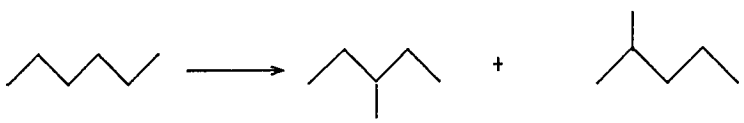


(c) Dehydrocyclization

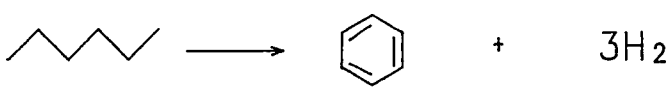


(d) Dehydroisomerization

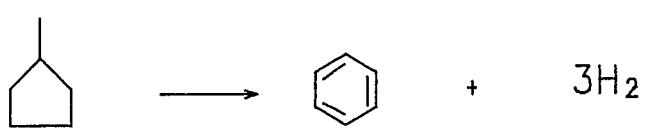


(e) Hydrocracking and Hydrogenolysis

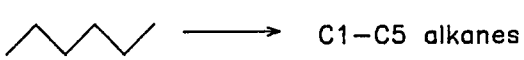


Figure I–1. Major Reactions in Reforming of C6 Hydrocarbons.

Table I-1. Octane Number of Pure Hydrocarbons

| Compound | Octane Number |
|---|---|
| Paraffins | |
| Methane | 120 |
| Ethane | 118 |
| n-Propane | 112 |
| n-Butane | 93 |
| n-Pentane | 62 |
| n-Hexane | 25 |
| n-Heptane | 0 |
| Branched Paraffins | |
| Trimethyl pentanes | 103-106 |
| Dimethyl hexanes | 55-75 |
| Methyl Heptanes | 22-33 |
| Naphthenes | |
| Cyclopentane | 101 |
| Methylcyclopentane | 91 |
| Cyclohexane | 83 |
| Aromatics | |
| Benzene | 100 |
| Toluene | 120 |
| m-Xylene | 117 |

instability in activity and selectivity. Thus, economic benefits may be realized with further improvements in the catalyst. One method which is widely used is the incorporation of a second metal component into the Pt based catalysts. The modified catalysts are called bimetallic or alloy catalysts. Some of the advantages offered by bimetallic catalysts include reduced rates of deactivation, higher reformate yields, and higher activities. In fact, bimetallic catalysts, $PtRe/Al_2O_3$ [Biloen et al., 1980] and $PtIr/Al_2O_3$ [Carter et al., 1982], have become the preferred catalysts for commercial reforming operations.

Of primary concern in reforming reactor operation is the start-up process, when fresh or regenerated catalysts are present. The high activity of fresh catalysts for the exothermic hydrogenolysis reactions adversely affects the overall selectivity (the rate of coking reactions increase), and possibly results in local temperature runaways that can alter the alloy structure. For these reasons, the activity of fresh reforming catalysts is moderated by partial poisoning with minute amounts of sulfur. The high toxicity of sulfur for hydrogenolysis reactions results in an increase in the stability of the catalyst and therefore has favorable effects on the start-up process.

Pre-sulfiding a fixed-bed reactor is a particularly delicate process in that sulfur compounds are strongly retained on the catalyst, resulting in a non-uniform deposition within the bed. The addition of enough sulfur to affect all of the catalyst causes severe poisoning near the reactor entrance.

Post-transition metals involving groups IVA, VA and VIA, such as Sb, Bi [Thoang et al., 1984], Te [Brignac and Swan, 1984], Sn and Pb [Völter et al., 1981] are candidate elements which may mimic the pre-sulfiding operation. The additives can suppress the hydrogenolysis reactions by either modifying the electronic structure of the Pt metal or by diluting the Pt metal surface into smaller ensembles which do not permit hydrogenolysis reactions. Although many investigations have been conducted, the precise role of these modifiers on the catalytic surface is poorly understood and therefore further studies are required. The remainder of this chapter reviews pertinent literature and defines the goal of the present work.

## A. Literature Review

### 1. Previous Studies on Te- and Sb-containing Reforming Catalysts

The use of tellurium as an additive to reforming catalysts was first demonstrated and patented by Eberly [1979]. 0.03 to 0.12 wt% tellurium was incorporated to 0.3 wt% platinum-0.3 wt% rhenium or iridium alloy using a solution containing sufficient $H_2TeO_4$. The resulting catalysts decrease the yield to hydrocracking products thereby increasing the selectivity to aromatics in naphtha reforming at 500°C.

Further investigation of Te-modified $PtRe/Al_2O_3$ catalysts was reported by Brignac and Swan [1984], who showed that the catalyst was more selective and active in naphtha reforming after the catalysts were calcined and reduced severely at temperatures greater than 450°C. On the other hand, the $PtRe/Al_2O_3$ counterpart (no Te) remains highly active for the hydrogenolysis reaction, when pretreated at the same conditions. Although both patents have shown that these catalysts offer the advantages of much greater resistance to deactivation and higher selectivity to aromatics, information concerning the effects of tellurium on the modification of platinum, in terms of surface science and the reaction mechanism, have not been reported.

Thoang et al., [1984] and Lanh et al., [1984] have investigated $PtSb/Al_2O_3$ catalysts, which were prepared by simultaneous impregnation of gamma-$Al_2O_3$ with an

aqueous solution containing $SbCl_3$ and $H_2PtCl_6$ followed by drying, calcination and reduction at 500°C. The investigators showed that modification of $Pt/Al_2O_3$ by Sb stabilizes the activity for cyclohexane dehydrogenation and n-heptane dehydrocyclization at high temperatures (450-500°C). Total catalytic activity as well as selectivity were shown to be a maximum when the Sb/Pt atomic ratio is 1:1. However, the catalysts are inactive at lower temperatures (≈ 300°C). The authors suggested that the inhibition of hydrogenolysis reactions is due to the dilution of the Pt sites by the second metal component, while the lower temperature inactivity is caused by electronic effects. In addition, bimetallic clusters of platinum and antimony were indicated by the results on the adsorption of hydrogen and oxygen. The bimetallic catalysts inhibit hydrogen adsorption but increase the capacity for oxygen adsorption when reduced with hydrogen at 700°C. Furthermore, temperature programmed reduction measurements found the presence of a nonzero oxidation state for antimony, and that the extent of its reduction decreases with increasing content of antimony.

**2. Other Catalysts**

Many studies have been published in the last twenty years on the modification of reforming catalysts by the addition of a second metal component. The studies are sometimes in good agreement with each other but in other cases are contradictory. Different theories have been postulated to explain the observed catalytic properties of the modified catalysts, i.e. electronic or geometric effects, and partial poisoning due to the surface heterogeneity. One theory may succeed in one alloy system but may totally fail in the others. Part of the failure is probably due to the fact that the chemical and physical properties of a catalyst are particularly strong functions of its composition and pretreatment history, including such factors as the metal composition, the chlorine content of the support, the metal crystallite size, the temperature and length of time for drying, calcination and reduction, and even the purity of the oxidizing and reducing gas stream. In spite of these difficulties, numerous investigations on the characterization of alloy reforming catalysts have been conducted either academically or because of their industrial importance. The examination of these results may provide information which is useful for the development of new and improved catalysts.

In exploring the information available in these

reports, emphasis was placed on, although not limited to, post-transition metal modifiers. It should be noted that elements such as Re and Ir have long been used for alloying with $Pt/Al_2O_3$ in commercial processes. Bimetallic systems such as PtAu [Biloen et al., 1977] and $PtCu/Al_2O_3$ [Dejongste et al., 1976] have been investigated and reported to provide desirable characteristics as reforming catalysts. It is therefore enlightening to compare the effects of these metals on platinum with those of the post-transition metals. The literature encompassing these earlier studies can be classified into a) kinetic studies, b) surface characterization using spectroscopic techniques and c) mechanistic considerations of reforming reactions. Each of these areas is discussed in greater detail.

**a. Kinetic Studies of Alloy Catalysts**

Davis and associates [1976] studied the dehydrocyclization reaction of n-octane at 482°C using a $PtSn/Al_2O_3$ catalyst containing 0.6 wt% Pt. The optimum ratio of Pt:Sn was found to be 1:4, at which the bimetallic catalyst showed the greatest improvement in selectivity and activity maintenance. It was concluded that these improvements are caused by changes in the electronic density of the platinum atoms which weaken

the Pt-C bond strength and thereby decrease the poisoning by coke. On the contrary, Bacaud and Bussiére [1981] believed that tin poisons the strong acidic sites of the alumina support, which are responsible for the hydrogenolysis and coking reactions.

The conversion of methylcyclopentane on $PtSn/Al_2O_3$ catalysts containing 1 wt% Pt and 0.06-4 wt% Sn has been investigated by Coq and Figueras [1984]. The Sn additive stabilizes the catalytic activity and suppresses the hydrogenolysis reaction. These improvements are attributed to dilution effects. However, an enhancement in aromatization was explained as an electronic modification of the Pt atoms by Sn.

Thoang et al. [1984] observed the same catalytic behavior for $PtBi/Al_2O_3$ as $PtSb/Al_2O_3$ previously described. Similar results were found using $PtSn/Al_2O_3$ and $PtPb/Al_2O_3$ catalysts [Völter et al., 1981].

Goldwasser and coworkers [1986] studied the isomerization and hydrogenolysis reactions of n-butane, and the hydrogenation of benzene, catalyzed by $PtGe/Al_2O_3$ (1 wt% Pt and 0-1 wt% Ge). The specific activities for hydrogenolysis and hydrogenation decreased with increasing Ge content while that of isomerization was only weakly influenced. The results were attributed to electron donation from Pt to reduced

Ge ions.

Sulfurization of naphtha-reforming catalysts has been extensively studied due to the presence of sulfur in the feedstock. Maurel et al. [1975] investigated benzene hydrogenation, cyclopentane hydrogenolysis, and benzene exchange reactions with deuterium on S-containing $Pt/Al_2O_3$ catalysts. The results indicated that benzene hydrogenation is a facile reaction, i.e. the rate of reaction is dependent only on the total metal surface area, whereas hydrogenolysis and exchange are identified as demanding reactions, i.e. reactions which proceed only on surface sites with a particular structure and environment. Furthermore, sulfurization was classified into selective poisoning and nonselective poisoning. When sulfur is added in the form of $H_2S$ or $SO_2$, it acts as a nonselective poison which only diminishes the total accessible metallic surface area. Atomic sulfur, produced by a mixture of $H_2S + SO_2$, is a selective poison which eliminates the unwanted active sites responsible for hydrogenolysis reactions.

$PtRe/Al_2O_3$ has been used in reforming operation since 1968 [Kluksdahl]. The addition of Re to $Pt/Al_2O_3$ reduces the coke formation and thereby increases the catalyst stability. However, it also increases the rate of hydrogenolysis reactions. Therefore, the catalyst is

usually sulfided prior to contact with naphtha. The resulting Pt-Re-S/$Al_2O_3$ favors the start-up of the reforming process by diminishing the hydrogenolysis activity. In fact, the combination of Re, S, and Pt is essential, as suggested by Sachtler [1984]. Coughlin et al. [1984] reported the catalytic properties of S-containing Pt/$Al_2O_3$ and PtRe/$Al_2O_3$ during dehydrogenation of methylcyclohexane. Sulfur causes the irreversible poisoning of hydrogenolysis activity and reduces the rate of deactivation. Parera et al. [1986] also found that the high hydrogenolysis activity of PtRe/$Al_2O_3$ diminished after the addition of sulfur.

Experiments by Barbier and Marecot [1986] on sulfided and nonsulfided Pt/$Al_2O_3$, Ir/$Al_2O_3$ and PtIr/$Al_2O_3$ showed that sulfur protects the Pt metal from coking reactions. The results were explained by the dilution of the Pt metal surface into small ensembles which are inactive for coking and hydrogenolysis reactions. It is also possible that pre-sulfurization causes an instability in the cyclopentadienyl ion, a precursor of coke, on the Pt metal by electron donation from Pt to sulfur.

**b. Surface Characterization**

All of the alloy catalysts, when properly treated, show the suppression of hydrogenolysis or hydrocracking reactions in favor of the formation of liquid products. In addition, they usually decrease the rate of deactivation although the overall activity is usually somewhat lower than a fresh $Pt/Al_2O_3$. Several types of surface characterization, which are described below, have been used to aid in the understanding of the platinum/metal interaction.

Two theories [Ponec and Sachtler, 1972; Soma-Noto and Sachtler, 1974] are conceivable to explain the suppression of hydrogenolysis or hydrocracking reactions by alloying.

i. Geometric effect (dilution effect)

This theory states that alloying of Pt with the other metal simply dilutes the Pt-Pt ensembles. The hydrogenolysis reaction, which requires multiple contiguous adsorption sites, is thereby suppressed.

ii. Electronic effect (ligand effect)

The electronic interaction between Pt and the second metal alters the strength of the adsorbate bond to the adsorption site. The different chemisorption bond strengths result in altered catalytic activity and selectivity.

Infrared spectroscopy together with the isotopic

dilution method [Bastein et al., 1984; Toolenaar et al., 1983; Stoop et al., 1982], which was also applied in the current research, is one of those methods frequently used in obtaining the information required to deduce which type of effect is prominent. The method can be illustrated in Figure I-2 and explained briefly as follows. Assuming only a single Pt atom to be present on the support, a CO molecule adsorbed on this single Pt atom exhibits a characteristic isolated C-O stretch band frequency (Figure I-2(a)). However, on the real catalytic surface, each Pt atom is surrounded by other Pt atoms and by additional X atoms for $PtX/Al_2O_3$ catalysts. Two effects on this band frequency result, namely dipole-dipole coupling and an electronic effect related to PtX alloying (Figure I-2(b)). The dipole-dipole coupling, which is an interaction force between adsorbed CO molecules and is inversely proportional to intermolecular distance cubed [Hammaker et al., 1965], will result in a higher band frequency than the isolated band frequency discussed above. In the presence of electronic effects related to Pt-X alloying, changes from the isolated stretching band frequency depend on electron transfer between outer orbitals of X and the Pt d-orbitals. If there is electron donation from X to Pt orbitals, then back

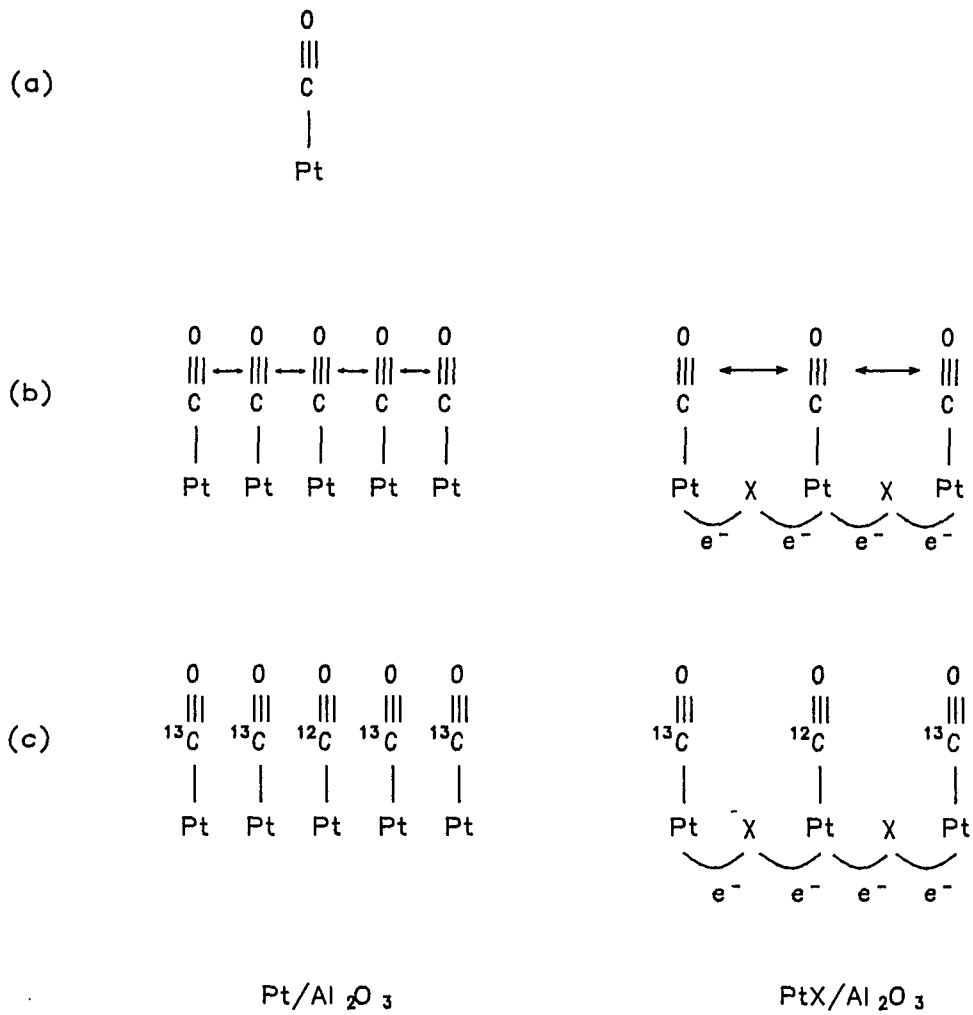


Figure I–2. A Schematic Diagram Showing the Method of Isotopic Dilution (see text for explanation).

donation from Pt to the CO antibonding orbitals causes the weakening of the CO bond and therefore decreases the band frequency. On the other hand, if X withdraws electron from Pt, the band frequency will shift to a higher value.

Dipole-dipole coupling can be eliminated by adsorbing dilute $^{12}CO$ in $^{13}CO$ on the surface (Figure I-2(c)), since the coupling between Pt-$^{12}CO$ and Pt-$^{13}CO$ is negligible. Any observed differences in band frequencies for CO adsorbed on $Pt/Al_2O_3$ and $PtX/Al_2O_3$ at this condition of isotopic dilution can therefore be ascribed to the electronic effects only. Experimentally, it is impossible to observe band frequencies at infinite dilution because the absorbance for the $^{12}CO$ band is too small. Alternatively, it is customary to extrapolate the curves for CO band frequency vs. gas mixture composition to infinite dilution. Figure I-3 shows two extreme cases in which only an electronic or a geometric effect is operative.

This method was used by Ponec and associates to study the supported alloy systems of Pt-Cu [Toolenaar et al., 1983], Pt-Pb, Pt-Sn and Pt-Re [Bastein et al., 1984]. Only Pt-Pb exhibits pronounced electronic effects. The decrease of the band frequency in $^{12}CO$, when the second metal component is added, can be

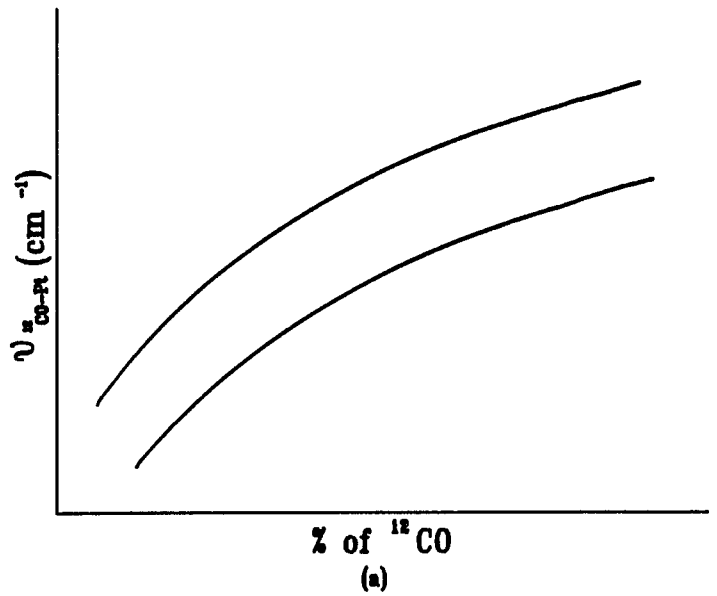


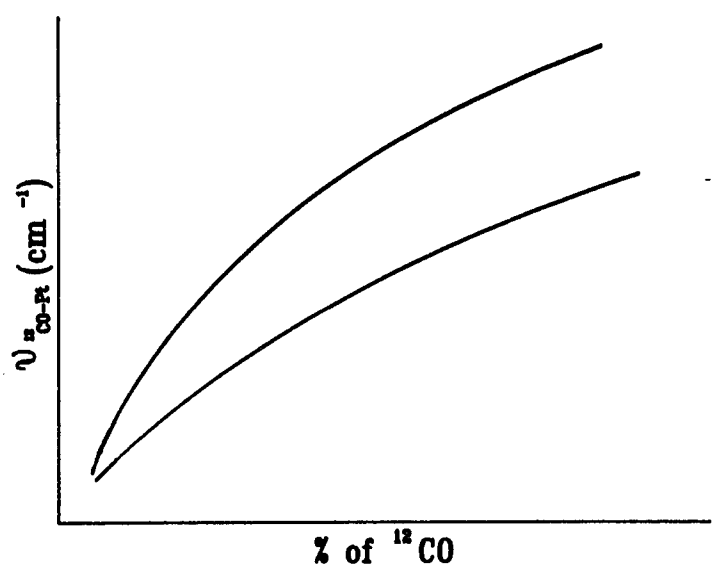


**Figure I-3. Two Extreme Cases Determined by Isotopic Dilution Method. (a) Electronic effect only. (b) Geometric effect only.**

ascribed totally to dilution effects for Pt-Cu and predominantly for Pt-Sn and Pt-Re systems. The changes in electronic properties of Pt for Pt-Pb, Pt-Sn and Pt-Re are caused by the electron transfer from the second metal component to Pt d-orbitals. The trend of such electronic effects seems to bear no apparent relationship to the exothermicity of the bulk alloy formation.

The transfer of electrons from Pb to Pt atoms was also demonstrated by Palazov et al. [1981], who suggested that both geometric and electronic effects are responsible for the suppression of the cyclohexane hydrogenolysis reaction.

Similar studies were performed by Apesteguia et al. [1984]. using $PtS/Al_2O_3$. However, unlike other additives, they found that electrons were transferred from Pt to S, as evidenced by an upward shift in the infrared band frequency of $^{12}CO$ from 2068 to 2083 $cm^{-1}$ when S was pre-deposited on $Pt/Al_2O_3$.

Other valuable information concerning the surface properties of bimetallic systems of interest is contained in the chemical states of the metal components on the surface. Although Pt is usually present in the metallic (zero-valent) state in the reduced catalysts, generally only a portion of the second metal component

is reducible to the zero valent state. Goldwasser et al. [1986] found no Ge(0) present on the surface of $PtGe/Al_2O_3$ when $Ge/Al_2O_3$ was calcined before the addition of Pt, and only part of Ge was reduced to Ge(0) after the calcination of a coimpregnated $PtGe/Al_2O_3$ at 400°C.

The studies of Lieske and Völter [1984] using temperature programmed reduction have shown that the majority of tin is present as Sn(II) in the reduced catalysts. Some Sn(0) is formed and is responsible for the alloying with Pt. Sexton et al. [1984], employing X-ray Photoelectron Spectroscopy (XPS), showed that both Pt and Sn can be reduced easily to the zero valent state in the unsupported complex. However, Sn(II) is the predominant oxidation state on the supported catalyst and is responsible for the electronic interaction with Pt. They pointed out that the low reducibility of Sn in the supported catalyst is caused by a strong interaction between Sn(II) and the alumina support. In contrast, Muller et al., [1979] found no Pt-Sn alloy formation and they also detected no Sn(0) present on alumina support. Alkins and Davis [1984] proposed the formation of an "eggshell" of tin aluminate surrounding the alumina support with the Pt(0) supported on the tin aluminate. The results from Bacaud and Bussière [1981] on

$PtSn/Al_2O_3$ using tin Mössbauer spectroscopy showed that the reducibility of tin to the metallic state increases with the Pt/Sn ratio. In addition, complete reduction was obtained for a $PtSn/Al_2O_3$ catalyst which was not calcined in air prior to reduction.

In other studies, Kirlin et al. [1986] have concluded that the presence of a hydrocarbon in the hydrogen stream used for reduction is essential for complete reduction of Re to the zero valent state in $PtRe/Al_2O_3$.

Thus, the surface properties of Pt alloy catalysts are still the subject of much debate. The discrepancies in the contrasting results seem strongly dependent on the catalyst preparation method and the pretreatment of the catalysts, i.e., temperature and length of time for drying, calcination, and reduction. However, a generalized theory encompassing all of the possible methods does not yet exist and therefore we can only speculate on the causes of the contrasting reports.

### c. Reaction Mechanisms

An important aspect of reforming catalysis is the mechanism by which each of the important reactions such as aromatization, isomerization, dehydrogenation, hydrogenation, and hydrogenolysis proceed. The determination

of this information provides us with the understanding which is required to produce better catalysts by promoting or poisoning specific pathways.

Commercial reforming catalysts are dual-functional, i.e., the catalysts possess both metal sites and acidic sites associated with the support. Both types of sites are thought to be necessary for successful reforming operations. Mills et al. [1953] proposed the scheme for the reforming reaction of n-hexane as illustrated in Figure I-4. The vertical abscissa represents the metal component which catalyzes the hydrogenation/dehydrogenation paths. The reactions parallel to the x-axis take place on the acidic support.

Via these reaction pathways, the metal sites catalyze the conversion of paraffins to olefins. Through carbonium ion intermediates, the olefins are converted to iso-olefins or a $C_5$ cyclic intermediate on the acidic centers. The iso-olefins return to the metal sites and are hydrogenated to isoparaffins. In another major pathway, the acid-catalyzed ring opening of the $C_5$ cyclic intermediates to $C_6$ cyclics followed by metal-catalyzed dehydrogenation results in the formation of aromatics.

The classical dual-functional mechanism cannot explain the skeletal rearrangement of hydrocarbons on Pt

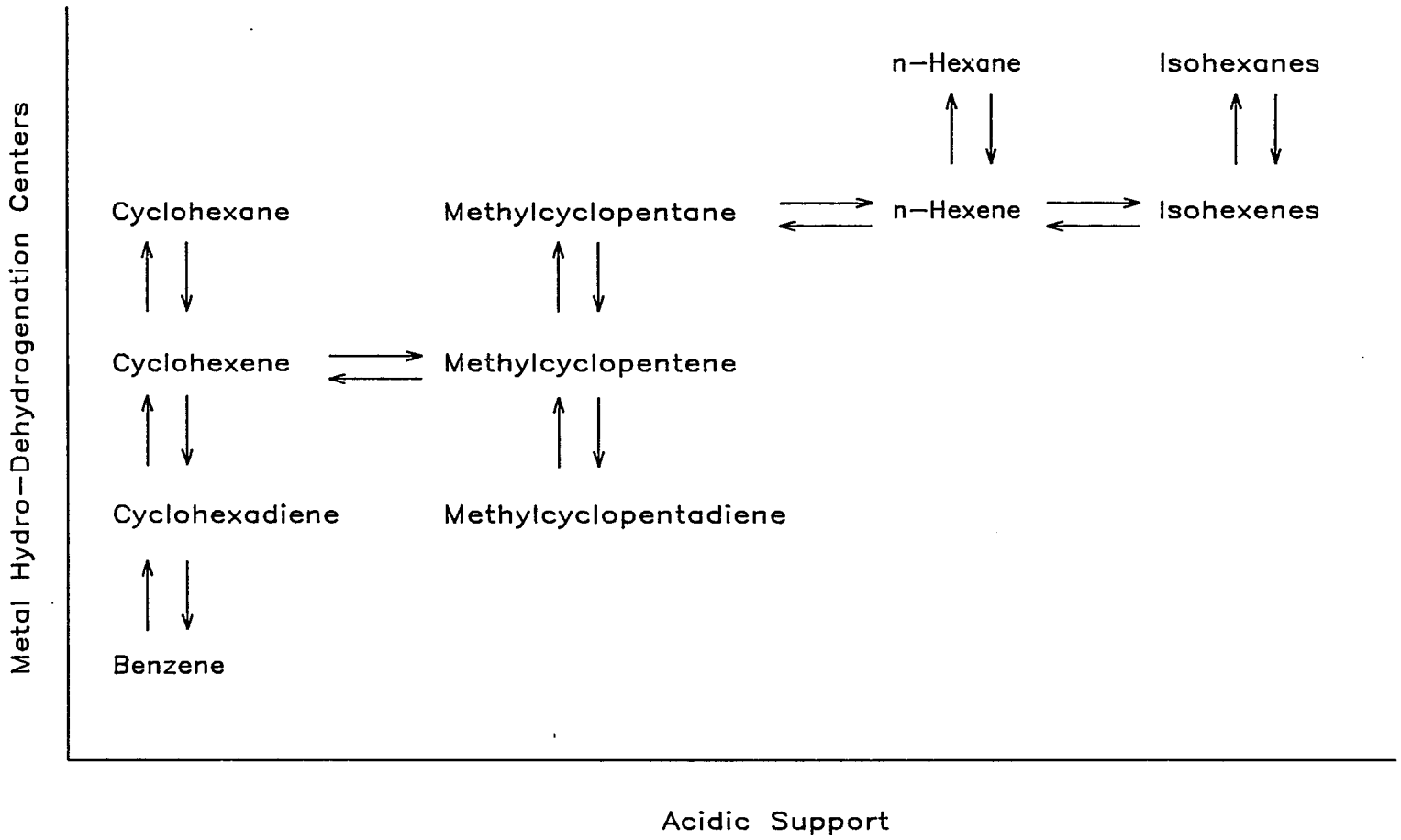


Figure I–4. Reaction Network for Catalytic Reforming of C6 Hydrocarbons [Mills et al.. 1953].

or Pd films and on Pt supported on an inert carrier [Anderson and Avery, 1966; Barron et al., 1963; Barron et al., 1966; Anderson and Baker, 1960, 1963]. In fact, reforming reactions are not restricted to dual-functional catalysts; they can occur on certain metals, notably Pt, without the acidic support. The current work focuses on the understanding of the effects of the second metal component on Pt metal. Metal-catalyzed reforming reactions are therefore discussed more thoroughly.

i. Aromatization

Aromatization of alkanes on metal sites can be divided into direct 1,6 ring closure and 1,5 ring closure followed by ring expansion and dehydrogenation.

The 1,6 ring closure [Dautzenberg and Platteeuw, 1972; Davis and Venuto, 1969] is proposed from the argument that benzene is an initial product from the n-hexane reaction but not from the 2-methylpentane reaction. Davis [1976] found evidence that this mechanism is more important on $Pt/Al_2O_3$ when the support is nonacidic.

Direct 1-6 ring closure cannot describe the formation of aromatics from a number of alkanes [Barron et al., 1966; Muller and Gault, 1972; Lester, 1969] with

only five carbons in the straight chain. In addition, the rapid formation of aromatics from substituted cyclopentanes suggests the mechanism of 1-5 ring closure followed by ring expansion and dehydrogenation. However, only limited information can be found in the literature about the relative effects of a second metal component on these two competing mechanisms.

**ii. Isomerization**

Skeletal isomerization over reforming catalysts has been the subject of many recent investigations. Two mechanisms [Anderson and Avery, 1966; Barron et al., 1963, 1966; Garin and Gault, 1975] have been well established to explain the skeletal isomerization of paraffins on metal sites. The bond shift mechanism, which involves simple carbon-carbon bond displacement, accounts for the isomerization of short chain molecules such as isobutane and neopentane on large metal crystallites (Figure I-5(a)). However, for larger molecules on small metal crystallites, the cyclic mechanism, which consists of the dehydrocyclization of the hydrocarbon molecule into a $C_5$ cyclic intermediate followed by the breakage of one of the carbon-carbon bonds in the ring, becomes more important (Figure I-5(b)). The cyclic mechanism was initially proposed to

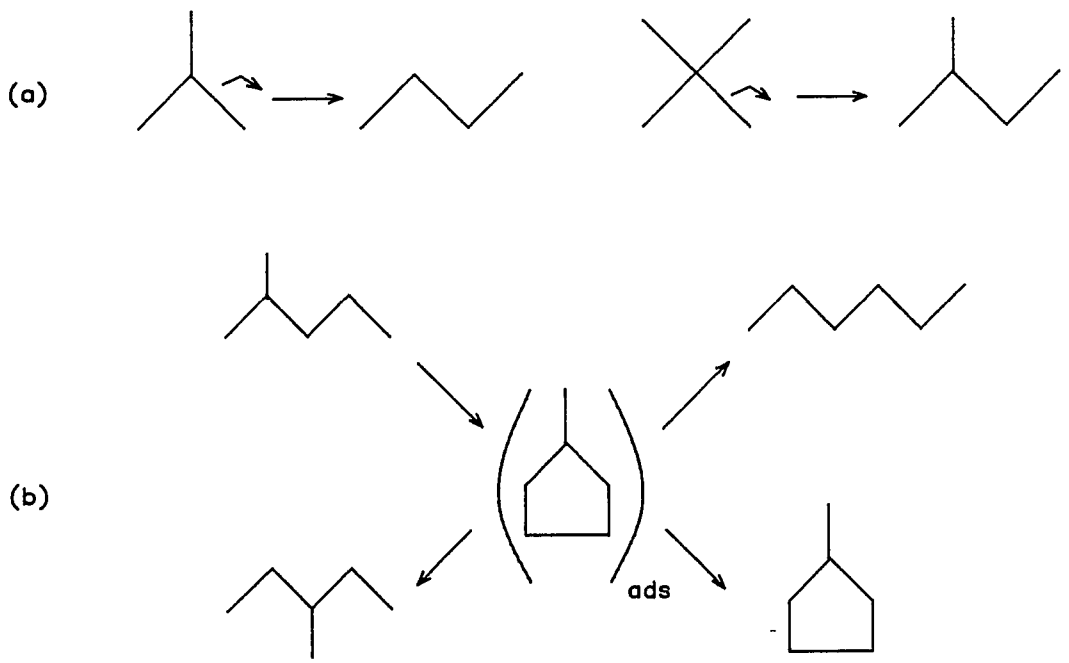


Figure I–5. (a) Bond Shift and (b) Cyclic Mechanism.
[Garin and. Gault, 1975]

explain the observation that the initial product distributions for 2-methylpentane isomerization and methylcyclopentane hydrogenolysis are the same.

The relative importance of these two mechanisms to metal-catalyzed isomerization reactions can be determined by carbon-13 tracer techniques, as suggested and reported by Gault and coworkers [Corolleur et al., 1972; Dartigues et al., 1976; Chambellan et al., 1977]. Typically, one of the carbon atoms in the reacting molecule is labeled with carbon-13 and by examining the distribution of the tagged species after reaction, one can determine the relative contributions of the bond shift and cyclic mechanisms.

Corolleur et al. [1972] studied the isomerization reactions of 2-methylpentane to 3-methylpentane and n-hexane using two $Pt/Al_2O_3$ catalysts with high and low dispersion (0.2 and 10 wt% Pt), at 265-275°C. The labeled reactants were 2-methylpentane ($2-^{13}C$) and 2-methylpentane ($4-^{13}C$). The approach is illustrated in Figure I-6. It was found that the cyclic mechanism is prominent on highly dispersed $Pt/Al_2O_3$, accounting for more than 70% of the isomerization of 2-methylpentane to 3-methylpentane, and 80% of that to n-hexane. For the 10 wt% $Pt/Al_2O_3$, the contribution of the cyclic mechanism to isomerization of 2-methylpentane to

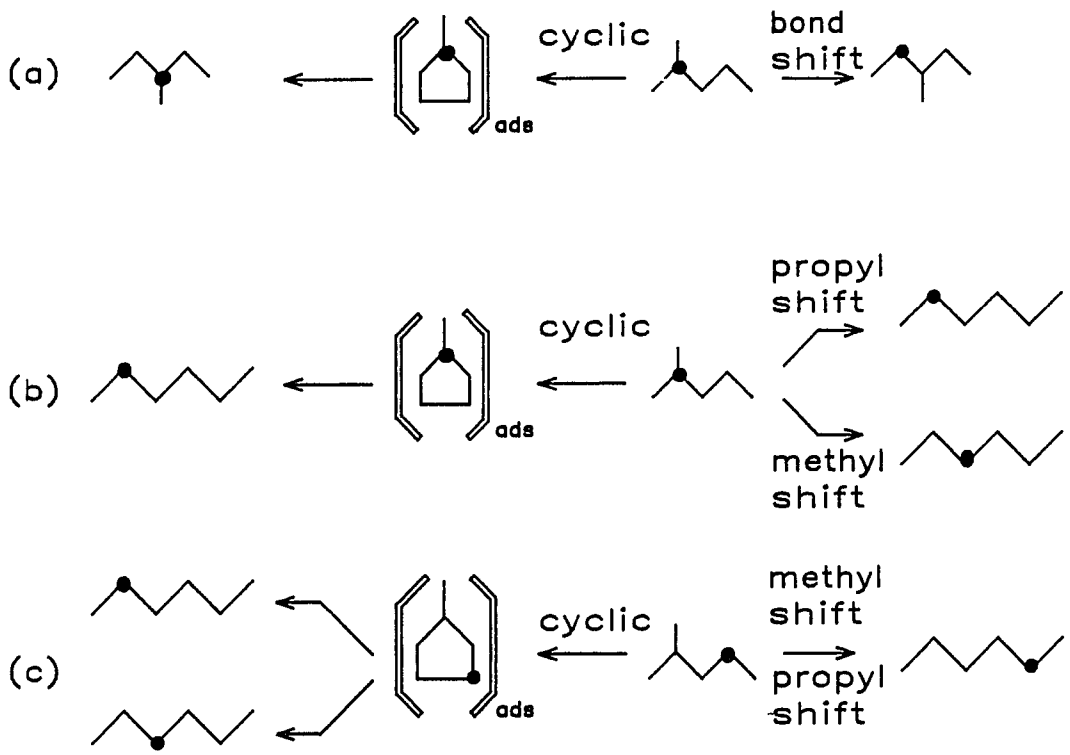


Figure I–6. Isomerization of 2–MP (2–$^{13}$C) and 2–MP (4–$^{13}$C) [Corolleur et al., 1972].

3-methylpentane decreases to approximately 30%, and successive rearrangements of n-hexane molecules via either bond shift or cyclic mechanism has occurred. A higher activation energy for the cyclic mechanism than the bond shift mechanism was also deduced.

Later, using the same method, O'Cinneide and Gault [1975] investigated isomerization in the hexane system over Pd-Au and Pt-Au supported catalysts containing 10 wt% Pt. They concluded that isomerization in the hexane system proceeded through the cyclic mechanism for both Pd and Pd-Au/$Al_2O_3$. However, PtAu/$Al_2O_3$ resembles a highly dispersed Pt/$Al_2O_3$ (0.2 wt% Pt) in both catalytic selectivity and mechanism.

Diaz et al. [1983] have investigated the 2-methylpentane isomerization reaction on PtRu/$Al_2O_3$ (10 wt% Pt, Pt/Ru atomic ratio = 2.4), from 220 to 300°C. In this study, the cyclic mechanism accounts for only 30-46% of the isomerization of 2-methylpentane to 3-methylpentane, and approximately 77-86% of that to n-hexane. Compared to Pt/$Al_2O_3$, the researchers discovered that the bimetallic catalyst can promote isomerization at a lower temperature, 220°C, and that the methyl shift, which is never observed on Pt/$Al_2O_3$, is roughly one to two times more favorable than propyl shift. No correlations between the temperature and the

relative importance of the two reaction mechanisms (bond shift and cyclic) were found.

Although the rough classification of metal catalyzed skeletal isomerization into cyclic and bond shift mechanisms is generally accepted, a precise description of the reactive species on the surface has not been attained. However, four basic types of bond shift mechanisms were reviewed by Gault [1981] and are presented in Figure I-7.

(a).Anderson-Avery mechanism

The proposed reactive species is an $\alpha,\alpha,\tau$-triad-sorbed species, which requires at least two metal sites on the surface. The isomerization products are formed through carbon-carbon bond breakage and then carbon-carbon bond recombination of this chemisorbed species.

(b).Garin-Gault mechanism

This mechanism is particularly successful in explaining the isomerization of neopentane to isopentane, which takes place in a metallocyclobutane species. Transient rearrangement of the metallocyclobutane intermediate by carbon-carbon bond breakage followed by recombination, and hydrogenation yields the isomerization products.

(c).Muller-Gault mechanism

This mechanism is a modification of the Anderson-Av-

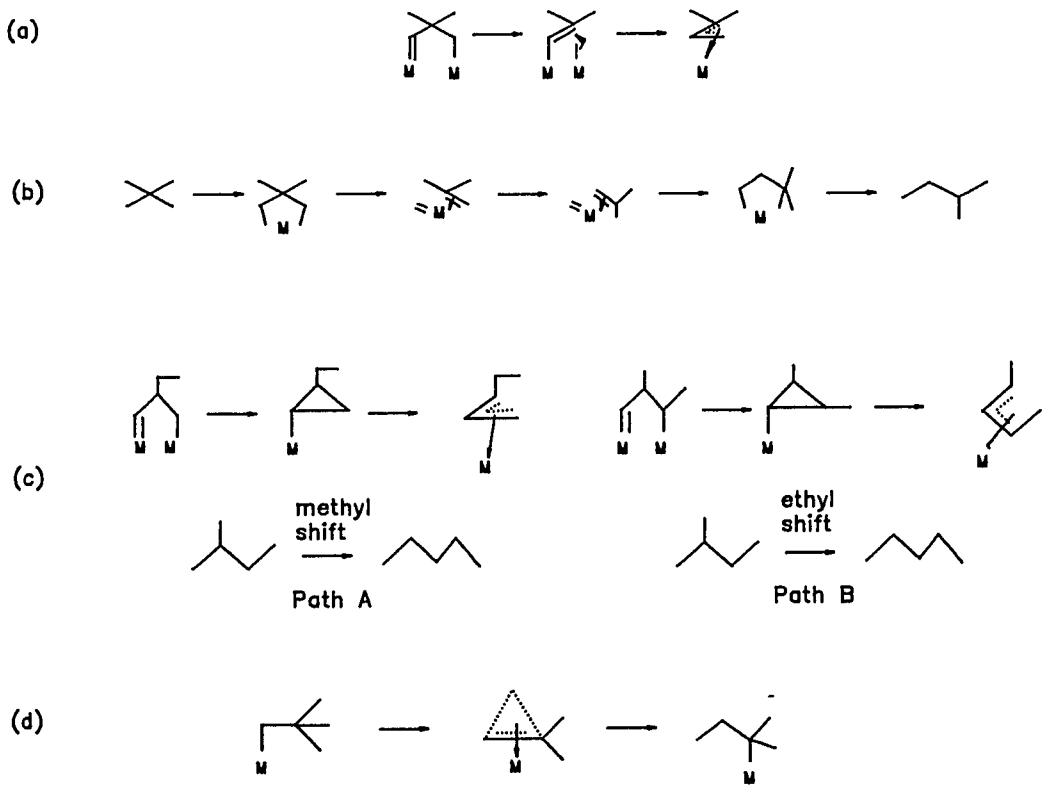


Figure I–7. (a) Anderson–Avery mechanism, (b) Garin–Gault mechanism, (c) Muller–Gault mechanism, and (d) Rooney–Samman mechanism for bond shift isomerization (Gault, 1981).

ery mechanism. The reactive species is a dissociatively adsorbed cyclopropane intermediate. The stabilization of this cyclopropane intermediate by methyl substituents explains the predominance of ethyl shift over methyl shift in the isomerization of isopentane to n-pentane.

(d).Rooney-Samman mechanism

This is a carbonium-ion like mechanism, which involves three-center orbitals with simultaneous Π-bonding to one metal site. The transient chemisorbed species is stabilized by lowering the energy of the antibonding orbital (one of the three associated molecular orbitals) upon the formation of the metal-free radical bond.

Isomerization via $C_5$ cyclic intermediates is generally classified into nonselective and selective cyclic mechanisms, which operate on small and large Pt metal crystallites, respectively. Reactive species on the metal surface for the corresponding mechanisms are illustrated in Figure I-8. In the case of the nonselective cyclic mechanism, the breakages of the secondary-secondary and the secondary-tertiary C-C bonds in the methylcyclopentane molecules are equally favorable (yielding 3-methylpentane and n-hexane).

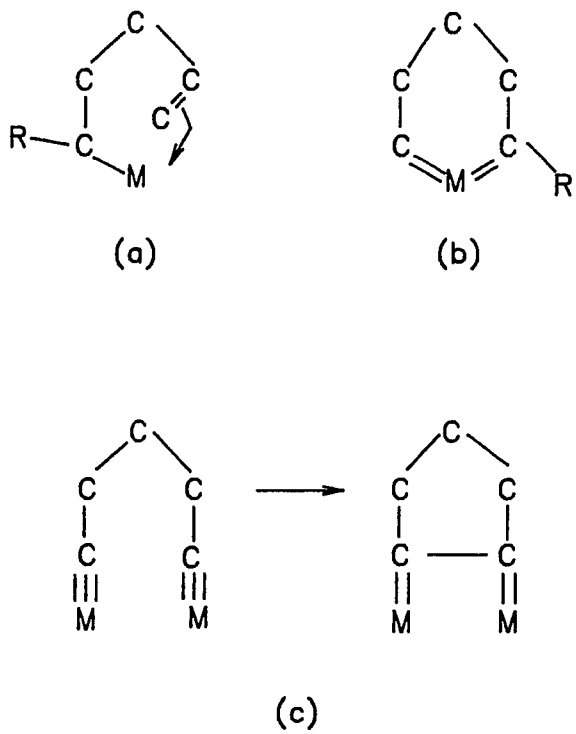


Figure I–8. Schematic Representation of Adsorbed Cyclic Species
(a), (b) nonselective, using one Pt atom
(c) selective, using two Pt atoms
[Gault, 1981].

However, the formation of n-hexane is not observed in the selective cyclic mechanism, possibly due to steric hindrances.

### iii.Dehydrogenation-Hydrogenation

Hydrogenation and dehydrogenation are generally considered as facile reactions, i.e. the rates are proportional only to the total metal surface area. The elementary steps of the reaction mechanism comprise (1) the adsorption of the hydrocarbon via single or multiple metal sites, (2) the addition or removal of hydrogen atoms to or from the adsorbed intermediate, and (3) the desorption of the products. All the elementary steps involve only the carbon-hydrogen bonds, as compared to the carbon-carbon bond scissions in isomerization, hydrocracking, or dehydrocyclization.

The reaction of hydrocarbons with deuterium has long been used to obtain mechanistic information related to hydrogenation/dehydrogenation reactions. The exchange reaction, in which hydrogen atoms in the molecules are substituted by deuterium atoms without a change in the total number of (H+D) atoms, may be governed by adsorption/desorption, whereas the hydrogenation or dehydrogenation is a surface reaction.

Classical theory divides catalytic exchange into dissociative [Farkas and Farkas, 1939] and associative [Horiuti and Polanyi, 1933] mechanisms, which are illustrated in Figures I-9 and I-10. According to the dissociative mechanism, the hydrogen atoms in the hydrocarbon molecules are substituted with deuterium through carbon-hydrogen bond breaking-making in the adsorption-desorption steps. The surface reaction is totally unrelated to the exchange reaction and occurs between two chemisorbed hydrogen atoms and a physically adsorbed hydrocarbon species. Although the dissociative mechanism is generally accepted for the catalytic exchange of saturated hydrocarbons, the associative mechanism is equally important in the exchange of unsaturated compounds, e.g. benzene. The associative mechanism involves a hydrocarbon molecule that is chemically adsorbed by the opening of a double bond. Hydrogenation and exchange reactions proceed via a common surface intermediate, a half-hydrogenated species.

Rooney and Webb [1964] applied a Π-complex adsorption mechanism for interpreting their results for the reactions of paraffins, olefins, and aromatics with deuterium. A schematic representation of this mechanism for the reaction of deuterium with benzene is shown in

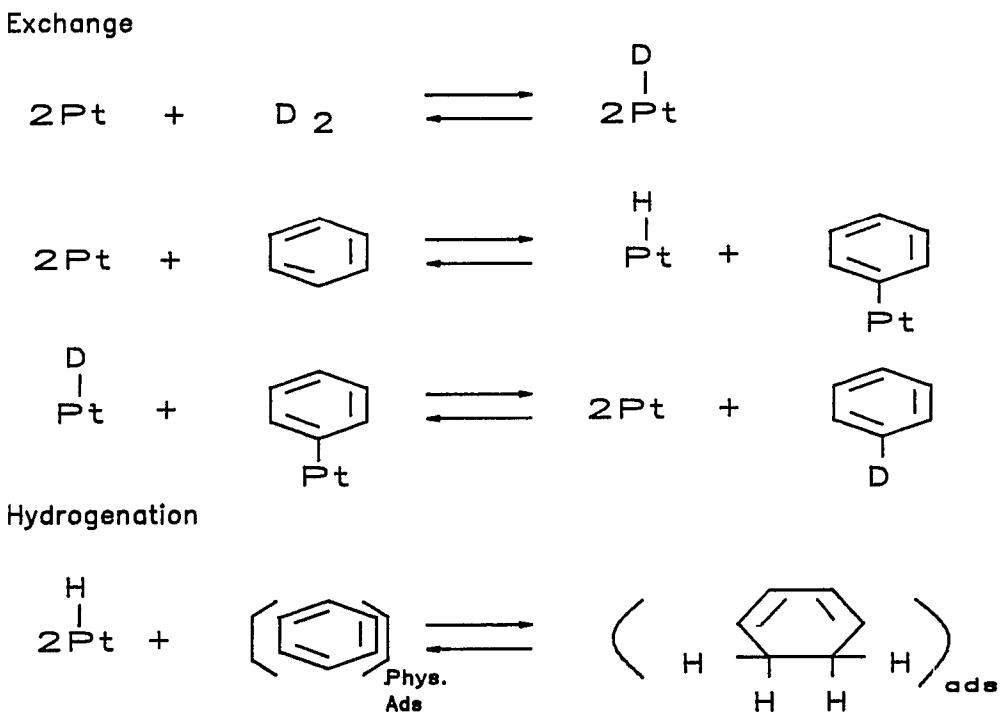


Figure I–9. Classical Dissociative Mechanism [Farkas and Farkas, 1939].

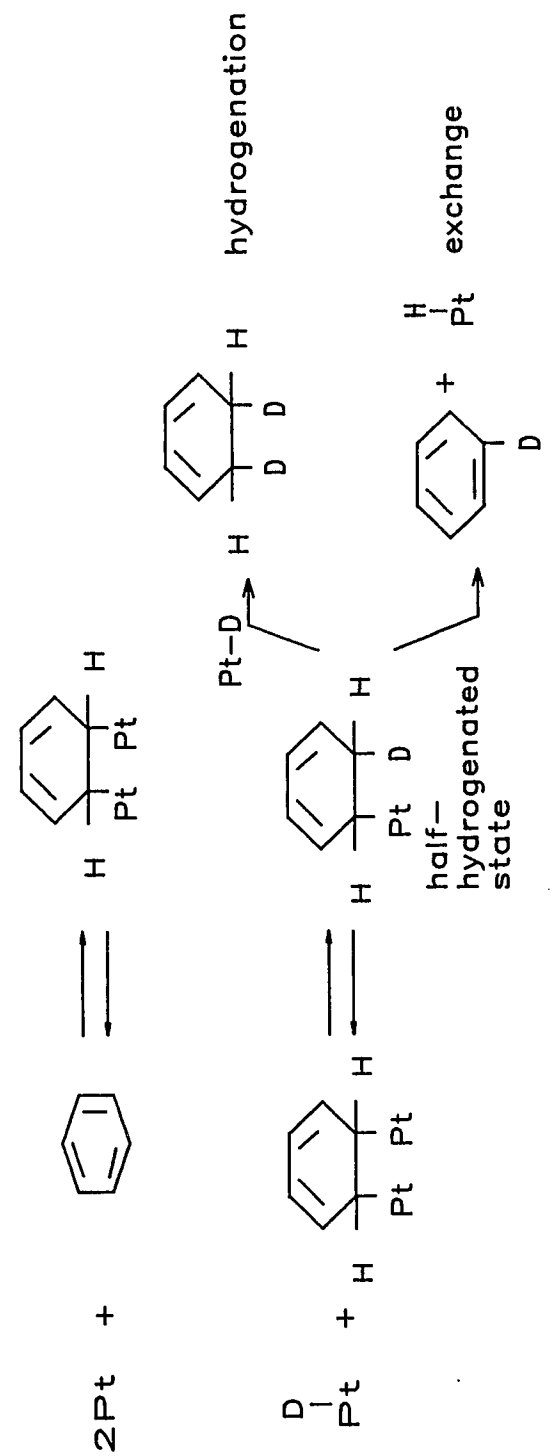


Figure I–10. Classical Associative Mechanism [Horiuti and Polanyi, 1933].

Figure I-11. It is suggested that benzene is Π-bonded to the metal sites and the plane of the ring is parallel to the catalyst surface forming a cyclohexadienyl complex. The catalytic activity of the transition metal was shown to depend on its position in the periodic table and is related to the stability of the cyclohexadienyl complex in benzene hydrogenation. In addition, a correlation between the chemisorption bond strength of the Π-intermediate and the chemical properties of the transition metals was observed.

Data on the catalytic exchange reaction can also be interpreted by determining the extent of single and multiple exchanges, which are directly related to geometric information on the surface intermediates. Possible surface species for allylic hydrocarbons are illustrated in Figure I-12 [Ponec and Sachtler, 1972]. In the case of a single exchange reaction, the distribution of deuterated hydrocarbons will be similar to that calculated by the binomial distribution. On the other hand, any deviation from the binomial distribution may be a clue to the presence of multiple exchange. Kemball [1959] proposed a parameter, M, which represents the mean number of hydrogen atoms exchanged in each of the hydrocarbon molecules in the initial stages of the reaction. Mathematically, M can be defined as the ratio

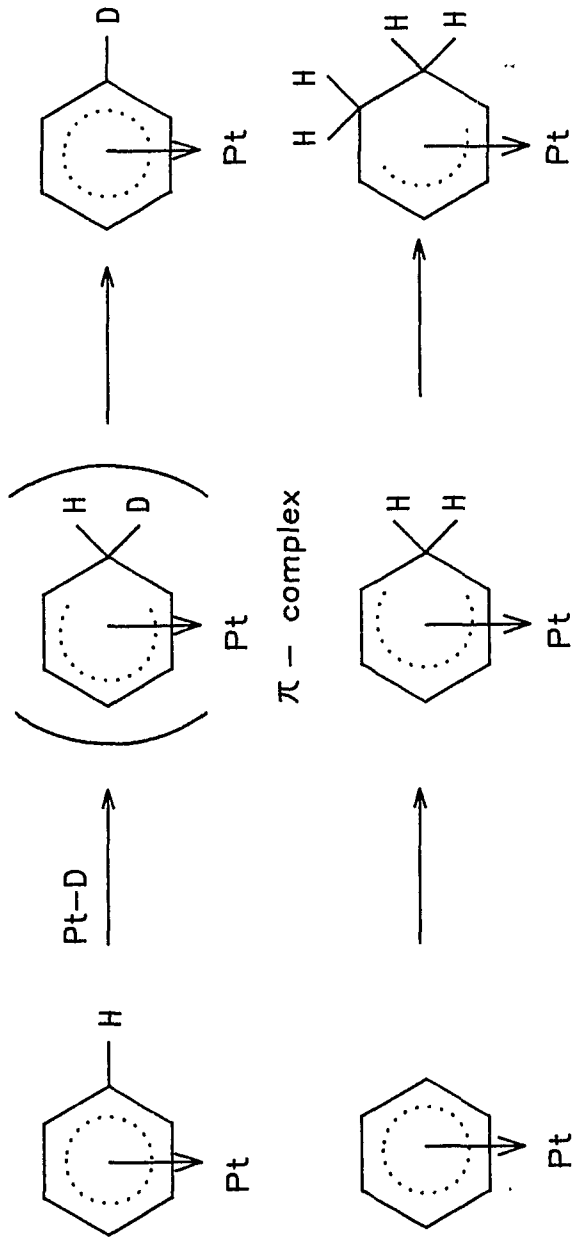


Figure I–11. π–Complex Adsorption Mechanism for Exchange and Hydrogenation of Benzene [Rooney and Webb, 1964].

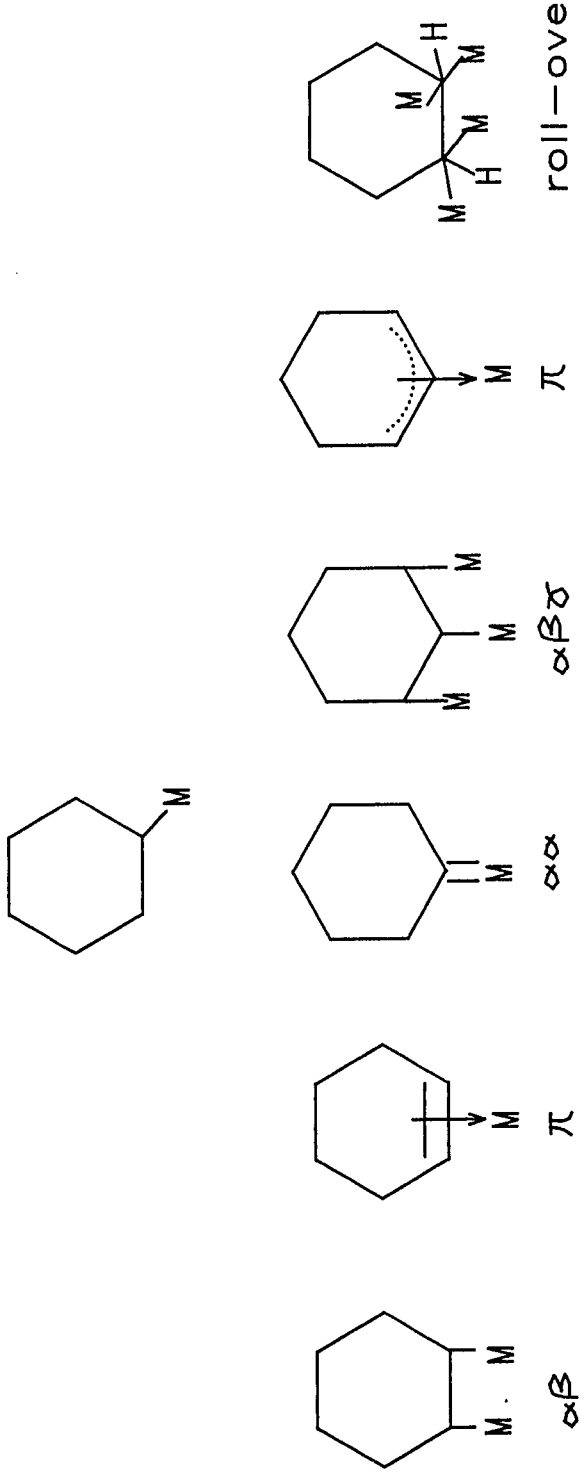


Figure I—12. Possible Surface Species [Ponec and Sachtler, 1972].

of $k_\bullet/k_{d0}$, where $k_\bullet$ is the initial rate of deuterium atoms entering the hydrocarbon molecules, and $k_{d0}$ is the initial rate of disappearance of the hydrocarbon molecules. Any value of M larger than one implies that multiple exchange is operative.

The work of Anderson and Kemball [1957] on benzene hydrogenation on evaporated metallic films, demonstrated that exchange and hydrogenation are independent reactions. The authors further suggested that the phenyl radical is the important surface intermediate for the exchange reaction. Multiple exchange is significant even at low temperature (≈ -20 to -40°C) and the most prominent type of adsorbed species for multiple exchange is the α-β type.

Ponec and Sachtler [1972] studied the exchange reactions between cyclopentane and deuterium on Ni and Ni-Cu alloys from -73 to 157°C. The M parameter remains approximately constant, 1.5, from -73 to 27°C, then, beginning at a temperature of about 67°C, increases with temperature. The function M(T) is similar for Ni and Ni-Cu alloy films, unlike hydrogenolysis and self-poisoning, which are inhibited by alloying. The increase in M(T) is due to a change, mainly in $D_1$ to $D_2$ at T < 107°C, and in $D_{10}$ at T > 107°C. At least two surface intermediates responsible for the multiple exchange are

proposed by the author.

Blakely and Somorjai [1976] investigated the dehydrogenation of cyclohexane and cyclohexene on a stepped Pt surface. They showed that the dehydrogenation of cyclohexane to cyclohexene is structure insensitive, whereas the dehydrogenation of cyclohexene to benzene is structure sensitive and the latter was identified as the rate determining step.

Ledoux et al., [1986], using a surface coverage type model, interpreted their results for the cyclohexane dehydrogenation on $Pt/Al_2O_3$ at 282-399°C at atmospheric pressure. The rate was found to go through a minimum with time. This was explained by a decrease in surface coverage of cyclohexane followed by complete regeneration of the catalyst as the gas phase hydrogen concentration increased with time. The slow steps are cyclohexane adsorption and hydrogen desorption as compared to the rapid surface reactions of the adsorbed molecules and benzene desorption.

**iv. Hydrogenolysis**

The primary steps for metal catalyzed hydrogenolysis reactions [Sinfelt, 1973] consist of (1) dissociative chemisorption of alkanes by the breakage of carbon-hydrogen bonds, (2) carbon-carbon bond rupture of the

surface species, (3) carbon-hydrogen bond formation and the desorption of the final products. The rate determining step appears to be carbon-carbon bond rupture on the surface.

As mentioned previously, the hydrogenolysis reaction requires multiple sites to occur and therefore is termed structure sensitive. Related surface intermediates include the α,β-dicarbene and the α,α,τ-triadsorbed species. It is clear that the rate of formation of these species should be slowed upon alloying by breaking up the contiguous sites required for the multiply adsorbed species. However, an adsorbed cyclobutane species (discussed in the Garin-Gault bond shift isomerization), which chemisorbs at only a single metal site, is also capable of promoting hydrogenolysis reactions. In such a case, electronic modification, rather than surface dilution, induced by alloying is a better explanation for the suppression of hydrogenolysis reactions by alloying.

## B. Research Goal and Plan

A newly developed catalyst requires fundamental studies to characterize its catalytic behavior and thereafter to evaluate its importance in industrial

applications. To achieve desired characteristics described previously, Te and Sb have received attention in the last five years as potential additives to $Pt/Al_2O_3$ or other bimetallic systems such as $PtRe/Al_2O_3$ and $PtIr/Al_2O_3$. A number of studies directed mainly at global selectivity of these catalysts have appeared in the literature [Eberly, 1979; Brignac and Swan, 1984; Thoang et al., 1984; Lanh et al., 1984]. However, the mechanistic aspects of catalyst modification have not been deduced. Consequently, the goal of the current research is to obtain fundamental information which may help explain exactly how Te and Sb modify Pt.

As industrially significant reforming catalysts are complex dual-functional materials, we have chosen to simplify the catalysts in two ways to improve our ability to recognize catalytic effects on the platinum function itself when we add a modifying element. First, we have eliminated acidity from the support so that we eliminate these complicating effects and also eliminate possible modifications to acidity. Second, we have refrained from calcining the catalysts in oxygen so that we are certain that metals are zero-valent. Thus, we are not seeing effects associated with the modification of the Pt oxidation state.

The research approach can be described as follows:

**1. Catalyst Preparation**

$PtTe/Al_2O_3$ and $PtSb/Al_2O_3$ were prepared by a conventional coimpregnation method. In addition, we took advantage of the low melting point of elemental tellurium by subliming Te directly onto the surface of $Pt/Al_2O_3$. We refer to this technique as vapor deposition modification. The unavailability of a suitable non-chlorided Sb compound forced us to abort the vapor deposition method for preparation of $PtSb/Al_2O_3$ without the incorporation of acidity.

**2. Catalyst Characterization**

a. The Pt metallic dispersion of the prepared catalysts was measured by chemisorption of hydrogen and carbon monoxide. The metallic dispersion combined with the kinetic data was used to calculate the specific activities of the test reactions.

b. n-Hexane and cyclohexane reactions were used as model reactions to test the activity and selectivity of the catalysts.

c. The existence of geometric and electronic effects by the modifying elements on Pt was determined using FTIR (Fourier Transform Infrared Spectroscopy) together with the isotopic dilution method. The spectroscopic results were compared with the kinetic results.

d. Carbon-13 labeled hydrocarbon reactions were used to determine the contribution of bond shift and cyclic mechanisms for the monometallic and bimetallic catalysts.

e. The reaction of benzene with deuterium on the catalysts was studied with an aim to understand the adsorption/desorption and surface reaction steps associated with hydrogenation.

The results thus obtained were then analyzed and compared with those obtained previously on similar alloy systems. Recommendations for additional investigations are also provided.

# II. EXPERIMENTAL

## A. Materials and Reagents

The materials and reagents used in this work are listed in Table II-1 with suppliers, specifications and lot numbers where available.

Hydrogen was deoxygenated by passing it through a CuO column at 400°C, followed by dehydration using a Linde type molecular sieve trap cooled with liquid nitrogen. The purified hydrogen was then stored in four 5-liter flasks for later use. Helium used in conjunction with catalytic reactions was pretreated only with the molecular sieve trap. All other chemicals were reagent grade or better and needed no further purification. Prior to experiments, any air in hydrocarbon reagents was removed by a freeze-evacuate-thaw procedure repeated three times. Water, used for catalyst preparation and atomic absorption analyses, was distilled and deionized. Chloroplatinic acid was kept under a positive pressure of argon to avoid contamination from the atmosphere. Gamma-alumina was ground, seived to 20-40 mesh, and calcined in a furnace maintained at 400°C for 3 hr before use.

## B. Equipment

### 1. Recirculation Batch Reactor System

TAble II-1. Materials and Reagents

| Compound | Supplier | Specification | Lot No. |
|---|---|---|---|
| $H_2PtCl_6 \cdot 6H_2O$ | Aldrich | ≥ 99.95% | 05128MM |
| $TeO_2 \cdot 2H_2O$ | Alfa Products | 99.95% | 051083 |
| $SbCl_3$ | Alfa Products | Ultrapure | 090484 |
| gamma-$Al_2O_3$ | Union Carbide Linde type 60-503 | Diameter 1/16" Length 1/8-1/4" Bulk Density 36 lbs/ft$^3$ Piece Density 0.98 g/cc Hg Pore Volume 0.71 cc/g Surface Area 215 m$^2$/g | 9647770004-1 |
| HCl | Baker | 37.5% | |
| $HNO_3$ | Fisher Scientific Company | 40° Baumè | |
| $NH_4OH$ | Baker | 29.2% | |
| $PtCl_2$ | Engelhard | 73.3% Pt | 22-300-19 |
| Amberlite IRA-400 | Diamond Shamrock | 4.3 meq/g.min | |
| SE-30 | Teklab | | |
| Carbowax 1540 | Teklab | | |
| Chromosorb | Teklab | | |
| 23% SP-1700 | Supelco | | |
| Chromosorb 102 | Supelco | | |
| Hydrogen | Liquid Carbonic | | |
| Helium | Lincoln Big Three | | |
| Nitrogen | Liquid Carbonic | | |

TAble II-1. Materials and Reagents (Cont'd)

| Compound | Supplier | Specification | Lot No. |
|---|---|---|---|
| Carbon Monoxide | Matheson | | |
| Carbon Monoxide $-^{13}C$ | MSD Isotopes | 99 atom % $^{13}C$ | |
| Deuterium | Liquid Carbonic | | |
| n-Hexane | Phillips | Reagent Grade | |
| 2-Methylpentane | Phillips | Reagent Grade | |
| Cyclohexane | Baker Analyzed | 100% | 404605 |
| Benzene | Matheson Coleman & Bell (MCB) | > 99% | |
| Acetone-2-$^{13}C$ | Sigma | 99.7 atom % $^{13}C$ | 105F3754 |
| Iodomethane-$^{13}C$ | Sigma | 99 atom % $^{13}C$ | 126F3753 |
| Magnesium | MCB | | |
| Ammonia Chloride | Allied | | |
| Isovaleraldehyde | Kodak | > 99% | D14A |
| n-Propyl Bromide | Fisher Scientific | | 783756 |
| Diethyl Ether | Mallinckrodt | ≤ 0.003% $H_2O$ | 0852 KBCK |
| Deuterated Chloroform | Aldrich | 99.8 atom % D | 4601HKHK |
| Iodine Crystal | Mallinckrodt | | KHRK |
| De-oxygenation Catalyst | Alfa | 3mmx5mm Pellets | 050283 |
| Molecular sieves (Linde Adsorbents) | Union Carbide | | |

All catalytic reactions were carried out in an all-pyrex recirculation batch reactor system, which is illustrated schematically in Figure II-1.

The heart of the circulation system consisted of two 300-ml flasks, a liquid nitrogen trap, a magnetically operated pump and a reactor section, interconnected with pyrex tubing and stopcocks. Only mixing flask 1 was used in this work, and the total volume of the reaction system in this configuration was approximately 580 cc. The liquid nitrogen trap could be used for the removal of compounds other than helium and hydrogen during reduction or activation processes. It could also be used to collect reaction products which were subsequently transferred to a glass bulb for other analyses, e.g. GC-MS and NMR.

The magnetically operated pump had a 7/8" diameter glass cylinder fitted with a teflon piston having an iron core. The piston could be alternated back and forth via switching magnetic fields, produced by two solenoids surrounding the glass cylinder. A gas flow of approximately 1000-1500 cc/min in the system was routinely obtained by the back and forth motion of the piston combined with four check valves, which forced the recirculating gas to flow counter-clockwise.

The reactor section, which is enlarged and shown in

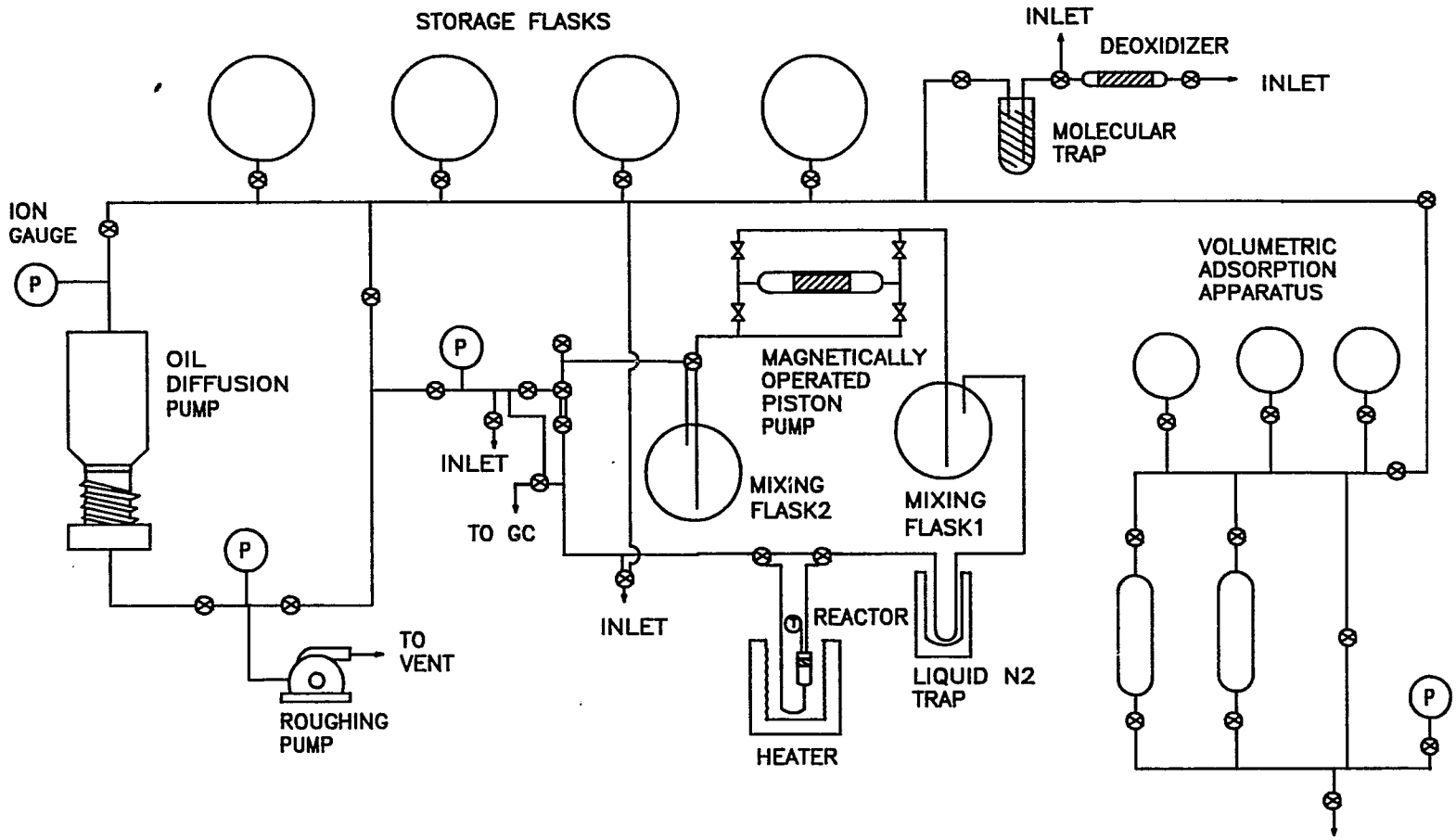


Figure II–1. Recirculation Batch Reactor System.

Figure II-2, included: a 10-mm O.D pyrex tube holding the catalyst in place with pyrex wool on each end of the catalyst bed, a thermowell immersed inside the catalyst bed permitting temperature measurments with a thermocouple, a four way high vacuum stopcock allowing the isolation of the catalyst from atmosphere, 6-mm O.D. pyrex tubing connecting the 10-mm O.D. tubing to the stopcock, and a pair of 10/30 ground glass joints which were used to connect the reactor to the recirculation system.

During reaction runs, the section below the four way stopcock was immersed in a concentric electric heater. The temperature of the catalyst was controlled by a PID controller (Love Model 151), with a reproducibility of ± 1°C.

Hydrocarbons could be introduced into the recirculation system through two inlets, each with a 12/30 ground glass joint. The partial pressure of the reactants were monitored by using a diaphragm pressure transducer (MKS), calibrated from 0 to 1000 torr.

Four 5-liter flasks and a vacuum manifold provided for purified gas storage and system evacuation. Vacuum was provided by a diffusion pump (Varian), and a rotary mechanical roughing pump (Sargent Walch). Vacuum was monitored by an ionization/thermocouple gauge (Varian).

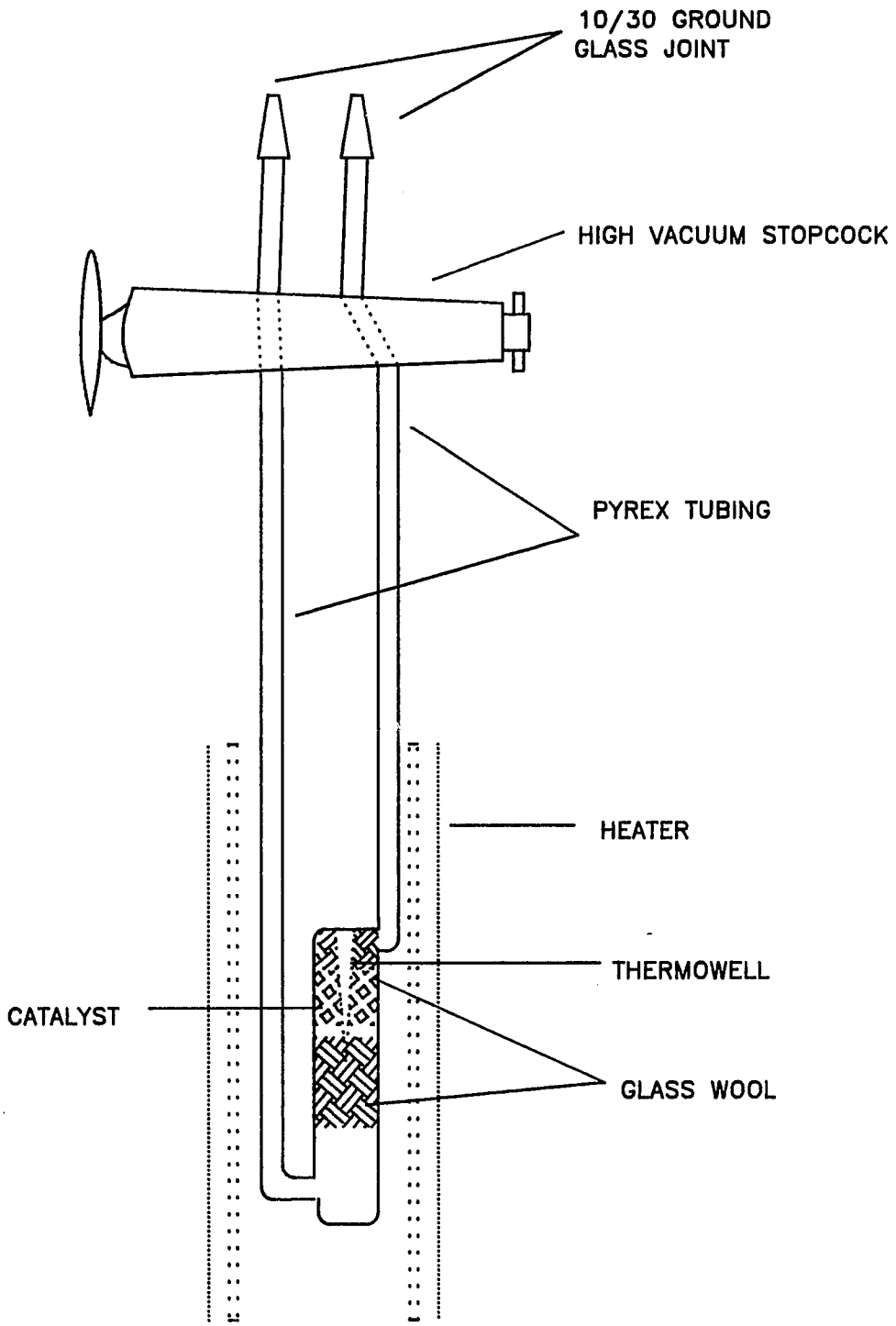


**Figure II–2. Reactor Section in the Recirculation System.**

The rotary pump could obtain an ultimate vacuum of $10^{-4}$ torr, while the diffusion pump could produce a vacuum of $10^{-7}$ torr. A liquid nitrogen trap was placed in front of each pump to avoid pump oil contamination of the system and the catalyst.

**2. Volumetric Adsorption Apparatus**

On the right side of Figure II-1, a static volumetric adsorption apparatus, used for the determination of the gas uptake of hydrogen and carbon monoxide on the catalysts, is shown. The volumetric adsorption apparatus shared the same vacuum system as the reactor system. Purified hydrogen, carbon monoxide, and helium were stored in three 1-liter flasks. The apparatus was constructed with capillary pyrex tubing in order to minimize its dead volume. The pressure in the gas phase was monitored with a diaphragm pressure transducer, calibrated from 0-100 torr (MKS). The catalyst was placed in the same pyrex reactor described previously, which was connected to the adsorption apparatus through a 10/30 ground glass joint. The catalytic surface could be degassed with the diffusion pump. The dead volume of the apparatus was measured by means of helium expansion from a gas bulb of known volume; detailed procedures and calculations are given in Appendix A.

### 3. Gas Chromatograph and Integrator

The gas chromatograph (GC) was a Carle Model-111H equipped with a hydrogen transfer system (HTS) and two thermistor detectors. The sample injection port was connected to the recirculation system using a 5-ft 1/16" stainless steel line, which was cleaned by evacuation and traced by a heating wire. The analytical columns used were a 20-ft 15% Carbowax on Chromosorb column, a 15-ft 23% SP-1700 column, and a 6-ft Chromosorb 102 column. The arrangement of the packed columns and the gas sampling valves are illustrated roughly in Figure II-3. The actual arrangement including backflushing valves and miscellaneous accessories is extremely complex. The sample loops of V1 and V2 were filled simultaneously with two identical samples from the recirculation system. First, V1 was switched to open allowing the sample to pass through the Carbowax column which separated cyclic $C_6$ hydrocarbons such as methylcyclopentane, benzene, cyclohexane, and cyclohexene. After the detection of cyclic compounds, V2 injected the stored sample onto the SP-1700 column which performed the separation of $C_3$ through $C_6$ alkanes, but light gases such as hydrogen, methane, and ethane were stored on the Chromosorb column. After the detection of

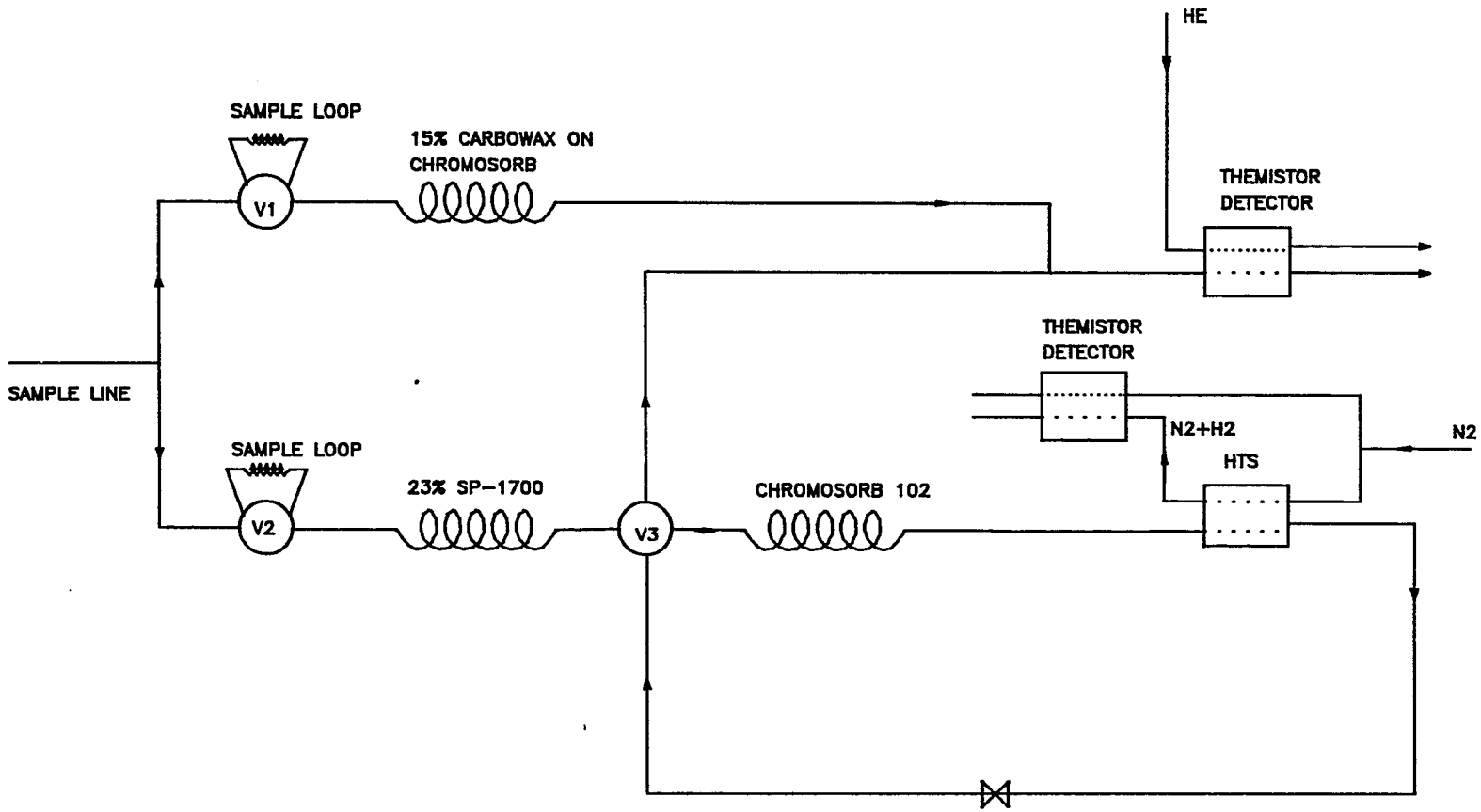


Figure II-3. Simplified Schematic Diagram of the Arrangement of Columns and Sampling Valves in the Carle-111H Gas Chromatograph.

hexanes, V3 was then switched allowing the separation of light gases to be made on the Chromosorb 102 column. Since hydrogen and helium have very similar thermal conductivities, hydrogen was transferred by the HTS into a nitrogen carrier prior to detection. The complete analysis of a sample took approximately 25 min. Each column was immediately backflushed with helium after the elution of the sample.

The switching of valves 1, 2, and 3 could be done manually or automatically according to a series of programmable time slots. Table II-2 lists the event times for the separation of C1 through C6 hydrocarbons. The GC conditions used in this work are given in Table II-3.

Peak area determination for quantitative analysis was handled by a Hewlett Packard 3390A integrator. Figure II-4 gives an example chromatogram of the reaction products for the n-hexane reaction. The integrator parameters are provided in Table II-4.

The calibration table was determined by preparing a standard mixture containing most of the components in the reaction products. Response factors of the components ascertained by using this standard mixture along with those from literature [Dietz, 1967] are shown in Table II-5. These values were generally in good

Table II-2. Events and Times for Carle-111H.

| Event | Time | Valve Position | | Purpose |
|---|---|---|---|---|
| 1 | 0 | V1 | CW | Injection of sample to column 1[a] |
| 2 | 10:50 | V2 | CW | Injection of sample to column 2[b] |
| 3 | 11:68 | V1 | CCW | Switch V1, reflush column 1 |
| 4 | 12:55 | V3 | CW | $C_3$-$C_6$ bypass column 3[c] and proceed to the detector |
| 5 | 20:25 | V2 | CCW | Switch V2, reflush column 2 |
| 6 | 20:50 | V3 | CCW | $H_2$, $C_1$ and $C_2$, separated on column 3, proceed to the detector |

a : 15% Carbowax on Chromosorb column
b : 23% SP-1700 column
c : Chromosorb 102 column

Table II-3. Gas Chromatograph Conditions.

| | |
|---|---|
| He Flow Rate | : 26 ml/min (66 psig) |
| HTS Temperature | : 580°C |
| Bridge Setting | : 6 |
| Output Attenuation | : 1 |
| $N_2$ Flow Rate | : 48 ml/min |
| Column Temperature | : 91°C |
| Cycle Time | : 25 min |

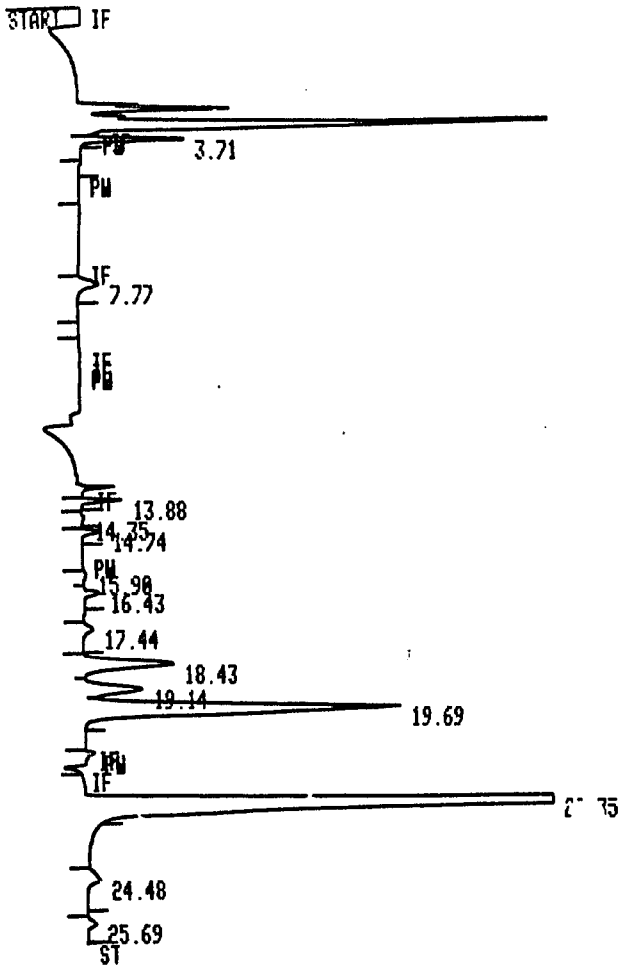


| COMPOUND | RT(MIN) | CAL# |
|---|---|---|
| METHYLCYCLOPENTANE | 3.71 | 1 |
| BENZENE | 7.77 | 4 |
| PROPANE | 13.88 | 5 |
| I-BUTANE | 14.35 | 14 |
| N-BUTANE | 14.74 | 6 |
| I-PENTANE | 15.90 | 15 |
| N-PENTANE | 16.43 | 7 |
| 2,2-DIMETHYLBUTANE | 17.44 | 16 |
| 2-METHYLPENTANE | 18.43 | 8 |
| 3-METHYLPENTANE | 19.14 | 9 |
| N-HEXANE | 19.69 | 10 |
| HYDROGEN | 22.35 | 11R |
| METHANE | 24.48 | 12 |
| ETHANE | 25.69 | 13 |

Figure II-4. Typical GC Chromatogram of Reaction Products.

Table II-4. Integrator Timed Events and Operation Settings.

| | |
|---|---|
| 0.00 INTG # = 9 | Disable Integration |
| 3.52 INTR # = -9 | Enable Integration |
| 3.60 PKWD = 0.09 | Set Peak Width |
| 4.80 PKWD = 0.16 | Set Peak Width |
| 7.30 INTG # = 0 | Set Baseline Now |
| 9.70 INTG # = 0 | Set Baseline Now |
| 10.00 INTG # = 9 | Disable Integration |
| 10.20 PKWD = 0.04 | Set Peak Width |
| 13.62 INTG # = -9 | Enable Integration |
| 15.50 PKWD = 0.16 | Set Peak Width |
| 20.90 INTG # = 9 | Disable Integration |
| 21.00 PKWD = 0.16 | Set Peak Width |
| 21.50 INTG # = -9 | Enable Integration |
| 26.30 STOP | Stop Integration |

ZERO = 0,0

ATT2 = 3

CHT SP = 0.5

PKWD = 0.04

THRSH = 0

AR REJ = 0

TAble II-5. GC Calibration.

| Cal # | Component | torrx$10^5$/area | RTR[a] | RTR [Dietz, 1967] |
|---|---|---|---|---|
| 1. | Methylcyclopentane | 2.047 | 0.896 | 0.935 |
| 2. | Cyclohexane | 2.072 | 0.885 | 0.927 |
| 3. | Cyclohexene | 2.214 | 0.828 | - |
| 4. | Benzene | 2.242 | 0.818 | 0.813 |
| 5. | Propane | 2.689 | 0.682 | 0.524 |
| 6. | n-Butane | 2.286 | 0.802 | 0.691 |
| 7. | n-Pentane | 2.123 | 0.863 | 0.854 |
| 8. | 2-Methylpentane | 1.900 | 0.965 | 0.976 |
| 9. | 3-Methylpentane | 1.907 | 0.961 | 0.967 |
| 10. | n-Hexane | 1.833 | 1.000 | 1.000 |
| 11. | Hydrogen | 15.374 | 0.119 | - |
| 12. | Methane | 5.176 | 0.354 | 0.290 |
| 13. | Ethane | 3.609 | 0.508 | 0.416 |
| 14. | Iso-butane | 2.370 | 0.773 | 0.667 |
| 15. | Iso-pentane | 2.185 | 0.839 | 0.829 |
| 16. | 2,2-Dimethylpentane | 1.964 | 0.933 | 0.943 |

*a* : Relative molar response (normalized to 1 on n-hexane)

agreement with each other. Part of the difference is possibly due to slightly different sample sizes injected to each column. Since our experimental values were reproducible within ± 2% using a series of standard mixtures, they were used in this work rather than the literature values.

**4. Gas Chromatograph - Mass Spectrometer (GC-MS)**

A Finnigan OWA/1000 Series system was used for the determination of the product distribution in deuterated hydrocarbons and, in some cases, for product identification. The analyses were automated with a dedicated data system. A Valco gas sampling valve with a 12/30 ground glass joint was used for the injection of the sample from a glass bulb into the instrument. A 12-ft 1/8" OD 15% Carbowax on Chromosorb packed column was used to perform separation of benzene and cyclohexane. The GC-MS used a jet separator, maintained at a temperature of 200°C, to remove most of the chromatographic carrier gas. The GC-MS system included an electron impact ionization source with a magnetically constrained electron beam. The mass analyzer was a quadrupole rod assembly producing a precision hyperbolic field for mass filtering in the range of 4 to 800 amu. The detector

was an off-axis continuous dynode electron multiplier. The voltage could be selected from 0 to 3000 volts in 10 volt increments. Resolution of 1600 at mass 800 M/$\Delta$ M at half peak height was obtainable. The operating vacuum, approximately $10^{-8}$ torr for the ion source, the mass analyzer, and the detector, was maintained by a turbomolecular pump together with a rotary vacuum pump. To reduce fragmentation, the ionization voltage was kept below 20 V for deuterium content analysis. Other related parameters for the operation of GC-MS are given in Table II-6.

5. Fourier-Transform Infrared Spectrometer (FTIR)

Infrared spectra for the isotopic dilution experiments were recorded on an IBM Instruments IR/32 FTIR spectrometer. The source of IR radiation was produced by a globar. The detector was a liquid nitrogen cooled MCT (mercury cadmium telluride) detector. The interferogram was created by a scanning Michelson interferometer. The Fourier transform calculations, which converted the interferogram into the final spectrum, was performed by an IBM 9000 computer system. The resulting spectrum covered the mid-infrared range from 4800-400 wavenumbers ($cm^{-1}$). The wave numbers were calibrated with a Buch Scientific 0.05 mm thick polystyrene film

Table II-6. GC-MS Operation Parameters.

| | |
|---|---|
| Packed Column | : 12 ft 15% Carbowax on Chromosorb |
| Zone Temp | : 150°C |
| Initial Temp | : 80°C |
| Final Temp | : 80°C |
| Initial Time | : 1 min |
| Ramp Rate | : 10 Deg/min |
| Final Time | : 10 min |
| Separator Oven | : 200°C |
| Manifold Temp | : 80°C |
| Solvent Divert Time | : 0 sec |

| | |
|---|---|
| Electrometer Range | 7.00 |
| Extractor | 2.94 |
| Elect Mult Volts | -1400.00 |
| Resolution High | 135.00 |
| Resolution Low | 128.00 |
| Ion Energy | 4.08 |
| Scope 1st Mass | 69.02 |
| Ion Program | 5.65 |
| Lens Voltage | -86.27 |
| Electrometer Zero | 2.80 |

and the resolution was set at 4 $cm^{-1}$.

6. Gas Adsorption System and IR Cell

A gas adsorption system together with an IR cell, which allowed in situ sample treatment in the infrared beam, was built for performing the isotopic dilution experiments; the schematic diagrams are given in Figure II-5 and II-6, respectively.

A diffusion pump and a backing rotary mechanical pump provided a vacuum of less than $10^{-6}$ torr. Two diaphragm pressure gauges with digital readout, calibrated from 0.1 to 1000 torr and $1x10^{-4}$ to 1 torr, monitored the amount of gas added to the system. Two inlets, each with a 12/30 ground glass joint, were used to introduce the gas samples from glass bulbs. Two 5-liter flasks could be used to store purified gas. In order to minimize the dead volume, the system was constructed with pyrex capillary tubing. The system was connected to the IR cell using two 3-way high vacuum stopcocks which could also be used for the isolation of the cell from the adsorption system during reduction processes.

The body of the IR cell was a 1" OD, 6.3" long pyrex tube. The wafer was mounted in a sample holder which allowed it to be slid to the center of the cell. A

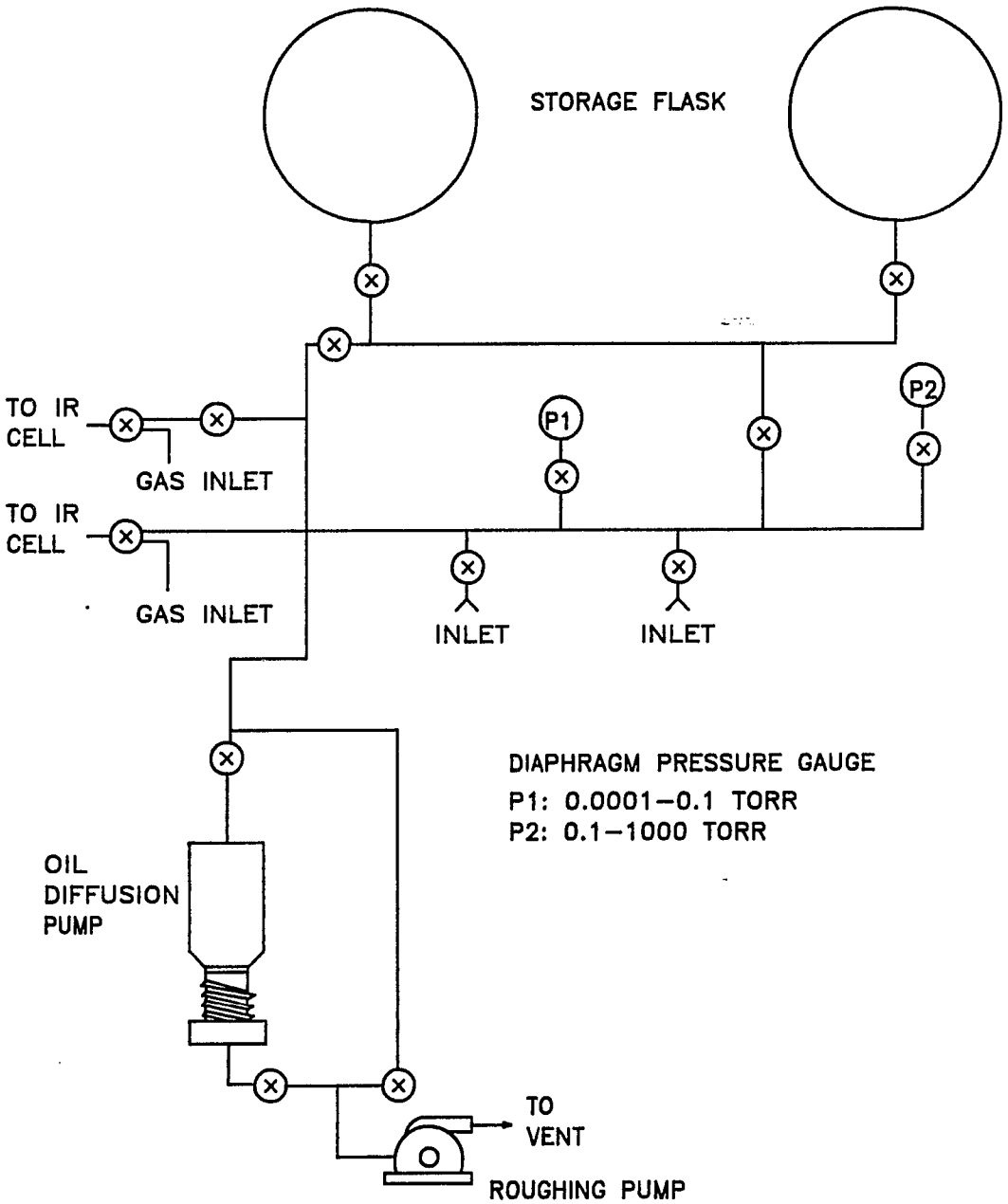


Figure II–5. Schematic Diagram of the Gas Adsorption System for FTIR Experiments.

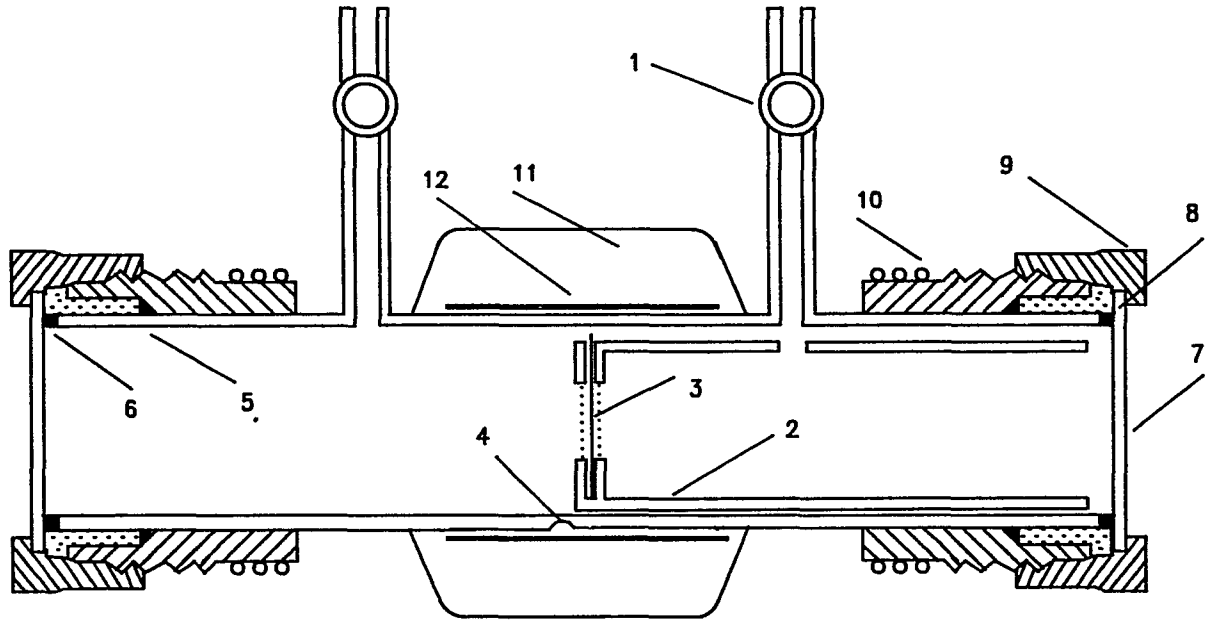


1 HIGH VACUUM STOPCOCK
2 SAMPLE HOLDER
3 CATALYST WAFER
4 THERMOCOUPLE
5,6 VITON O-RINGS
7 NaCl WINDOW
8 WINDOW ATTACHED TO SLEEVE
9 CAJON ULTRA-TORR ADAPTOR
10 COOLING WATER TUBING
11 THERMAL INSULATION
12 HEATING WIRE

Figure II-6. IR Cell.

furnace surrounded the sample for heating during reduction processes. The temperature measurement was made by a thermocouple placed between the furnace and the body of the cell. Infrared transmitting NaCl windows were attached to the ends of the cell with two Viton o-rings. The cooling of the windows was accomplished with cooling water flowing through tubing wound around the window adaptor. The cell had two ports for admission of gases and for evacuation.

**7. Atomic Absorption Spectrophotometer**

The metal content of the catalysts, $Pt/Al_2O_3$ (ion-exchange) and $PtTe/Al_2O_3$ (vapor deposition), were determined using a Varian AA-1475 atomic absorption spectrophotometer. The spectrophotometer was a double beam instrument which could also be operated in the single-beam mode. Hollow cathode lamps for external light sources and an air-acetylene flame for the atomizer were used for all analyses. The excitation wavelengths for Pt and Te were 266 and 214.3 nm, respectively. Background correction was provided by a deuterium lamp and the emission signal was measured by a photomultiplier detector. By supplying concentration values of up to three standards for calibration and

curve correction, sample concentration could be obtained directly from a digital readout. Table II-7 lists the operating conditions for the analyses of Pt and Te.

**8. Preparative-Scale Gas Chromatograph**

A preparative-scale gas chromatograph (prep-GC), as illustrated in Figure II-7, was built to perform separation and purification of isomerization products from $^{13}C$-labeled 2-methylpentane reactions for later $^{13}C$-NMR analyses. A glass bulb containing the reaction products could be connected to the system using a 12/30 ground glass joint. The hydrocarbons were vaporized and then condensed into a pyrex U-tube which functioned as a sample injector. The column used was a 35-ft 3/8" O.D. copper column packed with 4% SE-30 and 8% Carbowax 1540 on Chromosorb. The column was heated with a hot water bath maintained at 43°C. The effluent was detected by a thermal conductivity cell and an HP-3390A integrator provided a chromatographic trace. A typical chromatogram and the integrator parameters are shown in Figure II-8. The effluent was collected by condensation in a U-tube cooled with liquid nitrogen.

**9. Fourier Transform $^{13}C$ NMR**

Table II-7. Atomic Absorption Operation Conditions.

| | Pt | Te |
|---|---|---|
| Lamp | Fisher Scientific Hollow Cathode Tube Type 14-386-104K | Fisher Scientific Hollow Cathode Tube Type 14-386-103R |
| Lamp Current | 10 mA | 7 mA |
| Wavelength | 266 nm | 214.3 nm |
| Slit | 0.2 nm | 0.5 nm |
| Flame | Air-Acetylene | Air-Acetylene |
| Fuel Flow | 5 Units | 5 Units |
| Oxidant Flow | 20 Units | 20 Units |

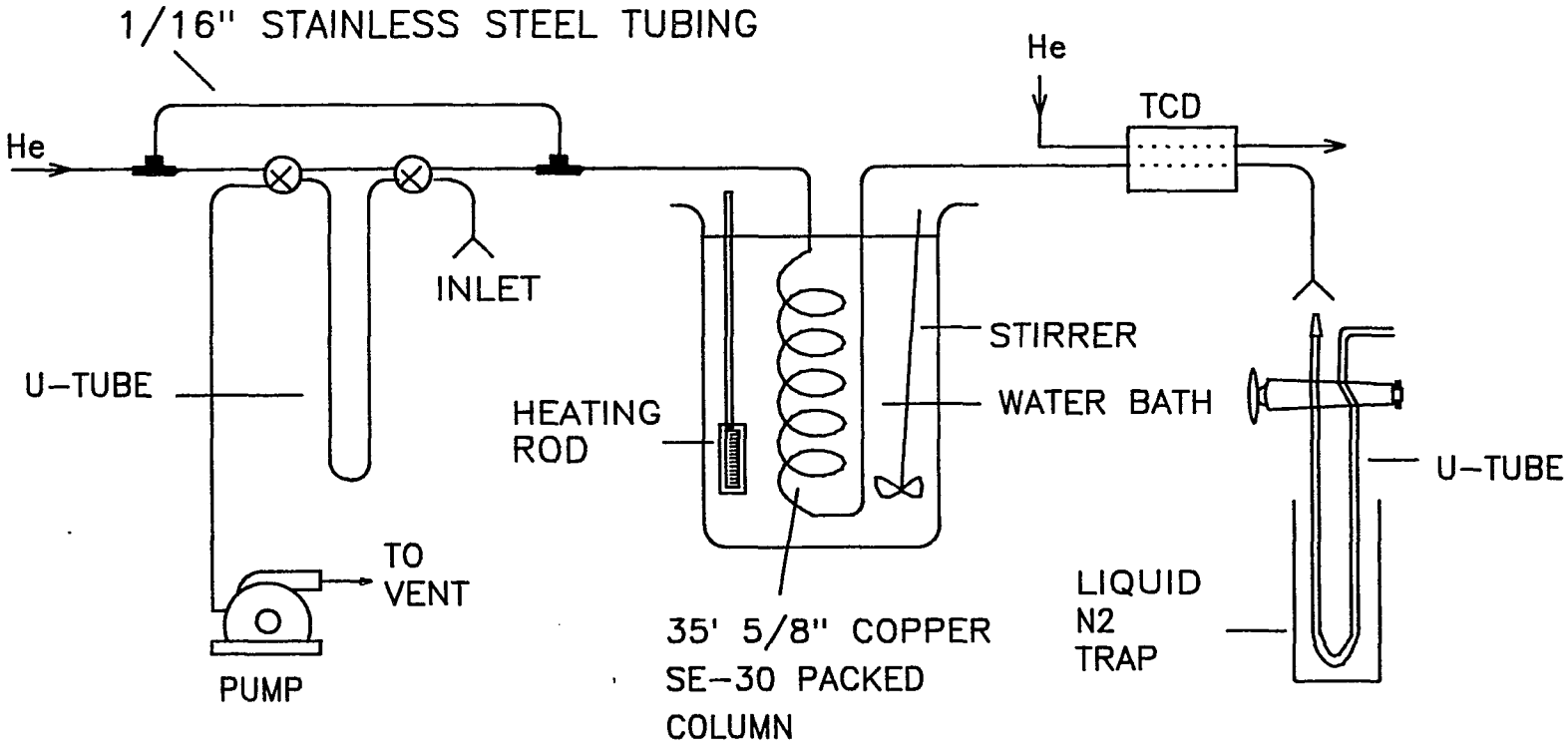


Figure II-7. Preparative Scale Gas Chromatograph.

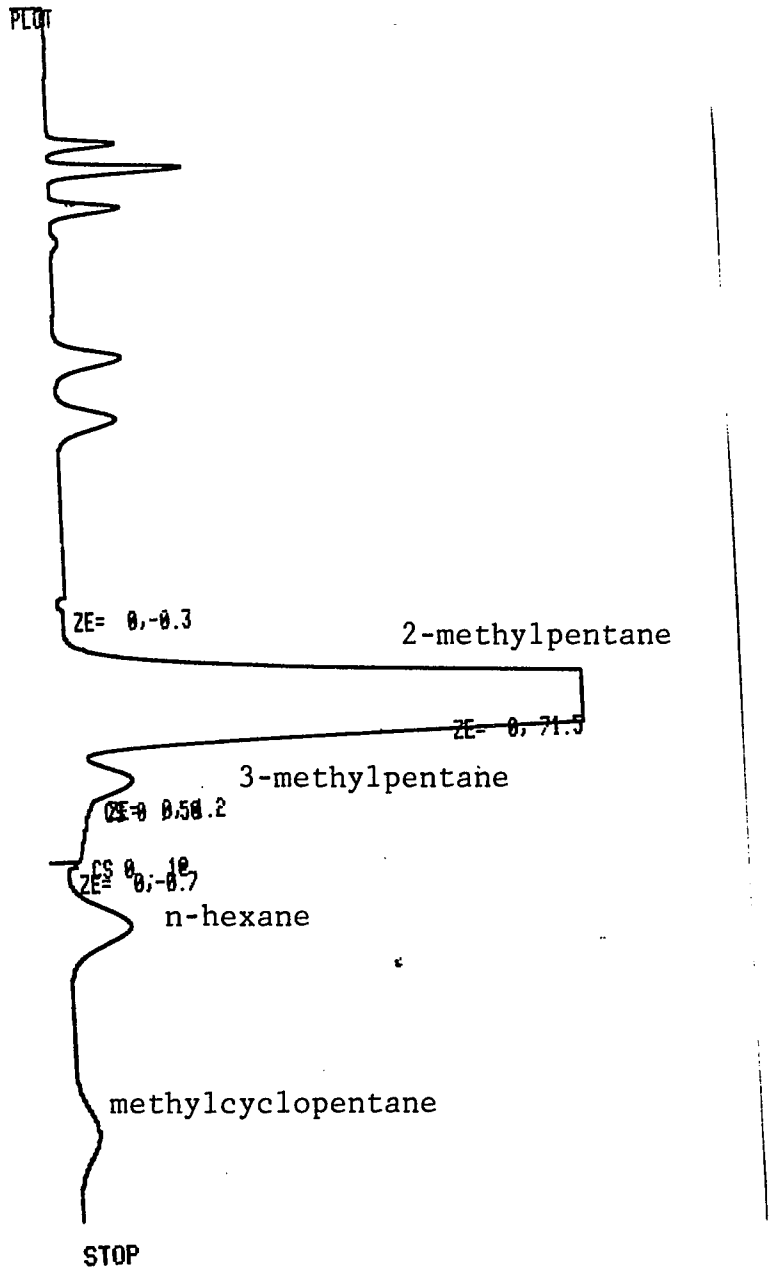


Figure II-8. Typical Prep-GC Chromatogram of Isomerization Products.

The $^{13}C$-NMR spectrocopy results were kindly obtained by Marcus Naumann at the Chemistry Department of Louisiana State University, Baton Rouge. All experiments were run at 50.32 MHz on a Bruker WP-200 FTNMR spectrometer at room temperature. A 5mm Carbon-13 probe was used for all samples.

All spectra obtained were routine $^{13}C$ with proton decoupling. A standard sweep width of 220 ppm was used. In order for the $^{13}C$ spectra to be integrated accurately, an inverse gated proton decoupling technique was used. In this experiment, the proton decoupler was switched off during the relaxation delay. This delay was required to be at least 5 times the longest spin-lattice relaxation, which describes the rate at which the thermal distribution of spin among the nuclear energy levels is reestablished after a perturbing event. The spin-lattice relaxation was determined by using a separate inversion recovery experiment. The proton decoupler was only switched on during the data acquisition.

The inversion recovery experiment determined that the longest T1 of a typical sample was approximately 30 sec. As a result, the relaxation delay was set to 3 min per scan. The concentration of most samples was high enough such that most spectra could be obtained in 1-3

hr (20-60 scans).

The location of the $^{13}C$ in the hydrocarbon molecule was identified by matching the chemical shift to reference spcetra from The Sadtler Standard Spectra for $^{13}C$-NMR [1969]. Table II-8 lists the $^{13}C$-NMR chemical shift of n-hexane, 2-methylpentane, 3-methylpentane and methylcyclopentane. Natural abundance of $^{13}C$ in the molecule was neglected since it exists only in 1/100 of the $^{13}C$-enriched molecule.

**10. Thermogravimetric Analyzer**

A thermogravimetric analyzer (Perkin Elmer, TGA 7) was used to determine the reducibility of telluric acid. The equipment consists of a furnace for measuring the temperature of the sample from room temperature to temperatures as high as 1000°C, a balance with 50 mg sample capacity capable of detecting weight changes to 0.1 μg, and a Perkin Elmer data acquistion computer system. The sample can be treated in situ with flowing helium or hydrogen.

## C. Experimental Procedures

### 1. Catalyst Preparation

#### a. $Pt/Al_2O_3$

Table II-8. $^{13}C$ NMR Chemical Shifts of 2-MP, 3-MP, n-$C_6$ and MCP.

| Compound | C-1 | C-2 | C-3 | C-4 | C-5 |
|---|---|---|---|---|---|
| 2-Methylpentane 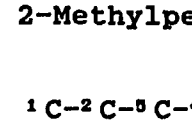 | 14.4 | 20.8 | 22.8 | 28.1 | 41.9 |
| 3-Methylpentane 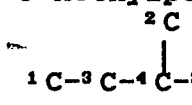 | 11.6 | 18.9 | 29.5 | 36.6 | |
| n-Hexane  | 14.2 | 23.0 | 32.1 | | |
| Methylcyclpentane 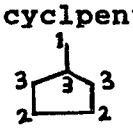 | 20.9 | 25.6 | 35.1 | | |

Ion-exchange [Benesi et al., 1968; Dorling et al., 1971] and impregnation methods [Castro et al., 1981; Gil'Debrand, 1966] were employed for the preparation of $Pt/Al_2O_3$ catalysts.

i. Ion-exchange method

0.002 M $PtCl_2$ solution containing 0.05 g Pt was prepared by dissolving $PtCl_2$ in a 0.1 M $NH_4OH$-$NH_4NO_3$ buffer. A clear solution was obtained after overnight stirring. The chloride ions were exchanged for hydroxyls by passing the solution through a 3/4" ID, 15.5" column packed with basic ion-exchange resin, (Amberlite IRA-400). In this manner, a non-chlorinated catalyst was prepared by ion-exchange of the tetrammine ion onto 5 g gamma-$Al_2O_3$ in excess $NH_3$ (PH > 10). After 8 hr, the solids were filtered from solution, washed with deionized water to remove all free salt, dried at 120°C for 20 hr, and calcined in air at 390°C for 9 hr. The resulting catalyst was then stored in a dessicator. The filtrate, after ion-exchange, was stored in a sample bottle sealed with Parafilm for later AA analyses.

ii. Impregnation Method

$H_2PtCl_6 \cdot 6H_2O$ was placed in a pre-weighed sample bottle in an argon glove box. It was then weighed and dissolved in a minimum amount of deionized water which

was just sufficient to cover the $Al_2O_3$. The solid was evaporated to dryness in a hot water bath followed by a deionized water washing. The catalyst was then dried with flowing He at 110°C for 20 hr, reduced in a hydrogen stream at 400°C for 17 hr, and cooled to room temperature. In order to remove the chlorine, the catalyst was washed thoroughly with 400 cc 5% ammonia [Adkins and Davis, 1984], then 200 cc deionized water. The washing was repeated three times. The resulting catalyst was then dried with flowing He at 120°C for 16 hr, and stored in a dissicator.

**b. $PtTe/Al_2O_3$**

**i. Vapor Deposition Method**

0.1 g $Pt/Al_2O_3$ prepared by the ion-exchange method was placed in the reactor of the recirculation system and reduced with $H_2$ at 400°C for at least 15 hr. Elemental tellurium, ground with pyrex glass, was placed upstream of the $Pt/Al_2O_3$ bed, and heated to vaporize the Te (Figure II-9). The Te vapor was carried by either $H_2$, He, or a reforming feed stream (a mixture of n-hexane, $H_2$ and He), and deposited onto the $Pt/Al_2O_3$ at 400°C. A high flow rate (≈ 25 cc/sec) of carrier gas caused most of the Te to bypass the bed, while at a low flow rate of the carrier gas, the entrance of the bed

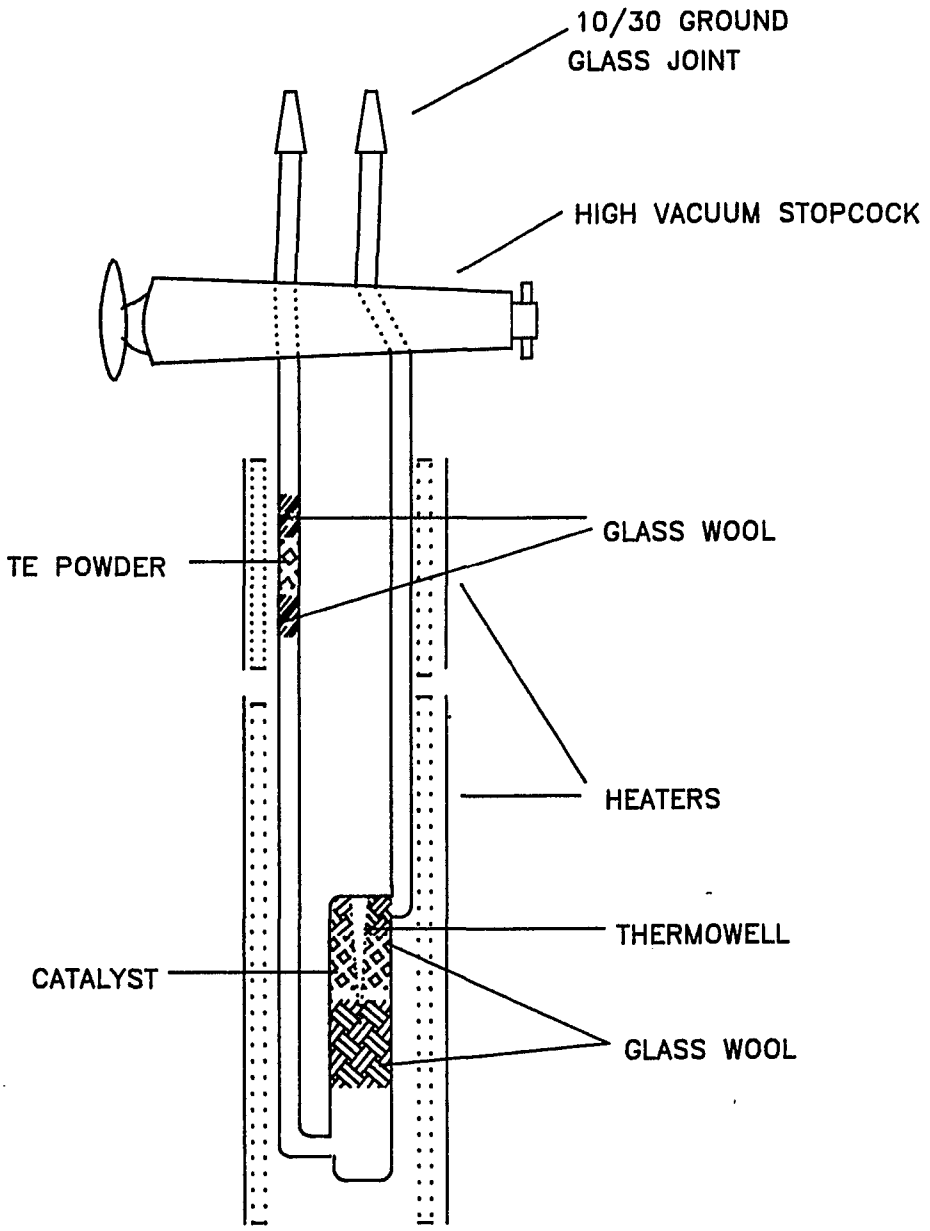


Figure II–9. Schematic Diagram of Vapor Deposition of Te on Pt/Al2O3.

was more heavily tellurided than was the exit. This was visually observed by the change in the color of the catalyst bed and by a silvery Te film formed on the cold glass wall downstream of the reactor. A uniformly tellurided catalyst was preferred; therefore high flow rates were used. The depostion was allowed to take place for 15 hr. Analyses by atomic absorption determined that only 1/3 to 1/2 of the original Te was successfully deposited. After deposition and prior to each reaction study, the catalyst was activated with 400 torr hydrogen at 400°C for 15 hr.

ii. Coimpregnation Method

The preparation procedures and the pretreatment of the catalysts were identical to that of impregnated $Pt/Al_2O_3$ with the exception that the solution contained $H_2PtCl_6 \cdot 6H_2O$ and $H_2TeO_4 \cdot 2H_2O$.

c. $PtSb/Al_2O_3$

$PtSb/Al_2O_3$ catalyst was prepared by the coimpregnation method as described above except that the solution contained $H_2PtCl_6 \cdot 6H_2O$ and $SbCl_3$. A minimum amount of concentrated HCl was added dropwise to the coimpregnation solution in order to dissolve all the $SbCl_3$ solids.

## 2. Gross Chemical Analysis

Only ion-exchanged $Pt/Al_2O_3$ and vapor deposited $PtTe/Al_2O_3$ catalysts were thoroughly examined for the metal content with the atomic absorption spectrophotometer. The metal content of the (co)impregnated catalysts was taken to be the calculated amount of the metal(s) in the (co)impregnation solution. However, the Pt content of some of the (co)impregnated catalysts was also examined for the purpose of testing the efficiency of extracting the noble metal from the support using aqua regia.

### a. Determination of Pt Content

Standard 100 ppm platinum solution was prepared by dissolving $PtCl_2$ in deionized water with stirring. Concentrated $NH_4OH$ was added dropwise until all the $PtCl_2$ was dissolved. Some of this solution was diluted to 50 ppm and 25 ppm with deionized water. The calibration curve for absorbance vs. concentration was then prepared using these three standard solutions.

The platinum content of the catalysts was determined using two methods. The first method involved the measurement of residual Pt in the filtrate which remained after catalyst preparation. The amount of platinum remaining in the filtrate solution allowed the

calculation of the amount of platinum which had been successfully ion-exchanged via difference. For the second method, platinum was extracted from the catalyst and measured directly. 0.1 g of the catalyst was ground and placed in a 50 cc pyrex beaker, to which 10 cc of aqua regia was added. The mixture was evaporated to dryness on a hot plate at 95-100°C. The aqua regia treatment was repeated three times. 25 cc of deionized water was then stirred into the dried sample to dissolve all soluble material. Insoluble material was filtered out. The metal content of the catalyst was then determined by atomic absorption.

b. Determination of Te Content

Standard solutions, containing 50, 25, and 12.5 ppm of tellurium, were prepared by dissolving $TeO_2 \cdot 2H_2O$ in deionized water. Tellurium was also extracted from the catalysts using aqua regia as above.

3. Reducibility of Telluric Acid

Approximately 30 mg of $H_2TeO_4 \cdot 2H_2O$ was loaded into the sample holder of the thermogravimetric analyzer (TGA). The temperature of the sample was then increased from 20°C to 500°C at a ramp rate of 10°C/min with flowing helium. This step removed all the water of

crystallization. The sample was then cooled to approximately 20°C. After purging the system with hydrogen, the temperature was raised from 20°C to 400°C at a ramp rate of 10°C/min in hydrogen. The reduction was allowed to occur overnight. The sample weight loss during these processes was recorded by the data acquisition system.

**4. Chemisorption of $H_2$ and CO**

Chemisorption capacities of all catalysts were determined with hydrogen and carbon monoxide using the static volumetric adsorption apparatus. The adsorption isotherms were obtained at 25°C and pressures ranging from 0.1 to 100 torr. Typically the experiment for obtaining the hydrogen chemisorption isotherm was carried out as follows.

First, the catalyst was reduced with flowing hydrogen at 400°C for 4 hr, and then evacuated ($\approx 10^{-6}$ torr) at the same temperature for 2 hr. It was then cooled to the adsorption temperature (ambient).

A known amount of hydrogen was admitted to the adsorption cell. After equilibrium was reached, the amount of hydrogen remaining in the gas phase was subtracted from the amount admitted to give the amount adsorbed, then another known amount of $H_2$ was added to

the cell and the process repeated. In this manner, a hydrogen chemisorption isotherm was constructed.

Langmuir-type isotherms were obtained when hydrogen was used as the adsorbate. However, when carbon monoxide was used, the weakly bound fraction on the support was apparent. Therefore, a double adsorption isotherm method was required to take into account the weakly bound fraction [Sinfelt et al., 1972]. After monolayer coverage was obtained, the catalyst was evacuated to remove the weakly bound fraction. The adsorption isotherm for the weakly bound fraction was then constructed by repeating the adsorption process. The difference between the total chemisorption isotherm and the weakly bound chemisorption isotherm yielded the strongly bound chemisorption isotherm which could then be used to calculate the metallic dispersion.

**5. Reaction Studies**

Before each reaction experiment, 20 to 200 mg of the catalyst was placed in the reactor, and was pretreated with the following procedure. The catalyst temperature was slowly raised to 120°C and evacuated under dynamic vacuum for 2 hr. The temperature was then slowly increased to 400°C and the catalyst was evacuated for an additional hour. This heating process was required to

remove the surface water on the support. The recirculation system was then filled with 400 torr hydrogen, and helium to 800 torr. The reduction process was conducted for at least 15 hr with a liquid nitrogen trap downstream of the reactor.

The reactor was cooled to the reaction temperature and bypassed. After removing the liquid nitrogen trap, the system was evacuated for 30 min while the catalyst was still blanketed with the pretreatment mixture of hydrogen and helium. Hydrocarbon reactant was then introduced into the system and its pressure monitored with a diaphragm pressure gauge as described previously. It was then condensed in the liquid nitrogen trap and hydrogen was then admitted to the system from the storage flasks. The hydrogen to hydrocarbon molar ratio was always kept at 17. The system was then filled with helium to 800 torr. The admission of helium improves heat transfer in the catalyst bed and assures minimal oxygen contamination by atmospheric leakage into the system. After the removal of the liquid nitrogen trap, the gas mixture was allowed to circulate for 15 min. A sample was injected into the GC prior to the admission of the gas mixture to the reactor. The partial pressure of hydrogen measured by GC was usually about 10% higher than that recorded by the diaphragm pressure gauge,

since a portion of the system was cooled by the liquid nitrogen trap at the time hydrogen was introduced.

The reactant was then admitted to the reactor establishing t=0. The temperature of the catalyst stabilized within one to two min, with a maximum offset of 4°C when the reactant mixture was first admitted. Reaction products were analyzed by GC periodically. After reaching a desirable conversion of the reactant, the hydrocarbons were collected by condensation in the liquid nitrogen trap. The reactor, which was still in the remaining hydrogen/helium atmosphere, was then bypassed and if no further analyses for the products were required, the liquid nitrogen was removed and the system was evacuated.

On the other hand, if subsequent product analysis (such as GC-MS and NMR) was to be performed, only hydrogen and helium were evacuated while the hydrocarbons were kept in the liquid nitrogen trap. A glass bulb was connected to the system using a 12/30 ground glass joint and evacuated. The hydrocarbons were then heated with a beaker of hot water or heat gun and collected in the glass bulb with a liquid nitrogen trap. The reaction products could be injected into the GC-MS for product identification. For $^{13}C$-NMR analyses, samples were separated using preparative scale gas

chromatography then dissolved in $CDCl_3$ (deuterated chloroform) in a 5 mm NMR sample tube.

The system was then filled with 400 torr hydrogen and 400 torr helium, and the catalyst was re-activated at 400°C overnight before the next test reaction.

### 6. $^{13}C$ Labeled Hydrocarbon Reactions

The contribution of cyclic and bond shift mechanisms for $C_6$ isomerization reactions is normally determined by studying the reactions of 2-methylpentane (2-$^{13}C$) and 2-methylpentane (4-$^{13}C$) and the product distribution of the $^{13}C$-labeled species has been determined by analyzing the mass spectral fragmentation pattern of the products [Corolleur et al., 1972; Dartigues et al., 1976; Chambellan et al., 1977]. In this work, slight modifications were made. 2-methylpentane (5-$^{13}C$) was substituted for 2-methylpentane (4-$^{13}C$) because the reagents required to make the 5-$^{13}C$ compound were more readily available and because there is little difference in the ultimate information which can be extracted from the data. Also, Fourier transform $^{13}C$-NMR was used for analytical purposes. The advantages of $^{13}C$-NMR over MS includes easier spectrum interpretation and NMR does not require that all possible labeled molecules be synthesized to serve as reference compounds. However,

$^{13}$C-NMR requires a larger sample size. The details of the syntheses of 2-methylpentane (2-$^{13}$C) and 2-methylpentane (5-$^{13}$C) are given later in this chapter.

The catalyst pretreatment and reaction procedures were conducted in the usual manner. The hydrocarbon products were collected in a glass bulb after 5 to 15% conversion of 2-methylpentane and were separated by preparative scale GC. For the 2-methylpentane (2-$^{13}$C) reaction, the C6 hydrocarbon fraction, including 2-methylpentane, 3-methylpentane, n-hexane and methylcyclopentane, was recovered in the prep-GC procedure and transferred into an NMR tube containing $CDCl_3$. However, for the 2-methylpentane (5-$^{13}$C) reaction, n-hexane and methylcyclopentane were separated from 2-methylpentane and 3-methylpentane and analyzed individually since the chemical shift corresponding to the 2 position in n-hexane could not be resolved from the 5 position of 2-methylpentane. Fractions other than $C_6$ were discarded.

Figure II-10 shows a typical $^{13}$C-NMR spectrum of the reaction products, including 2-methylpentane, 3-methylpentane, n-hexane and methylcyclopentane, for 2-methylpentane (2-$^{13}$C) isomerization on $Pt/Al_2O_3$ at 290°C. The assignment of the bands is somewhat complex and will be discussed in the result section.

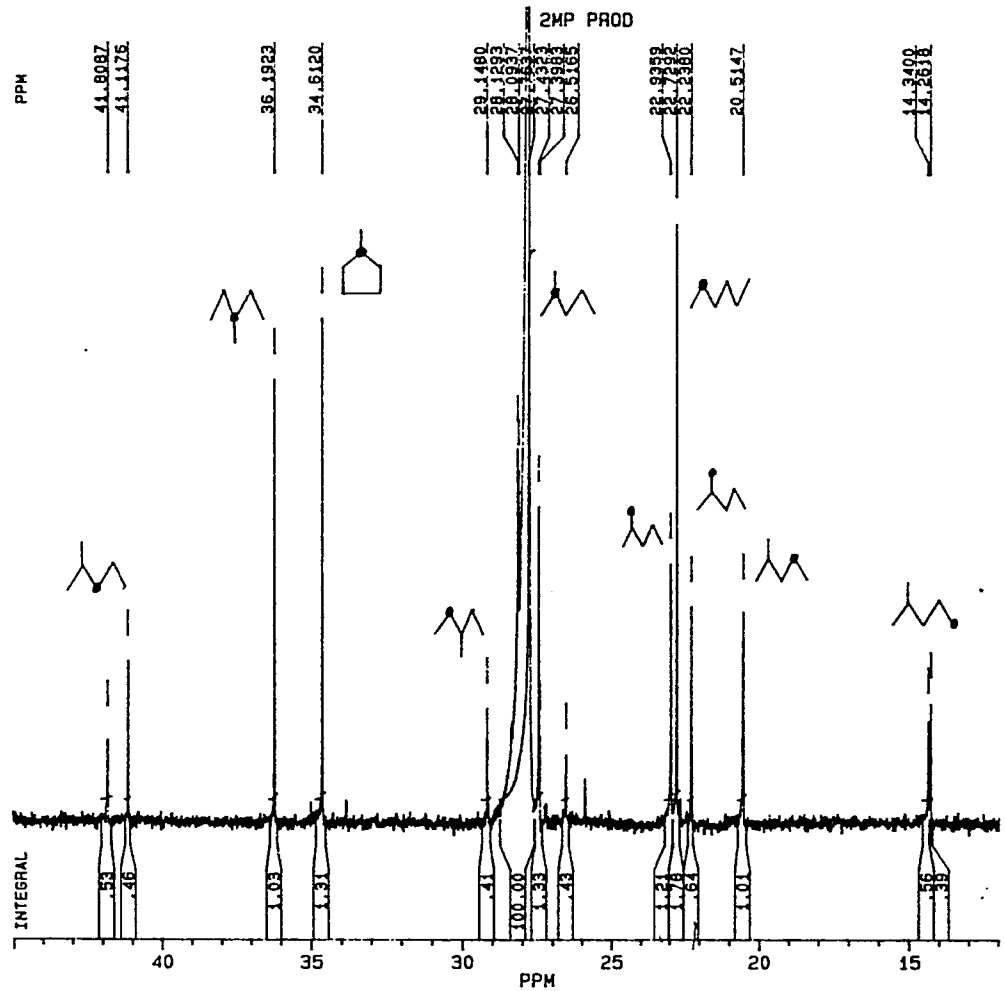


Figure II-10. $^{13}C$ NMR Spectrum of Reaction Products from 2-MP (2-$^{13}C$) Isomerization.

## 7. Syntheses of Labeled 2-methylpentane

Labeled 2-methylpentane (2-$^{13}$C) and 2-methylpentane (5-$^{13}$C) were prepared by first making the corresponding alcohols via Grignard synthesis followed by dehydration and hydrogenation (Figure II-11). Detailed procedures follow.

### a. 2-methylpentane (2-$^{13}$C)

0.45 g (0.018 mole) magnesium was placed in a 25-cc round-bottomed flask with three 14/20 THREAD-TITE outer joints and a 2-mm teflon stopcock. Two of the joints were fitted with an efficient stirrer and a dropping funnel, pressure equalizing (Figure II-12). The flask was flushed with nitrogen and heated with a heat gun to remove atomspheric moisture. This step is essential since water is acidic enough to decompose a Grignard reagent. After cooling, the flask was filled with 3 cc anhydrous diethyl ether. 7 cc of a mixture of 0.018 moles of n-propyl bromide and 5.4 cc of dry diethyl ether was placed in the dropping funnel. The reactor was filled with nitrogen, and a plastic balloon was used as a stopper for the dropping funnel. The ballon, which allowed a flexible reactor volume, kept the reactor under 1 atm pressure. Approximately 2 cc of the mixture was added directly onto the magnesium. After the

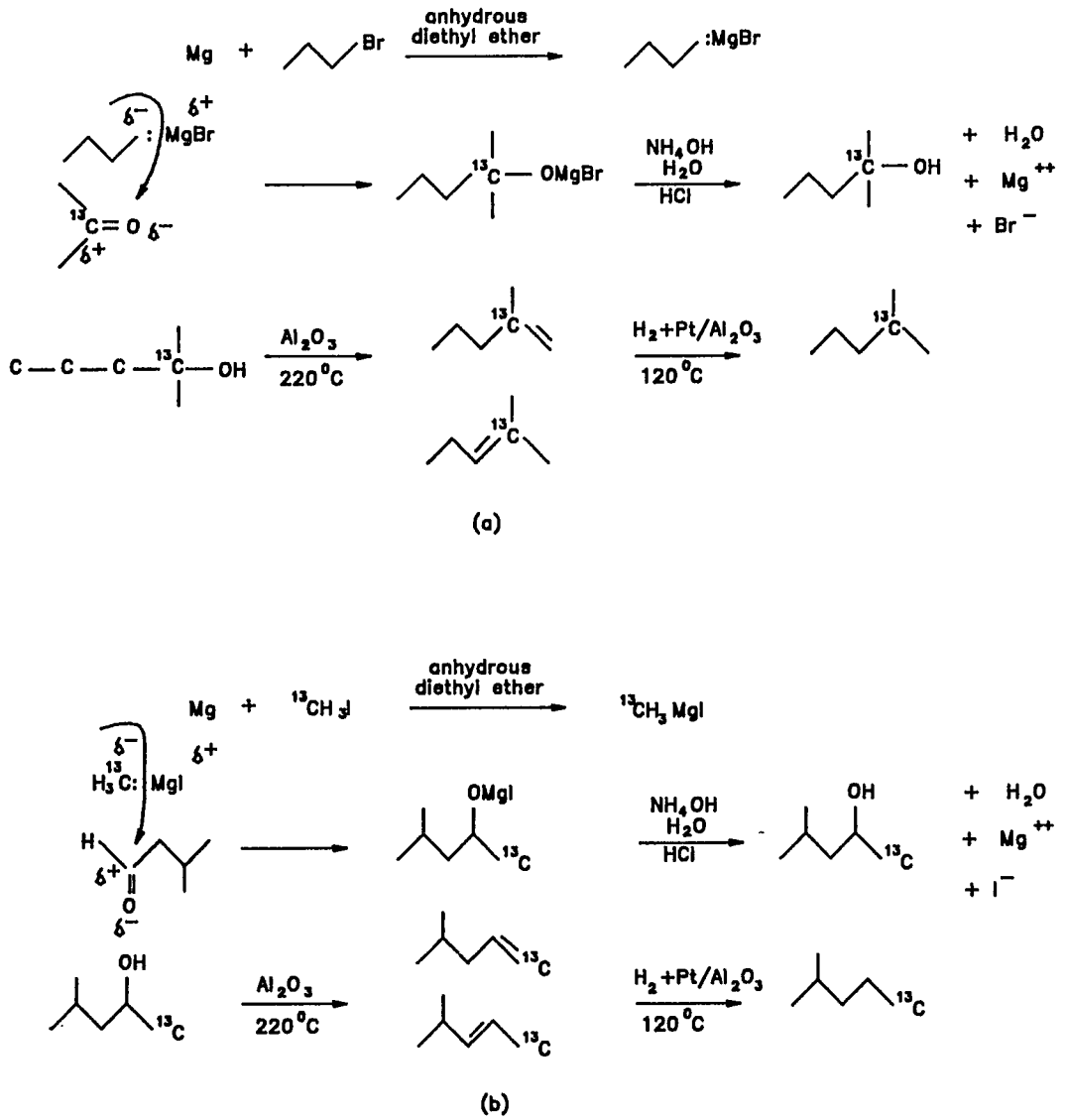


Figure II–11. Syntheses of (a) 2–methylpentane (2– $^{13}C$) and (b) 2–methylpentane (5– $^{13}C$).

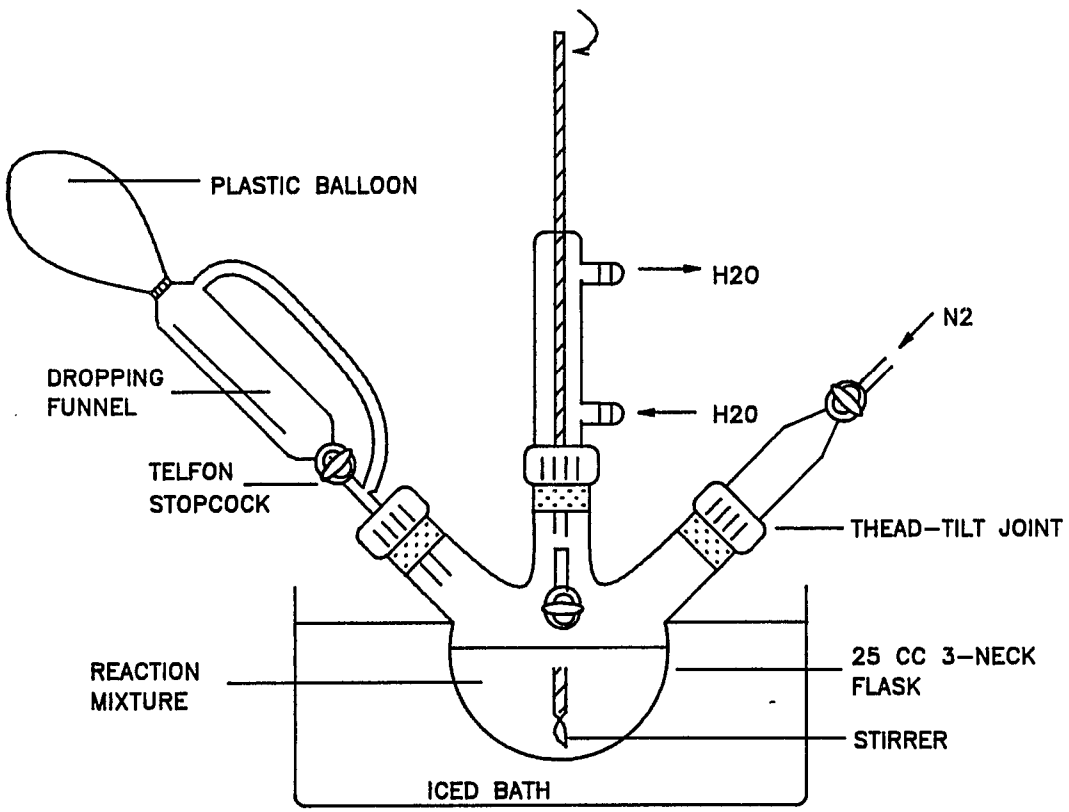


Figure II–12. Apparatus for Carbon–13 Labeled 2–Methylpentanol Synthesis.

reaction started and progressed for a few minutes, the rest of the mixture was added dropwise to the reactor which was cooled with an ice bath and mechanically stirred. After all of the halide-ether solution had been added, the stirring was allowed to continue for an hour at ambient temperature. A solution of 1g (0.017 mole) acetone-2-$^{13}$C and 3 cc diethyl ether was then placed in the dropping funnel and the flask was cooled with an ice bath. The acetone solution was added at a rate not faster than one drop every second. After all the acetone had been added, the cooling bath was removed, and the mixture was allowed to stay at room temperature with stirring for 2 hr or longer.

The ether solution was poured slowly, with stirring, onto a mixture of 1.1 g ammonium chloride and 6 g of crushed ice. Ammonia escaped and an emulsion of magnesium oxychloride was separated, which was clarified by adding dilute hydrochloric acid. After neutralizing the liquid with sodium hydroxide, the mixture was transferred to a separatory funnel. The organic layer (upper layer) was collected and the aqueous layer was extracted with 15 cc diethyl ether. The crude carbinol 2-methylpentanol (2-$^{13}$C) was obtained by fractional distillation (Figure II-13) of the ether solution in the temperature range of 115-124°C.

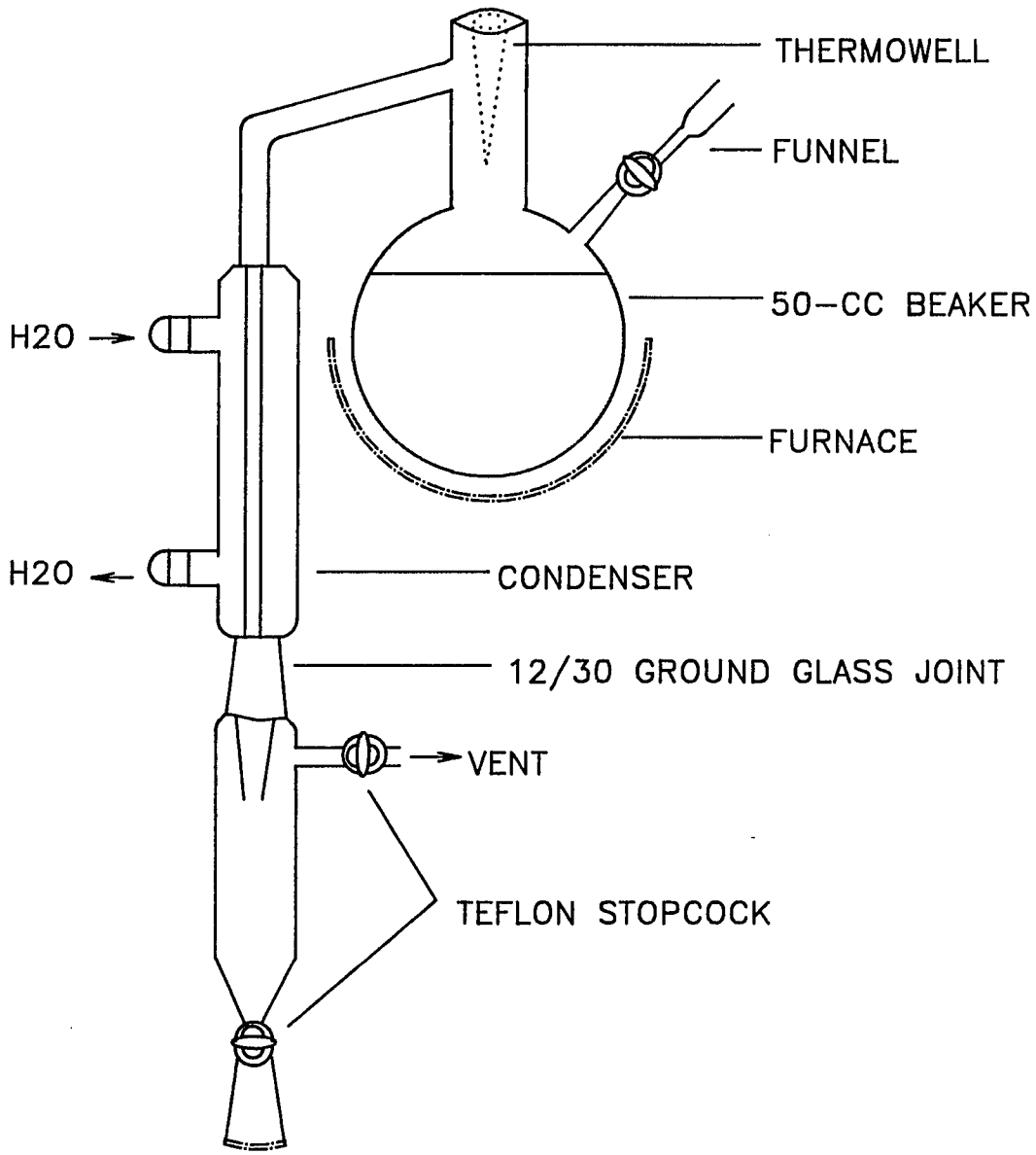


Figure II–13. Fractional Distillation Apparatus.

The alcohol was dehydrated and hydrogenated in the recirculation batch reactor in portions. Approximately 30 torr of the alcohol was mixed with 750 torr He, as a diluent, and reacted on 0.5 g alumina at 220°C for 3 hr. The resulting olefins, 2-methyl-4-pentene and 2-methyl-3-pentene, confirmed by GC-MS, were then hydrogenated using 0.1 g $Pt/Al_2O_3$ under one atmosphere of hydrogen at 120°C for 1 hr. The purification of the final product, 2-methylpentane (2-$^{13}$C) was done by prep-GC.

b. 2-methylpentane (5-$^{13}$C)

The preparation procedure for 2-methylpentane (5-$^{13}$C) was the same as that for 2-methylpentane (2-$^{13}$C) except that:

1) A small crystal of iodine was added with the magnesium to initiate the reaction.

2) The 2-methylpentanol (5-$^{13}$C) was prepared by reacting the Grignard reagent, $^{13}CH_3MgI$, with 0.022 mol isovaleraldehyde. The Grignard reagent was prepared from 0.51 g (0.021 mole) magnesium and 3 g (0.021 mole) $^{13}CH_3I$.

3) The distillate was collected in the temperature range of 120-138°C during the fractional distillation step.

4) The alcohol synthesized had a very low vapor pressure, ≈10 torr at room temperature, and therefore was dehydrated in smaller portions.

8. Isotopic Dilution Method and FTIR

Isotopic mixtures of $^{12}CO$ and $^{13}CO$ were prepared in the gas adsorption system. A 30 cc glass bulb and a flask containing $^{13}CO$ were connected to the two inlets of the system. After evacuation, the glass bulb was filled with the desired amount of $^{13}CO$. It was then isolated, and the rest of the system evacuated. $^{12}CO$, which was previously stored in a 5-liter flask, was then slowly admitted to the glass bulb until the gas mixture reached the desired composition. In this manner, three isotopic mixtures of ≈24, 37, and 68% $^{12}CO$ were prepared. These mixtures together with the pure $^{12}CO$ in the 5-liter flask were used as adsorbates to perform the isotopic dilution experiments.

The catalyst wafer for IR analysis was prepared by pelletizing 20 mg of the finely ground catalysts into a disk 13 mm in diameter at 15,000 psi using a hydraulic press. A minimum amount of fine graphite was used as a lubricant for the die. The wafer was mounted in the sample holder which was subsequently slid to the center of the IR cell, to which the gas adsorption system was

connected. The wafer was reduced with flowing hydrogen at 400°C for at least 13 hr, evacuated at the same temperature for 3 hr, and cooled to room temperature under dynamic vacuum. A background spectrum was taken, then 20 torr of the gas mixture of $^{12}CO$ and $^{13}CO$ was admitted. After 15 min, the cell was evacuated to a pressure of approximately 0.1 torr. The IR spectrum was recorded and the background spectrum was subtracted. These procedures were determined based upon the reproducibility of the data.

## III. Results

### A. Catalysts

Table III-1 lists the catalysts prepared and studied in this work. The nominal values of metal loading correspond to the amount of metal which was intended to be loaded onto the catalyst. 70 to 80% of the platinum was successfully exchanged in ion-exchanged $Pt/Al_2O_3$ catalysts. Atomic absorption analysis on the filtrate solution containing the unexchanged platinum and on the solution obtained from aqua regia extraction agree quite well. The tellurium content for the vapor-deposited $PtTe/Al_2O_3$, measured after the test reactions, indicated that only a fraction of the original tellurium was successfully deposited. The platinum content for the (co)impregnated catalysts, determined by atomic absorption analysis, was within 10% of the nominal value in all cases This provided evidence that the aqua regia dissolution procedure was efficient and that the uncertainty in atomic absorption analysis was less than ±10%. The chlorine content analysis was performed at Exxon Research and Development Laboratories using X-ray fluorescence. Only three catalysts, $Pt/Al_2O_3$, $PtTe/Al_2O_3$, and $PtSb/Al_2O_3$, prepared by the (co)impregnation method, were examined. The measurements showed that

Table III-1.
Catalysts

| Catalysts | Prep. Method | Pt (wt%) | | Te, Sb (wt%) | | [a]Cl (ppm) |
|---|---|---|---|---|---|---|
| | | Nominal | AA | Nominal | AA | |
| $Pt/Al_2O_3$ | Ion Exchange | 1.0 | 0.70 | - | - | - |
| $Pt/Al_2O_3$ | Ion Exchange | 1.0 | 0.82 | - | - | - |
| $Pt/Al_2O_3$ | Impregnation | 1.0 | 0.95 | - | - | 80 |
| $PtTe/Al_2O_3$ | Vapor Dep. (He) | 1.0 | 0.70 | 1.0 | 0.24 | - |
| $PtTe/Al_2O_3$ | Vapor Dep. (He) | 1.0 | 0.70 | 0.2 | 0.16 | - |
| $PtTe/Al_2O_3$ | Vapor Dep. ($H_2$) | 1.0 | 0.70 | 1.0 | 0.25 | - |
| $PtTe/Al_2O_3$ | Vapor Dep. (Re[b]) | 1.0 | 0.70 | 1.0 | 0.26 | - |
| $PtTe/Al_2O_3$ | Vapor Dep. (Re[b]) | 1.0 | 0.70 | 0.2 | 0.09 | - |
| $PtTe/Al_2O_3$ | Vapor Dep. (Re[b]) | 1.0 | 0.82 | 1.0 | 0.22 | - |
| $PtTe/Al_2O_3$ | Coimpregnation | 1.0 | 0.92 | 0.04 | - | 50 |
| $PtTe/Al_2O_3$ | Coimpregnation | 1.0 | - | 0.15 | - | - |
| $PtTe/Al_2O_3$ | Coimpregnation | 1.0 | 1.04 | 0.50 | - | - |
| $PtTe/Al_2O_3$ | Coimpregnation | 1.0 | 1.10 | 0.80 | - | - |
| $PtSb/Al_2O_3$ | Coimpregnation | 1.1 | - | 0.10 | - | - |
| $PtSb/Al_2O_3$ | Coimpregnation | 1.1 | - | 0.28 | - | - |
| $PtSb/Al_2O_3$ | Coimpregnation | 1.1 | - | 0.47 | - | - |
| $PtSb/Al_2O_3$ | Coimpregnation | 1.1 | - | 0.67 | - | 130 |
| $PtSb/Al_2O_3$ | Coimpregnation | 1.1 | - | 0.85 | - | - |

[a] : measured by X-ray fluorescence.

[b] : A "reforming" gas mixture consisting of 25 torr n-hexane, 440 torr $H_2$, and He to 800 torr.

insignificant amounts of chlorine were present on the catalyst surface as anticipated.

The results of temperature programmed reduction experiments showed that $H_2TeO_4 \cdot 2H_2O$ was reduced to the zero valent tellurium in flowing hydrogen at 400°C after a time period of about 12 hr, though this time period was impossible to measure accurately because elemental tellurium also vaporizes slowly and is observed as a mirror on the cool sections of the quartz enclosure. The low metal content of the supported catalyst prevented us from obtaining similar results on the actual catalyst. However, reduction of the actual catalyst should require less time as the surface area of $H_2TeO_4 \cdot 2H_2O$ is greatly enhanced upon dispersion on the $Al_2O_3$ support.

**B. Chemisorption of $H_2$ and CO**

The accessible platinum metal fractions of all the catalysts were determined by chemisorption of hydrogen and carbon monoxide. Preliminary studies showed that the support, $Te/Al_2O_3$, and $Sb/Al_2O_3$ had no or insignificant adsorption capacities. The platinum metallic dispersion, which is defined as the ratio of the number of surface platinum atoms to the total platinum atoms present in the metal crystallites, was calculated by:

$$Pt\ \%\ dispersion = \frac{no.\ surface\ Pt\ atoms}{total\ no.\ of\ Pt\ atoms}$$

$$= \frac{no.\ H\ (CO)\ atoms\ adsorbed\ /\ surface\ adsorption\ stoichiometry}{total\ no.\ of\ Pt\ atoms}$$

The surface adsorption stoichiometry was taken as H/Pt = 1, CO/Pt = 1.15 for $Pt/Al_2O_3$, and CO/Pt = 1.0 for $PtTe/Al_2O_3$ and $PtSb/Al_2O_3$ after Spenadel and Boudart, [1960], Dorling et al. [1968], and Freel et al. [1972].

Figures III-1 and III-2 give typical chemisorption isotherms of hydrogen and carbon monoxide at 25°C on a $PtTe/Al_2O_3$ catalyst containing 1 wt% platinum, Te/Pt atomic ratio = 0.23. The dashed lines in the figure represent the amounts of strongly adsorbed hydrogen and carbon monoxide on this catalyst.

The results of hydrogen and carbon monoxide chemisorption were similar for the coimpregnated $PtTe/Al_2O_3$ and $PtSb/Al_2O_3$. These results are given in Figures III-3 and III-4. The amounts adsorbed decrease with increasing post-transition metal content; a drastic fall is evident upon initial addition of tellurium or antimony. Tellurium inhibits the adsorption more strongly than does antimony.

When the same experiments were performed on $PtTe/Al_2O_3$ catalysts prepared by vapor deposition,

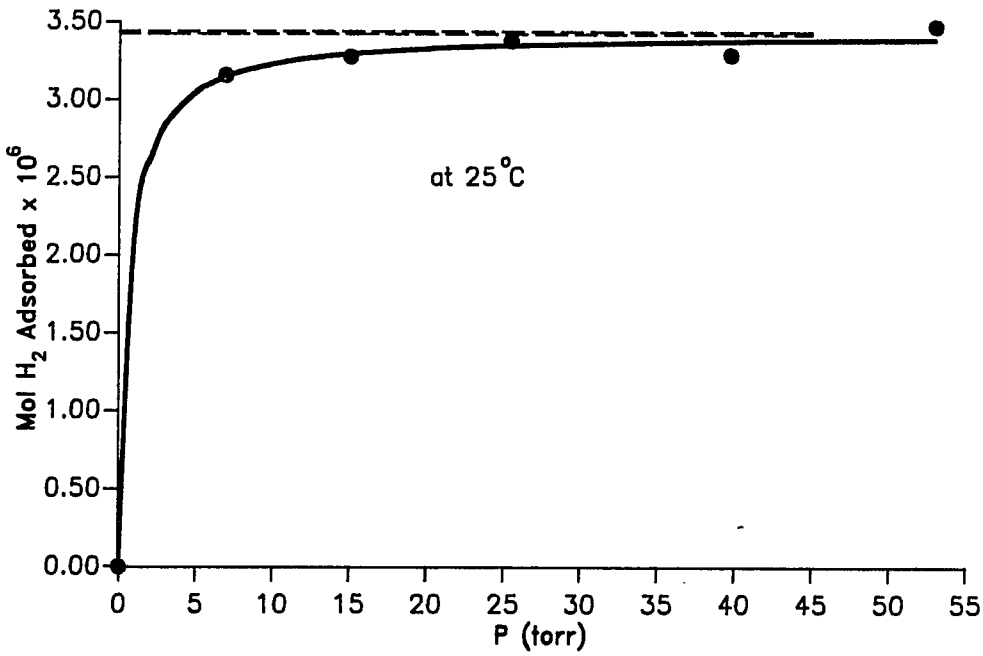


Figure III–1. Adsorption Isotherm of Hydrogen on Coimpregnated $PtTe/Al_2O_3$ (Te/Pt=0.23).

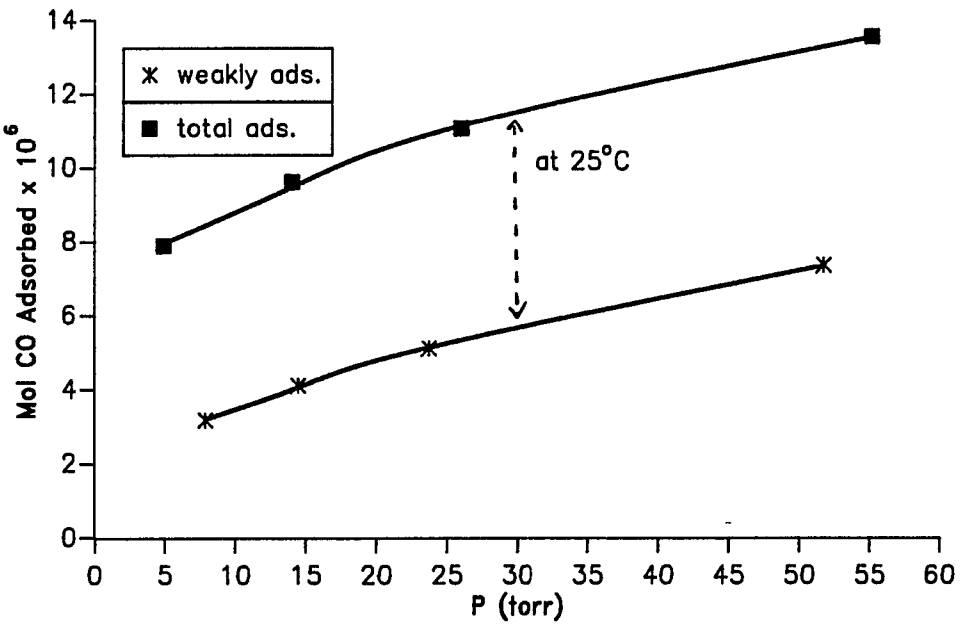


**Figure III–2.Isotherms for Total Carbon Monoxide Adsorption and Weakly Adsorbed Carbon Monoxide on Coimpregnated $PtTe/Al_2O_3$ (Te/Pt=0.23).**

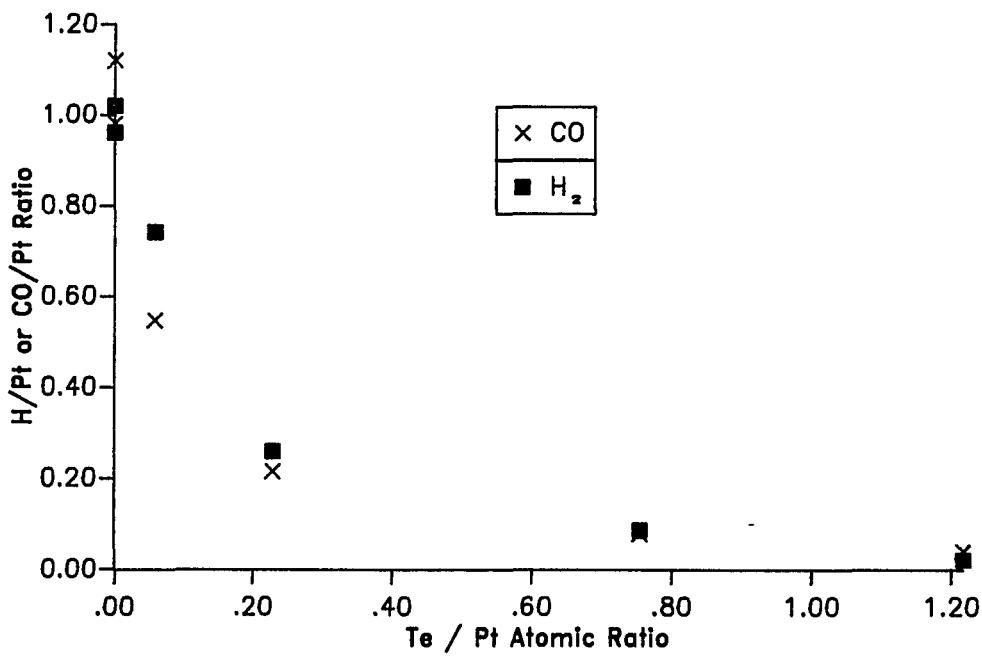


Figure III–3. Chemisorption of H2 and CO on Coimpregnated $PtTe/Al_2O_3$ Catalysts, measured at 25°C.

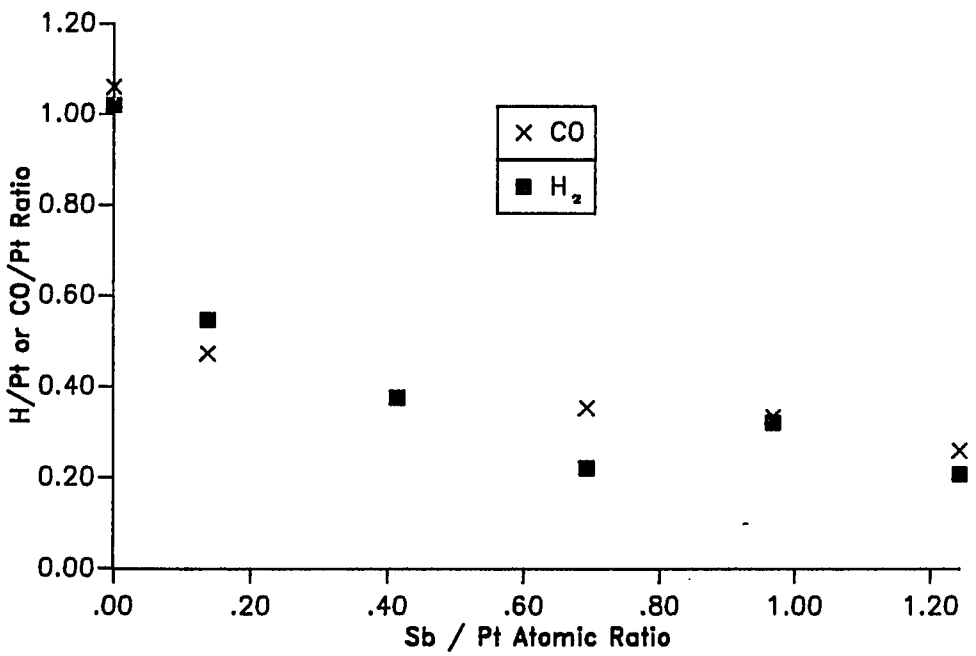


Figure III–4. Chemisorption of H2 and CO on Coimpregnated $PtSb/Al_2O_3$ Catalysts, measured at 25°C.

insignificant amounts of hydrogen were adsorbed. The carbon monoxide uptake, however, was approximately 20 to 30% of that on $Pt/Al_2O_3$. Table III-2 provides the adsorption data in terms of H/Pt and CO/Pt ratios. The PtTe bimetallic clusters formed using coimpregnation and vapor deposition methods are therefore different. This is further demonstrated by the catalytic results, reported below.

## C. Kinetic Measurements

### 1. Blank Runs

0.2 g $Al_2O_3$, which was washed with 5% $NH_4OH$ to simulate actual catalysts, was loaded into the reactor. The test reactions were carried out at 400°C using 25 torr hydrocarbon (n-hexane, methylcyclopentane, cyclohexane, or 1-hexene), 440 torr hydrogen, and helium to atmospheric pressure. No product formation was observed for the n-hexane, methylcyclopentane, or cyclohexane reactions after 2 hr on stream. Carbon skeletal isomerization of 1-hexene was less than 5% after 2 hr on stream, although 1-hexene was readily converted to double-bond isomers (2- and 3-hexene). Similar results were obtained using $Sb/Al_2O_3$ catalysts. Tellurium is not stable on $Al_2O_3$ at 400°C; therefore, $Te/Al_2O_3$ could not

Table III-2.
$H_2$ and CO Adsorption Data for Vapor-deposited $PtTe/Al_2O_3$, measured at 25°C.

| Catalysts | Prep. Method | wt% Pt | Te/Pt[a] | H/Pt | CO/Pt |
|---|---|---|---|---|---|
| $Pt/Al_2O_3$ | Ion-exchange | 0.70 | 0 | 0.85-0.97 | 0.92 |
| $Pt/Al_2O_3$ | Ion-exchange | 0.82 | 0 | 0.92 | 0.87 |
| $PtTe/Al_2O_3$ | Vapor Dep.(Re[b]) | 0.82 | 0.33 | ≈0 | 0.18 |
| $PtTe/Al_2O_3$ | Vapor Dep. (He) | 0.70 | 0.37 | ≈0 | 0.22 |
| $PtTe/Al_2O_3$ | Vapor Dep. (He) | 0.70 | 0.24 | ≈0 | - |
| $PtTe/Al_2O_3$ | Vapor Dep. ($H_2$) | 0.70 | 0.38 | ≈0 | 0.25 |
| $PtTe/Al_2O_3$ | Vapor Dep. (Re[b]) | 0.70 | 0.40 | ≈0 | - |
| $PtTe/Al_2O_3$ | Vapor Dep. (Re[b]) | 0.70 | 0.14 | ≈0 | 0.27 |

[a] : Atomic ratio.

[b] : A "reforming" gas mixture consisting of 25 torr n-hexane, 440 torr $H_2$, and He to 800 torr.

be tested. These results suggest that the global activities for all the catalysts studied in this work can be attributed to the platinum metal function.

## 2. Internal Mass Diffusion Limitations

Two approaches were used for determining the importance of internal mass transfer limitations on the conversion rates of n-hexane and cyclohexane reactions. The first approach compared the observed initial rates over two $Pt/Al_2O_3$ catalysts with particle sizes of 20/40 and 40/60 mesh. Figures III-5 and III-6 show the data for the rate of disappearance of n-hexane at 400°C and cyclohexane at 300°C, respectively. The respective relative errors of the initial rates corresponding to the two different particle size catalysts were 4% and 7%.

The second approach calculated the effectiveness factors for the n-hexane and cyclohexane reactions on $Pt/Al_2O_3$ under the same reaction conditions, assuming that each reaction was first order in n-hexane or cyclohexane. This is generally true for reforming reactions with high hydrogen to hydrocarbon ratio [Christoffel and Paál, 1982; Hosten and Froment, 1971; Voorhies, and Bryant, 1968]. The bulk gas diffusivities for both reactions were estimated by the Chapman-Enskog

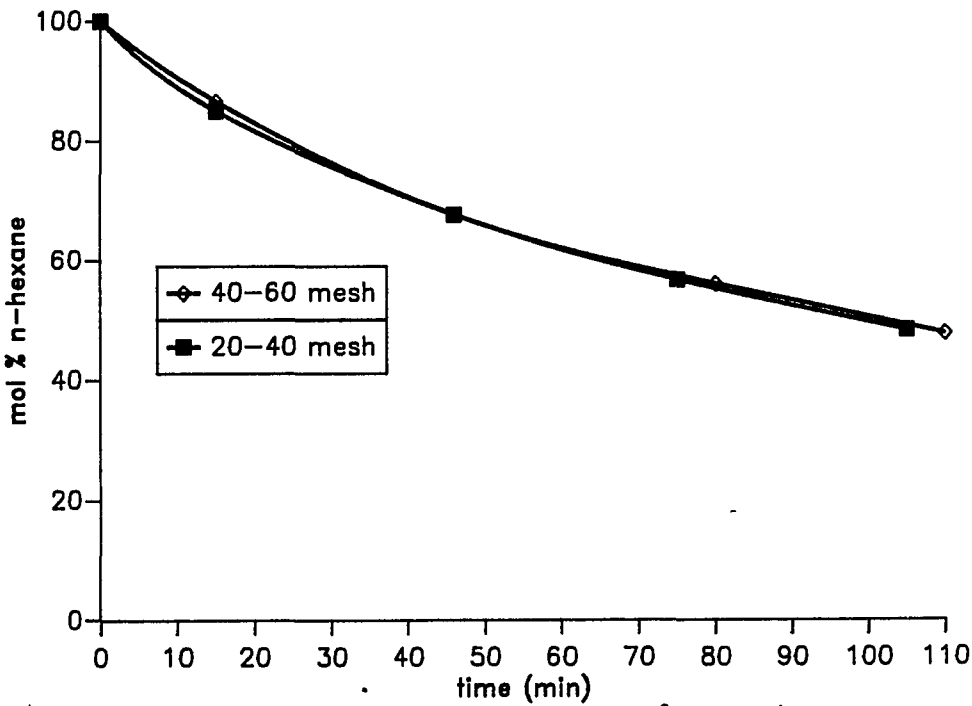


Figure III-5. n-Hexane Conversion at 400°C on $Pt/Al_2O_3$.

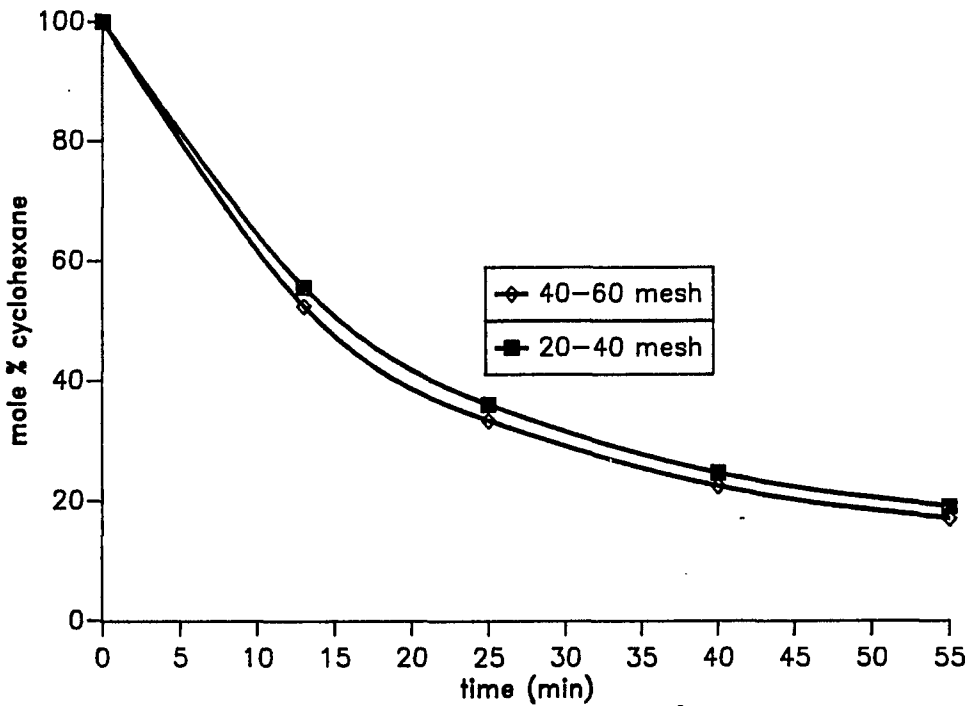


Figure III–6. Cyclohexane Conversion at 300°C on $Pt/Al_2O_3$.

equation [Bird, Stewart, and Lightfoot, 1960], and were found to be unimportant relative to the Knudsen diffusivities since the pore size of the $Al_2O_3$ is relatively small. The effectiveness factor for the n-hexane reaction at 400°C was found to be 0.97. However, a lower value of 0.88 was obtained for the cyclohexane reaction at 300°C. Detailed calculations are given in Appendix B.

Keeping in mind that the relative errors for obtaining the initial activities based on the initial slopes of the accumulation curves were no better than ±15%, we conclude that pore diffusion limitations are not significant. This conclusion can be applied to all the bimetallic catalysts, since they have considerably lower overall activity than $Pt/Al_2O_3$ and essentially identical physical properties.

### 3. n-Hexane Reaction

For the n-hexane reaction, the % yield to a particular product was defined as the mole percent of n-hexane converted to that product and corresponds to a carbon yield:

$$Y_i = \frac{iP_i}{\sum_{i=1}^{6} iP_i} x\,100\%$$

where i = number of carbon atoms in the molecule

$Y_i$ = mol percent of n-hexane converted to species $C_i$

$P_i$ = partial pressure of $C_i$ in the reaction mixture

For the sake of simplicity, the results using different catalysts were interpreted based on 30% conversion of n-hexane unless otherwise specified. The products were grouped as aromatic (benzene), isoparaffins [2- and 3-methylpentane (MP)], methylcyclopentane (MCP), and cracking products (the C1-C5 paraffins). Complete product distribution data for all the catalysts can be found in Appendix C. $Pt/Al_2O_3$ catalysts, prepared by ion-exchange and impregnation methods, were used for the comparisons with vapor-deposited $PtTe/Al_2O_3$ and coimpregnated catalysts, respectively. The initial activities for the isomerization and cracking reactions of the catalysts were determined by the initial slopes of the product vs. time accumulation curves. It was assumed that the active sites available for the reactions are those which can adsorb hydrogen or carbon monoxide; therefore, the catalytic activities are reported as moles hydrocarbon converted per time per mole surface Pt atom.

This calculation, based on the initial slopes of the accumulation curves, is no better than ±15%, but it provides data for rudimentary comparisons of rate and selectivity.

a. $Pt/Al_2O_3$

Table III-3 contains the product distributions for 0.1 g ion-exchanged $Pt/Al_2O_3$ at 30% conversion of n-hexane. The data given in run 1 were obtained by the interpolation of data between 20.7 and 49.0% conversion of n-hexane. The product distribution for run 2 was obtained after the reaction had proceeded 20 min. The reproducibilities of the data are evident.

Similar data are also provided in Table III-3 for impregnated $Pt/Al_2O_3$. Impregnated $Pt/Al_2O_3$ displays a higher yield to benzene but a lower yield to branched isomers, when compared to ion-exchanged $Pt/Al_2O_3$. This is possibly caused by a different particle size distribution and support-metal interactions, which are sensitive to the catalyst preparation techniques.

b. Vapor-Deposited $PtTe/Al_2O_3$

Table III-3.
Product Distributions for n-Hexane Reaction at 400°C on $Pt/Al_2O_3$ Catalysts at 30% Conversion of n-Hexane.

| | 0.1g $Pt/Al_2O_3$ (Ion-exchange 0.7 wt% Pt) | | 0.02g $Pt/Al_2O_3$ (Impregnation, 1 wt% Pt) |
|---|---|---|---|
| | Run 1 | Run2 | |
| Time (min) | 20 | 20 | 43 |
| $C_1$ | 0.69 | 0.69 | 0.88 |
| $C_2$ | 1.01 | 0.99 | 1.25 |
| $C_3$ | 2.50 | 2.25 | 2.78 |
| i-$C_4$ | 0.14 | ≈0 | ≈0 |
| n-$C_4$ | 1.78 | 1.93 | 2.30 |
| i-$C_5$ | 0.38 | ≈0 | 0.22 |
| n-$C_5$ | 2.40 | 3.15 | 3.56 |
| | 8.90 | 9.01 | 10.99 |
| 2-MP | 7.37 | 7.16 | 4.60 |
| 3-MP | 4.63 | 4.45 | 2.62 |
| | 12.00 | 11.61 | 7.22 |
| MCP | 6.00 | 5.88 | 6.02 |
| Benzene | 3.10 | 2.82 | 5.77 |
| | 30.00 | 29.32 | 30.00 |

The deposited tellurium is not completely stable for the duration of the activation period and reaction experiments. A film of tellurium was visually observed on the downstream cold wall of the glass reactor. Therefore, we have more uncertainty in our results.

In order to determine the dependence of the catalytic behavior on tellurium content and method of deposition (using different carrier gases), each catalyst was subjected to several test reactions at the same conditions, 400°C and 25 torr initial pressure of n-hexane. Before each test reaction, the catalyst was activated with hydrogen for at least 12 hr. In Tables III-4 and III-5, the yields to hydrocracking and isomerization products for the different catalysts are compared based on 30% conversion of the reactant n-hexane. Typical product distributions obtained using $Pt/Al_2O_3$ and $PtTe/Al_2O_3$ are given in Table III-6. The yields reported in the tables are mole percent of reactant converted to products. As indicated in Tables III-4 to III-6, the addition of tellurium to $Pt/Al_2O_3$ generally increased the yield to isomerization products (2-methylpentane and 3-methylpentane) at the expense of both dehydrocylization and hydrocracking products. The overall activity also decreased by about one order of

Table III-4.

Yield % to Cracking Products, $PtTe/Al_2O_3$ (Vapor Deposition) [a]Catalysts at 400°C,

| | | | Yield % at 30% Conversion | | | | |
|---|---|---|---|---|---|---|---|
| Carrier Gas | Te/Pt | [b]time | [c]1st | 2nd | 3rd | 4th | 5th |
| He | 0.37 | 77 | 6.6 | 3.8 | 3.4 | 3.4 | 3.5 |
| He | 0.24 | 110 | 6.3 | 5.0 | 4.3 | 4.5 | - |
| $H_2$ | 0.38 | 38 | 8.1 | 4.2 | 4.7 | 5.2 | - |
| Re[d] | 0.40 | 325 | 3.0 | 3.1 | 3.4 | - | - |
| Re[d] | 0.14 | 350 | 3.0 | 3.4 | 4.5 | 5.2 | 5.6 |
| $H_2$+He | 0.00 | 20 | 8.9 | - | - | - | - |

[a] Catalysts, 0.1 g, 0.7 wt% Pt.

[b] Time to reach 30% conversion for the first test reaction, min.

[c] Test number.

[d] A "reforming" gas mixture consisting of 25 torr n-hexane, 440 torr $H_2$, and He to 800 torr.

Table III-5.

Yield % to 2MP + 3MP, $PtTe/Al_2O_3$ (Vapor Deposition)

[a]Catalysts at 400°C.

| | | | Yield % at 30% Conversion | | | | |
|---|---|---|---|---|---|---|---|
| Carrier Gas | Te/Pt | [b]time | [c]1st | 2nd | 3rd | 4th | 5th |
| He | 0.37 | 77 | 14.2 | 17.8 | 19.8 | 19.7 | 19.6 |
| He | 0.24 | 110 | 17.6 | 16.9 | 19.1 | 19.7 | - |
| $H_2$ | 0.38 | 38 | 11.1 | 15.8 | 14.7 | 15.2 | - |
| Re[d] | 0.40 | 325 | 18.5 | 18.1 | 18.1 | - | - |
| Re[d] | 0.14 | 350 | 21.9 | 19.1 | 18.7 | 15.6 | 15.3 |
| $H_2$+He | 0.00 | 20 | 12.0 | - | - | - | - |

[a] Catalsts, 0.1 g, 0.7 wt% Pt.

[b] Time to reach 30% conversion for the first test reaction, min.

[c] Test number.

[d] A "reforming" gas mixture consisting of 25 torr n-hexane, 440 torr $H_2$, and He to 800 torr.

Table III-6.

Product Yields, $Pt/Al_2O_3$ and $PtTe/Al_2O_3$ (Vapor Deposition) Catalysts at 400°C.

| | [a] $Pt/Al_2O_3$ | $PtTe/Al_2O_3$ [b] | |
|---|---|---|---|
| time (min) | 20 | 325 | 95 |
| C1 | 0.69 | ≈ 0.00 | ≈ 0.00 |
| C2 | 1.01 | 0.59 | 0.34 |
| C3 | 2.50 | 0.95 | 0.45 |
| i-C4 | 0.14 | 0.49 | ≈ 0.00 |
| n-C4 | 1.78 | 0.61 | 0.33 |
| i-C5 | 0.38 | ≈ 0.00 | ≈ 0.00 |
| n-C5 | 2.40 | 0.36 | ≈ 0.00 |
| ΣC1-C5 | 8.9 | 3.0 | 1.12 |
| i-C6 | 12.0 | 18.5 | 6.88 |
| MCP | 6.0 | 6.6 | 3.18 |
| benzene | 3.1 | 1.9 | 0.52 |
| % Conv. | 30.0 | 30.0 | 11.7 |

[a] 0.7 wt% Pt, catalyst was prepared by ion-exchange method.

[b] The carrier gas was a "reforming" mixture consisting of 25 torr n-hexane, 440 torr $H_2$, and He to 800 torr. Final Te/Pt atomic ratio was 0.40.

magnitude. These changes in product distribution took place only after the PtTe catalysts were exposed to a feed stream which included n-hexane at 400°C. The $PtTe/Al_2O_3$ catalysts which were prepared using a hydrogen or helium carrier gas initially exhibited higher yields to hydrocracking products (Table III-4); these yields decreased with the successive runs (in which the reactant included n-hexane) in the reforming reaction. The selectivity toward isomerization products eventually approached a steady value which was considerably higher than that of $Pt/Al_2O_3$ (Table III-5). However, when a feed stream containing n-hexane was used as the carrier gas for tellurium deposition, the $PtTe/Al_2O_3$ immediately displayed a high selectivity for isomerization products. The yield to hydrocracking products for these catalysts was the lowest among all those tested, but for those samples of low Te/Pt ratio (0.14), the yield to hydrocracking products increased in successive reactions. This activation phenomenon was not observed for the other catalysts of higher tellurium content, whose selectivities remained relatively constant. Finally, it is noted that the fragmentation pattern for hydrogenolysis products is also altered after alloying. $PtTe/Al_2O_3$

displays a clear preference for scission of internal C-C bonds instead of terminal cleavage. Such hydrocracking leads primarily to the formation of C2-C4 products.

### c. Coimpregnated $PtTe/Al_2O_3$

$PtTe/Al_2O_3$ catalysts prepared by the coimpregnation method exhibited even greater stabilities than vapor-deposited $PtTe/Al_2O_3$ during reaction experiments. No tellurium was evolved from the catalyst surface during these tests. The product distribution results at 400°C and 30% conversion of n-hexane are given in Table III-7. Similar to the $PtTe/Al_2O_3$ catalysts prepared by vapor deposition, coimpregnated catalysts caused a decrease in the yield to cracking products and favored the formation of isomerization products. The methylcyclopentane and benzene in the product were similar for all the catalysts. Note that even the introduction of a small amount of tellurium (Te/Pt atomic ratio = 0.06) was sufficient to dramatically alter the selectivities for isomerization and hydrocracking.

The initial reaction rates for these coimpregnated catalysts for isomerization and hydrogenolysis are given in Table III-8. At low tellurium content, the turnover frequency of Pt/Te catalysts for isomerization is

Table III-7.

Product Yields, $PtTe/Al_2O_3$ (Coimpregnation) Catalysts at 400°C.

| [a]Catalyst | | | Yield % at 30% Conversion | | | |
|---|---|---|---|---|---|---|
| Te/Pt | wt cat (mg) | rxn time (min) | 2MP+3MP | C1-C5 | MCP | Benzene |
| 0.00 | 20 | 43 | 7.2 | 11.0 | 6.0 | 5.8 |
| 0.06 | 20 | 40 | 11.6 | 6.3 | 6.6 | 5.5 |
| 0.23 | 100 | 39 | 11.2 | 6.8 | 6.8 | 5.2 |
| 0.76 | 200 | 51 | 12.5 | 7.1 | 6.4 | 4.0 |
| 1.2 | 200 | 80 | 11.3 | 8.4 | 6.3 | 4.0 |

[a] 1 wt% Pt.

Table III-8.

Initial Rates of Isomerization and Cracking (n-Hexane, 400°C) and Dehydrogenation (Cyclohexane, 300°C).

| Catalyst | Initial Rate (mols of reactant/s/surf.Pt)x10² | | |
|---|---|---|---|
| | Isom. | Crack. | Dehydrog. |
| $Pt/Al_2O_3$ | 3.4 | 4.8 | 58 |
| $PtTe/Al_2O_3$ | | | |
| Te/Pt | | | |
| 0.06 | 7.7 | 5.3 | 99 |
| 0.23 | 3.8 | 2.1 | 62 |
| 0.76 | 3.6 | 1.6 | 68 |
| $PtSb/Al_2O_3$ | | | |
| Sb/Pt | | | |
| 0.14 | 3.4 | 1.0 | 41 |
| 0.41 | 4.0 | 1.5 | 39 |
| 0.69 | 3.3 | 0.8 | 32 |
| 0.97 | 2.6 | 0.9 | 40 |
| 1.24 | 3.0 | 1.5 | 43 |

significantly higher than that of $Pt/Al_2O_3$, while the specific cracking activity of both catalysts are practically the same. Therefore, the increase in the isomerization selectivity is due to an increase in specific isomerization activity. However, at high tellurium content, the increase in isomerization selectivity observed for PtTe catalysts is due more to a decrease in the specific hydrogenolysis activity.

### d. Coimpregnated $PtSb/Al_2O_3$

The product distributions for n-hexane conversion using coimpregnated $PtSb/Al_2O_3$ catalysts are given in Table III-9, and the initial turnover frequencies for isomerization and hydrocracking are provided in Table III-8. Similar in behavior to the coimpregnated $PtTe/Al_2O_3$ catalysts, the Sb-containing bimetallics display a substantial increase in the yield to isomerization products and inhibit the hydrogenolysis reactions, when compared to $Pt/Al_2O_3$ (Table III-9). The yield to cyclic products is relatively constant with respect to Sb/Pt ratio. As shown in Table III-8, the changes in observed selectivities using the $PtSb/Al_2O_3$ catalysts can be attributed to a decrease in the specific hydrocracking activity.

Table III-9.

Product Yields, $PtSb/Al_2O_3$ (Coimpregnation) Catalysts at 400°C.

| [a] Catalyst | | | Yield % at 30% Conversion | | | |
|---|---|---|---|---|---|---|
| Sb/Pt | wt cat (mg) | rxn time (min) | 2MP+3MP | C1-C5 | MCP | Benzene |
| 0.0 | 20 | 43 | 7.2 | 11.0 | 6.0 | 5.8 |
| 0.14 | 50 | 44 | 12.8 | 5.1 | 6.8 | 5.3 |
| 0.41 | 50 | 70 | 13.5 | 5.4 | 6.7 | 4.4 |
| 0.69 | 50 | 108 | 15.4 | 4.5 | 6.6 | 3.5 |
| 0.97 | 50 | 115 | 13.7 | 5.1 | 6.8 | 4.4 |
| 1.24 | 50 | 120 | 13.9 | 4.5 | 7.4 | 4.2 |

[a] 1.1 wt% Pt.

**4. Cyclohexane Reaction**

The dehydrogenation activity for cyclohexane catalyzed by $PtTe/Al_2O_3$ and $PtSb/Al_2O_3$, prepared by coimpregnation, has been investigated at 300°C. The results are presented in Table III-8. Benzene was found to be the only dehydrogenation product for all the catalysts. No or insignificant amounts of hydrogenolysis products were observed, even at high conversion (> 90%). The low Te-content $PtTe/Al_2O_3$ has a higher specific dehydrogenation activity than $Pt/Al_2O_3$. High Te-content catalysts show specific dehydrogenation activity at about the same levels as $Pt/Al_2O_3$, while $PtSb/Al_2O_3$ show moderately lower dehydrogenation activities.

**D. FTIR**

Typical infrared spectra of carbon monoxide chemisorbed on $Pt/Al_2O_3$, $PtTe/Al_2O_3$ and $PtSb/Al_2O_3$ are shown in Figures III-7 to III-9. Of the catalysts studied, only a single $Pt-^{12}CO$ peak appeared (2040-2080 $cm^{-1}$). This suggests the absence of phase separation in bimetallic catalysts at the adsorption temperature. As anticipated, the $Pt-^{12}CO$ peak continued to shift to lower frequencies with increasing amounts of $^{13}CO$. A peak ascribed to $Pt-^{13}CO$ appeared simultaneously at ≈2010

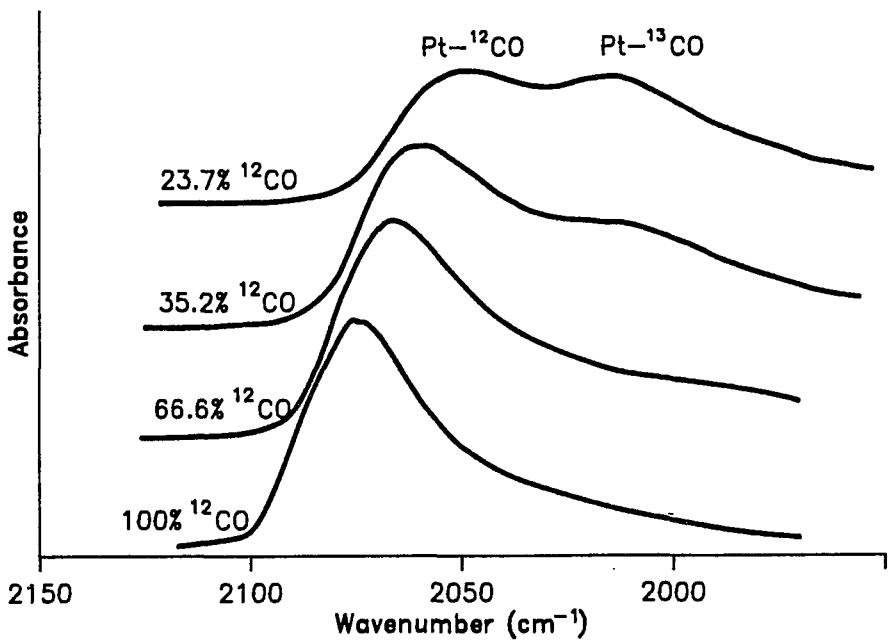


Figure III–7. Infrared Spectra of Isotopic Mixtures of $^{12}CO$ and $^{13}CO$ at 25°C on $Pt/Al_2O_3$.

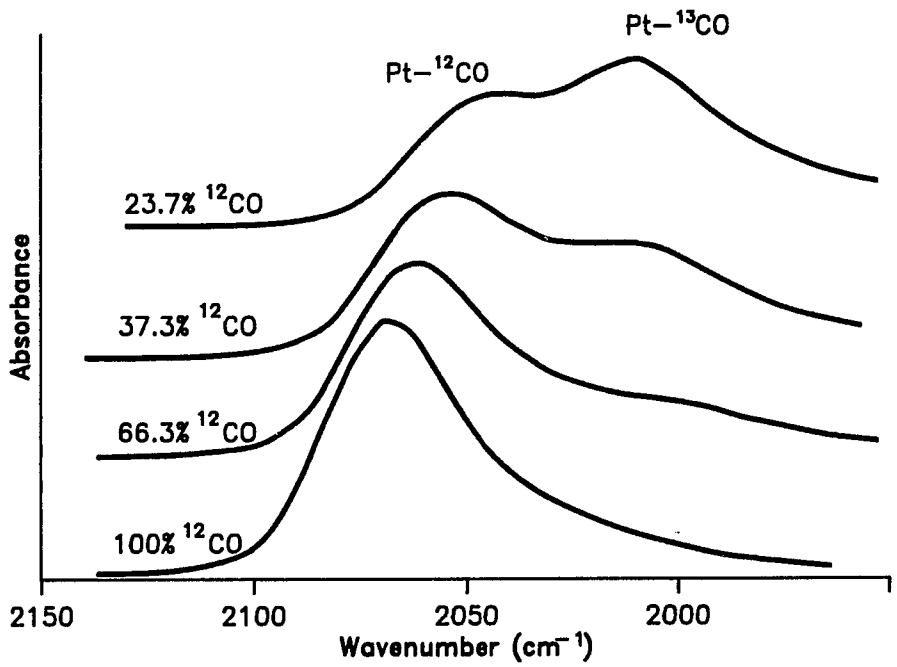


Figure III–8. Infrared Spectra of Isotopic Mixtures of $^{12}CO$ and $^{13}CO$ at 25°C on $PtTe/Al_2O_3$ (Coimpregnation, Te/Pt=0.06).

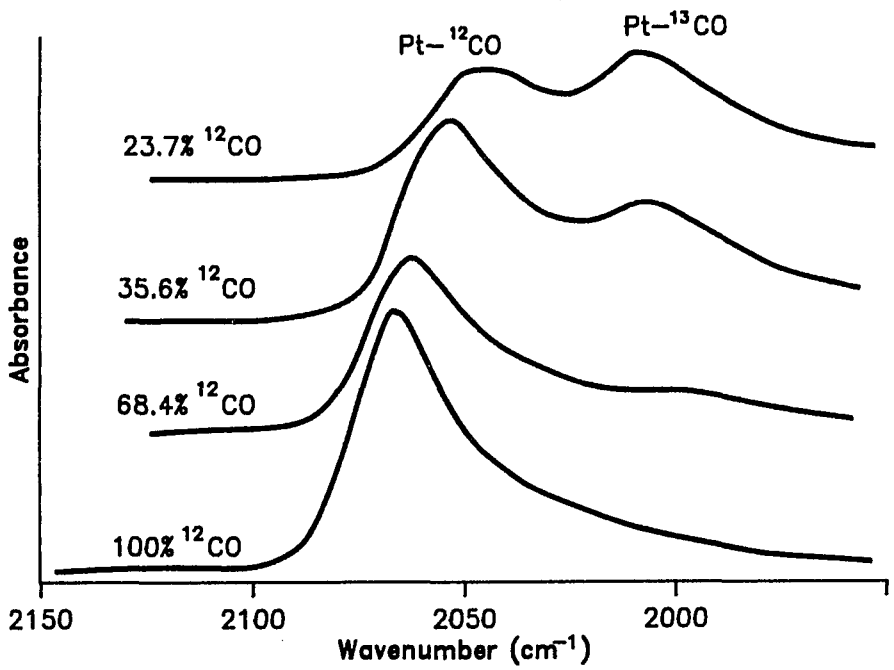


Figure III–9. Infrared Spectra of Isotopic Mixture of $^{12}CO$ and $^{13}CO$ at 25 °C on $PtSb/Al_2O_3$ (Coimpregnation, Sb/Pt=0.41).

$cm^{-1}$. The relative area of the Pt-$^{12}$CO and Pt-$^{13}$CO peaks does not correspond to the isotopic composition. Such intensity transfer (from a low frequency band to a high frequency band) is reduced by the addition of tellurium or antimony. This phenomenon has also been observed in other bimetallic systems, e.g. Pt-Cu, Pt-Pb, and Pt-Sn [Toolenaar et al., 1983; Bastein et al., 1984].

The Pt-$^{12}$CO band frequencies vs. the isotopic compositions are plotted in Figures III-10 and III-11. For $PtTe/Al_2O_3$, only the set of data for the low Te/Pt atomic ratio (0.06) catalyst is presented; the higher Te/Pt atomic ratio catalysts exhibited a peak of such low intensity that the data were not reliable. Based on these data, an electronic effect is possibly in operation, because the band frequency curves for $Pt/Al_2O_3$ and $PtTe/Al_2O_3$ apparently do not coincide at infinite dilution, though scatter in the data make the extrapolation somewhat uncertain (Figure III-10). Geometric effects are seemingly minimal for this low Te-content catalyst, since the two curves are separated by almost equal frequencies at all points. The $PtTe/Al_2O_3$ curve lies below $Pt/Al_2O_3$, suggesting that electrons have been transferred from tellurium s or p orbitals to platinum d orbitals. This electron transfer

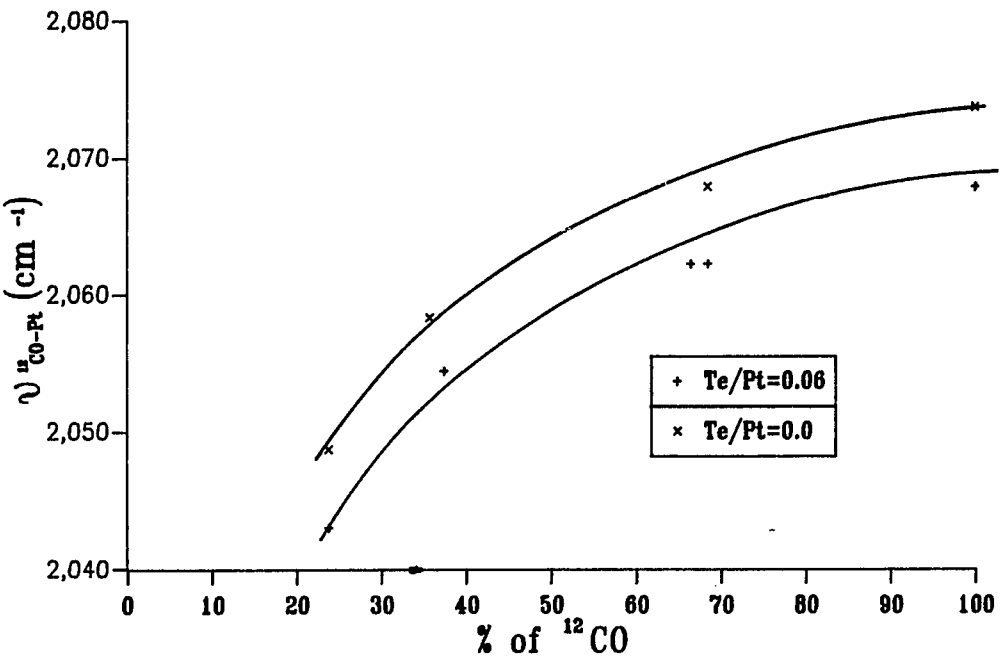


Figure III–10. Isotopic Dilution Experiments, Coimpregnated Catalysts.

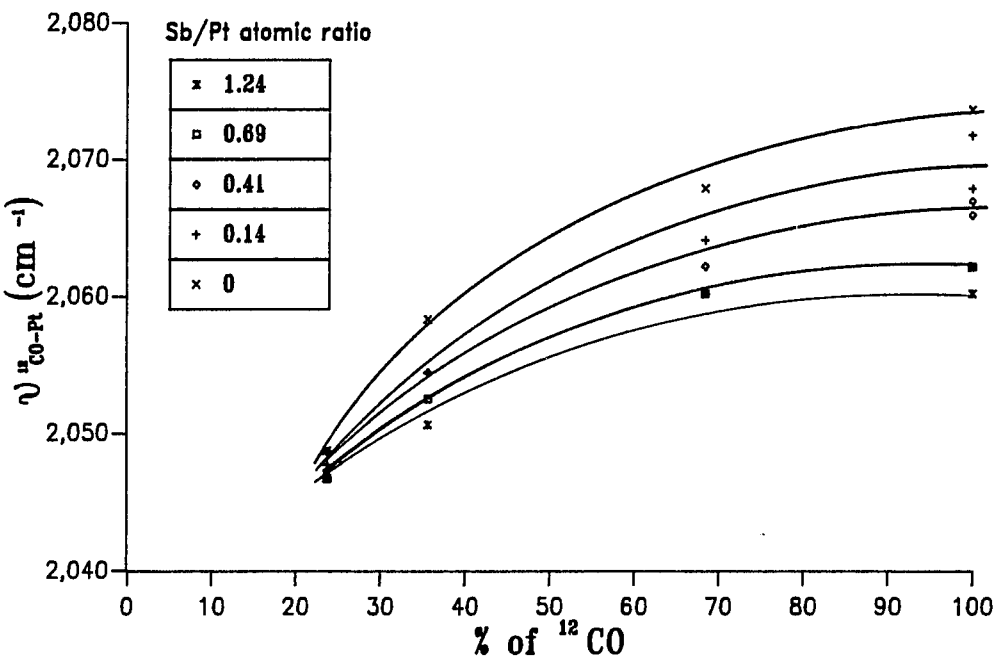


Figure III–11. Isotopic Dilution Experiments, Coimpregnated Catalysts.

increases the back-donation of electrons to the CO antibonding orbitals and thereby decreases the CO bond strength. Such a phenomenon has been observed for $PtSn/Al_3O_3$ and $PtPb/Al_2O_3$ [Bastein et al., 1984; Palazon et al., 1981], but is contrary to that observed for $PtS/Al_2O_3$ [Apestehuia et al., 1984] (electron withdrawal by S from Pt) and $PtCu/Al_2O_3$ [Toolenaar et al., 1983] (no observable electronic effects).

The isotopic dilution method for $PtSb/Al_2O_3$ gave results which differed from those of $PtTe/Al_2O_3$ (Figure III-11). All of the band frequencies for CO adsorbed on $PtSb/Al_2O_3$ converge to the frequency associated with adsorption on $Pt/Al_2O_3$ at infinite dilution. Therefore all band frequency deviations at higher $^{12}CO$ amounts are attributable to dipole-dipole coupling and geometric rather than electronic effects are therefore in operation. This behavior is similar to that found using $PtCu/Al_2O_3$ [Toolenaar et al., 1983].

## E. Isotopic Tracer Experiments

### 1. 2-methylpentane (2-$^{13}C$) and 2-methylpentane (5-$^{13}C$) Reactions

Because of the limited amount of labeled hydrocarbons synthesized, the investigations were performed on only a few of the catalysts prepared: $PtTe/Al_2O_3$ (coimpregnation, 1 wt% Pt, Te/Pt atomic ratio = 0.06), $PtSb/Al_2O_3$ (1.1 wt% Pt, Sb/Pt atomic ratio = 0.97) and $Pt/Al_2O_3$ (impregnation, 1 wt% Pt). The experiments were conducted in the recirculation batch reactor. $PtTe/Al_2O_3$ and $PtSb/Al_2O_3$ were studied at 290°C and 340°C respectively, and $Pt/Al_2O_3$ was studied at both temperatures. It should be noted that preliminary studies indicated that $PtSb/Al_2O_3$ was inactive for skeletal isomerization at 290°C. The hydrogen to hydrocarbon ratio was kept at 17 and the system was filled with helium to 800 torr as usual. The initial partial pressure of the hydrocarbon was 25 torr for 2-methylpentane ($2-^{13}C$) and 20 torr for 2-methylpentane ($5-^{13}C$) reactions, respectively. A smaller amount of 2-methylpentane ($5-^{13}C$) was used because the amount synthesized was less than expected.

Table III-10 provides the product distribution data for the 2-methylpentane reaction on $Pt/Al_2O_3$, $PtTe/Al_2O_3$ (Te/Pt=0.06), and $PtSb/Al_2O_3$ (Sb/Pt=0.97). The data were taken at low conversion to ensure that secondary reactions had not occurred. This was also evident in the absence of extensive cracking, which would lead to the

Table III-10.
Comparison of Product Distribution Data for 2-MP Reaction on $Pt/Al_2O_3$, $PtTe/Al_2O_3$, and $PtSb/Al_2O_3$.

| | $Pt/Al_2O_3$ | [a] $PtTe/Al_2O_3$ | $Pt/Al_2O_3$ | [b] $PtSb/Al_2O_3$ |
|---|---|---|---|---|
| Temp, °C | 290 | 290 | 340 | 340 |
| C1 | 0.60 | 0.46 | 0.33 | 0.27 |
| C2 | 0.49 | 0.41 | 0.21 | 0.31 |
| C3 | 0.69 | 0.58 | 0.53 | 0.47 |
| i-C4 | 1.01 | 0.75 | 0.41 | 0.62 |
| n-C4 | 0.00 | 0.00 | 0.00 | 0.00 |
| i-C5 | 1.39 | 1.09 | 0.81 | 0.67 |
| n-C5 | 1.50 | 1.17 | 0.68 | 0.68 |
| ΣC1-C5 | 5.68 | 4.46 | 2.68 | 3.03 |
| MCP | 0.95 | 0.94 | 2.68 | 2.83 |
| 3-MP | 2.11 | 1.55 | 2.89 | 3.81 |
| n-C6 | 2.36 | 1.37 | 2.83 | 2.24 |
| % Conv. | 11.10 | 8.32 | 11.08 | 11.91 |

[a] : Te/Pt atomic ratio = 0.06.

[b] : Sb/Pt atomic ratio = 0.97.

formation of n-butane and higher $C_1/C_5$ and $C_2/C_4$ ratios. Unlike the results from n-hexane reactions previously reported, a slight increase in hydrocracking selectivity was observed on $PtTe/Al_2O_3$ catalysts and no major effects were found on the selectivity toward hydrocracking products by the addition of antimony. However, the Sb and Te-containing catalysts exhibit lower $n\text{-}C_6$/3-MP ratios than does $Pt/Al_2O_3$.

The possible "tagged" species present in the reaction products of the labeled 2-methylpentane isomerization, according to bond shift and cyclic mechanisms, are illustrated in Figure III-12. The chemical shifts and their integral areas of the reaction products for both 2-methylpentane ($2\text{-}^{13}C$) and 2-methylpentane ($5\text{-}^{13}C$) isomerization using various catalysts can be found in Appendix D.

Table III-11 lists and identifies the chemical shifts of the reaction products, including 2-methylpentane, 3-methylpentane, n-hexane and methylcyclopentane, for 2-methylpentane ($2\text{-}^{13}C$) isomerization on $Pt/Al_2O_3$ at 290°C. The band assignments were made by comparing the corresponding $^{13}C$ chemical shifts with those given in Table II-8 (Chapter 2). The natural occurrence of $^{13}C$ in

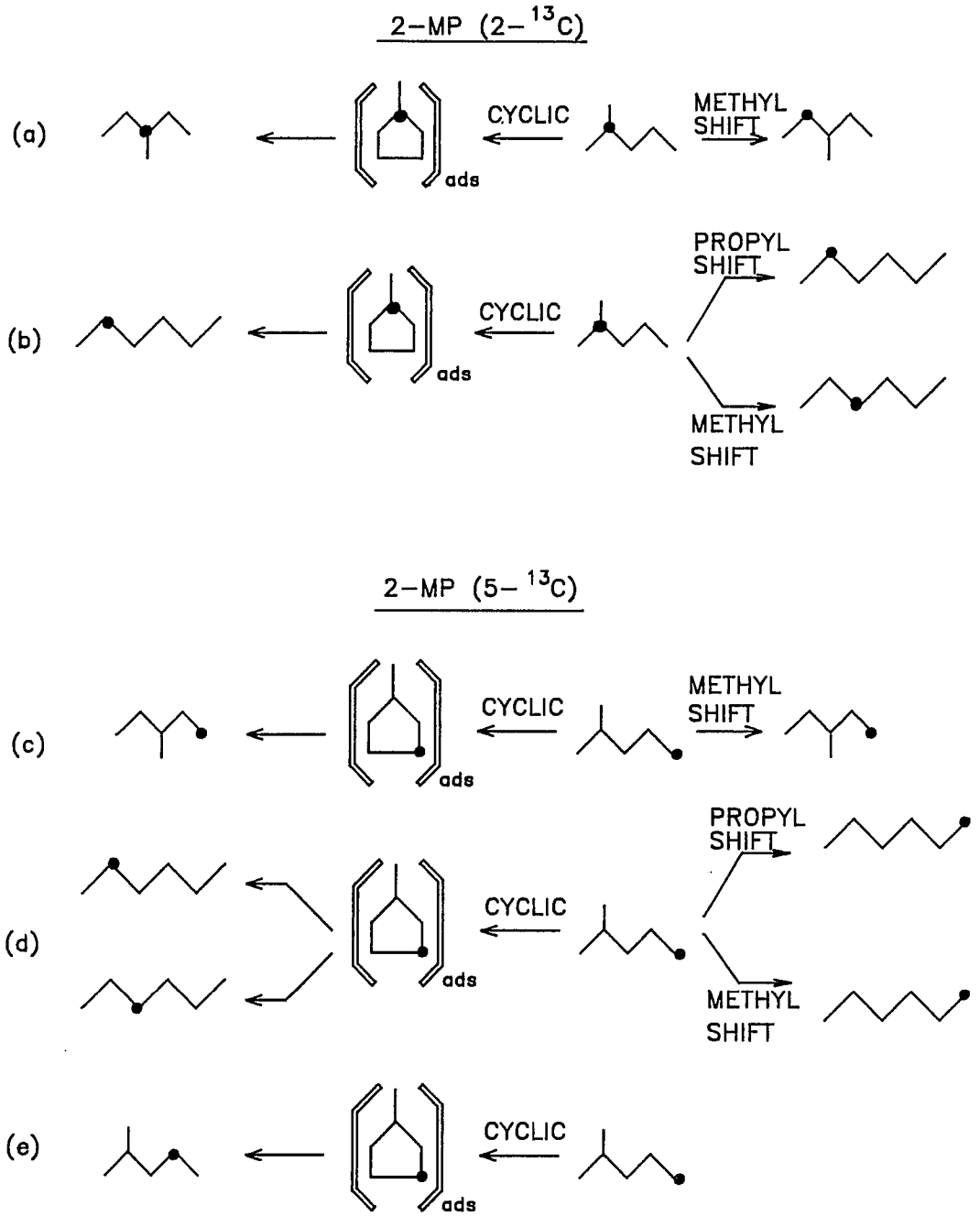


Figure III-12. Cyclic and Bond Shift Mechanisms for the Reactions of 2-MP (2-$^{13}$C) and 2-MP (5-$^{13}$C).

Table III-11. Chemical Shifts of Reaction Products from 2-MP (2-$^{13}$C) Isomerization on $Pt/Al_2O_3$ at 290°C.

| Position (ppm) | Assignment | Area |
|---|---|---|
| 14.26[c] | 2-MP (5-$^{13}$C) | 0.95 |
| 14.34[c] | | |
| 20.51[c] | 2-MP (4-$^{13}$C) | 1.01 |
| 22.24[c] | 2-MP (1-$^{13}$C) | 1.85 |
| 22.94[c] | | |
| 22.73 | n-C6 (2-$^{13}$C) | 1.78 |
| 27.40[a] | | |
| 27.43[a] | | |
| 27.76[b] | 2-MP (2-$^{13}$C) | 101.33 |
| 28.09[a] | | |
| 28.13[a] | | |
| 29.15 | 3-MP (2-$^{13}$C) | 0.41 |
| 34.61 | MCP (1-$^{13}$C) | 1.31 |
| 36.19 | 3-MP (3-$^{13}$C) | 1.03 |
| 41.12[c] | 2-MP (3-$^{13}$C) | 0.99 |
| 41.81[c] | | |

*a* satellite peak due to spin-spin splitting.

*b* main band.

*c* naturally abundant $^{13}$C in 2-MP (2-$^{13}$C) reactant.

positions 1, 3, 4, and 5 of the unreacted 2-methylpentane reactant molecules also appeared in the spectrum. $^{13}C$ spin-spin splitting, which is usually not observed for naturally abundant $^{13}C$ atoms in $^{13}C$-NMR spectra, was found for naturally abundant $^{13}C$ next to the enriched $^{13}C$ atom in 2-methylpentane. The enriched $^{13}C$ in the 2 position of 2-methylpentane also experiences spin-spin splitting by all neighboring naturally abundant $^{13}C$ atoms, resulting in a complex multiplet with a very intense main line and several satellites. The satellites represent areas consistent with natural abundance of $^{13}C$ and are grouped with the main band. Enriched $^{13}C$ positions in the products of the reaction, 3-methylpentane, n-hexane, and methylcyclopentane are those predicted according to the cyclic and bond shift mechanisms. The absence of other products indicates that secondary reactions or other rearrangements not predicted by bond shift or cylic routes had not occurred. It should be mentioned that, in some spectra, the resonance from the 2 position of n-hexane overlapped with the 1 position of 2-methylpentane. This did not upset our studies, since n-hexane (2-$^{13}C$) was the only n-hexane species observed. n-Hexane (3-$^{13}C$), expected from methyl shift, was not detected in any experiment. Therefore,

the production of n-hexane (2-$^{13}$C) can be attributed totally to propyl shift and cyclic mechanisms (Figures III-12(b)).

For the 2-methylpentane (5-$^{13}$C) reaction, the products were separated into two groups, 2-methylpentane + 3-methylpentane and n-hexane + methylcyclopentane, which were analyzed individually. The results for a typical spectrum of the former are presented in Table III-12. The relative areas of the peaks corresponding to $^{13}$C in positions 1, 2, and 3 of 2-methylpentane are in close agreement with those calculated based upon the natural abundance of $^{13}$C and therefore, these species are not formed via catalytic reactions. The spectrum also shows a triplet which was assigned to 2-methylpentane (4-$^{13}$C). The two satellite peaks appearing at 20.15 and 20.84 ppm are caused by $^{13}$C spin-spin splitting of the naturally abundant $^{13}$C at position 4 by the enriched neighboring $^{13}$C in position 5, as expected. The central peak at 20.48 ppm is ascribed to the 2-methylpentane (4-$^{13}$C) product from the ring opening of the cyclic intermediate, methylcyclopentane (3-$^{13}$C). 3-methylpentane (1-$^{13}$C), produced from both cyclic and bond shift mechanisms, was also detected, but, since both mechanisms give this product, it bears no useful information.

Table III-12. Chemical Shifts of Reaction Products from 2-MP (5-$^{13}$C) Isomerization on PtTe/$Al_2O_3$ at 290°C.

| Position (ppm) | Assignment | Area |
|---|---|---|
| 11.43 | 3-MP (1-$^{13}$C) | 0.34 |
| 14.32[a] | 2-MP (5-$^{13}$C) | 10.86 |
| 14.62[b] | | |
| 20.15[c] | 2-MP (4-$^{13}$C) | 0.10 |
| 20.84[c] | | |
| 20.48 | 2-MP (4-$^{13}$C) | 0.26 |
| 22.61[c] | 2-MP (1-$^{13}$C) | 0.21 |
| 22.67 | n-C6 (2-$^{13}$C) | 2.93 |
| 25.29 | MCP (3-$^{13}$C) | 3.28 |
| 27.68[c] | 2-MP (2-$^{13}$C) | 0.10 |
| 27.74[c] | | |
| 31.60 | n-C6 (3-$^{13}$C) | 2.61 |
| 41.39[c] | 2-MP (3-$^{13}$C) | 0.11 |

*a* satellite peak due to spin-spin splitting.

*b* main band.

*c* naturally abundant $^{13}$C in 2-MP (5-$^{13}$C) reactant.

The chemical shifts observed for the n-hexane and methylcyclopentane group from the isomerization of 2-methylpentane (5-$^{13}$C) are also given in Table III-12. It is evident that the cyclic mechanism is operative as indicated by the formation of methylcyclopentane (3-$^{13}$C) (refer to Figure III.12). Surprisingly, no n-hexane (1-$^{13}$C), expected via bond shift of 2-methylpentane (5-$^{13}$C), was observed in three of the four experiments. Only a small amount was observed in the fourth experiment ($Pt/Al_2O_3$ at 340°C). The peaks at 22.67 and 31.60 ppm were identified as n-hexane (2-$^{13}$C) and n-hexane (3-$^{13}$C), respectively, and must be produced by ring opening of methylcyclopentane.

The contribution of cyclic and bond shift mechanisms for the conversion of 2-methylpentane to 3-methylpentane were determined directly by the relative area of the 3 and 2 positions of 3-methylpentane. (Figure III-12(a)).

For the conversion of 2-methylpentane to n-hexane, it is necessary to couple the results from the reactions of 2-methylpentane (2-$^{13}$C) and 2-methylpentane (5-$^{13}$C) in order to evaluate the relative contributions of cyclic and methyl & propyl shift mechanisms. For 2-methylpentane (5-$^{13}$C), the ratio of cyclic to the "total" bond shift is (see Figure III-12(d)):

$$\frac{cyclic\ \ mech.}{propyl\ \ shift\ +\ \ methyl\ \ shift} = \frac{n\text{-}C6(2\text{-}^{13}C)+n\text{-}C6(3\text{-}^{13}C)}{n\text{-}C6(1\text{-}^{13}C)}$$

This ratio is then used in the analysis of data obtained with 2-methylpentane (2-$^{13}$C). n-Hexane (2-$^{13}$C) can be produced from both cyclic and bond shift mechanisms from 2-methylpentane (2-$^{13}$C) (Figure III-12(b)). The fraction of n-hexane (2-$^{13}$C) produced by the cyclic mechanism is calculated from the ratio obtained from the 2-methylpentane (5-$^{13}$C) reaction. The remaining n-hexane (2-$^{13}$C) corresponds to propyl shift while the n-hexane (3-$^{13}$C) corresponds to methyl shift.

The relative importance of cyclic and bond shift mechanisms for the isomerization of 2-methylpentane to 3-methylpentane and n-hexane using $Pt/Al_2O_3$, $PtTe/Al_2O_3$ (Te/Pt=0.06), and $PtSb/Al_2O_3$ (Sb/Pt= 0.97) were determined by these procedures and the results are summarized in Table III-13 and III-14.

The cyclic mechanism accounted more than 70% of the conversion of 2-methylpentane to 3-methylpentane on $Pt/Al_2O_3$ at both 290 and 340°C. This is in agreement with other studies using highly dispersed $Pt/Al_2O_3$ catalysts [Corolleur et al., 1972] under similar

Table III-13.
Product Distribution of Isotopic Species for the Isomerization Reactions of 2-MP (2-$^{13}$C) and 2-MP (5-$^{13}$C) on $Pt/Al_2O_3$, $PtTe/Al_2O_3$, and $PtSb/Al_2O_3$.[a]

| Catalyst | Reactant | T (°C) | 3-MP (3-$^{13}$C) | 3-MP (2-$^{13}$C) | n-C6 (1-$^{13}$C) | n-C6 (2-$^{13}$C) | n-C6 (3-$^{13}$C) |
|---|---|---|---|---|---|---|---|
| $Pt/Al_2O_3$ | 2-MP (2-$^{13}$C) | 290 | 71.5 | 28.5 | 0 | 100 | 0 |
| | 2-MP (5-$^{13}$C) | 290 | * | * | 0 | 52.7 | 47.3 |
| $PtTe/Al_2O_3$ | 2-MP (2-$^{13}$C) | 290 | 64.4 | 35.6 | 0 | 100 | 0 |
| | 2-MP (5-$^{13}$C) | 290 | * | * | 0 | 52.9 | 47.1 |
| $Pt/Al_2O_3$ | 2-MP (2-$^{13}$C) | 340 | 71.9 | 28.1 | 0 | 100 | 0 |
| | 2-MP (5-$^{13}$C) | 340 | * | * | 9.3 | 44.3 | 46.4 |
| $PtSb/Al_2O_3$ | 2-MP (2-$^{13}$C) | 340 | 39.7 | 60.3 | 0 | 100 | 0 |
| | 2-MP (5-$^{13}$C) | 340 | * | * | 0 | 60.0 | 40.0 |

* Not predicted from cyclic or bond shift reactions and none observed.
*a* Naturally abundant $^{13}$C in the labelled reactant has been removed.

Table III-14.
Contribution of Cyclic and Bond Shift Mechanisms for the Isomerization Reactions of 2-MP (2-$^{13}$C) and 2-MP (5-$^{13}$C) on $Pt/Al_2O_3$, $PtTe/Al_2O_3$, and $PtSb/Al_2O_3$.

| Catalysts | T (°C) | 2-MP to 3-MP | | 2-MP to n-C6 | | |
|---|---|---|---|---|---|---|
| | | C.M.[a] | M.S.[b] | C.M.[a] | P.S.[c] | M.S.[b] |
| $Pt/Al_2O_3$ | 290 | 71.5 | 28.5 | 100 | 0 | 0 |
| $PtTe/Al_2O_3$ | 290 | 64.4 | 35.6 | 100 | 0 | 0 |
| $Pt/Al_2O_3$ | 340 | 71.9 | 28.1 | 90.7 | 9.3 | 0 |
| $PtSb/Al_2O_3$ | 340 | 39.9 | 60.3 | 100 | 0 | 0 |

[a] : Cyclic mechanism.
[b] : Methyl shift.
[c] : Propyl shift.

conditions. However, the relative importance of the cyclic mechanism falls significantly with the addition of tellurium or antimony to $Pt/Al_2O_3$. These results are similar to those obtained using $PtRu/Al_2O_3$ [Diaz et al., 1983], but is contrary to those using $PtAu/Al_2O_3$ [O'Cinneide and Gault, 1975].

The cyclic mechanism is almost totally responsible for the formation of n-hexane from 2-methylpentane on all the catalysts tested. Methyl shift was not found and only 9% propyl shift was detected using $Pt/Al_2O_3$ at 340°C. The predominance of the cyclic mechanism over bond shift mechanisms for the conversion of 2-methylpentane to n-hexane has been observed on $PtAu/Al_2O_3$ and $PtRu/Al_2O_3$ bimetallic systems as well as on highly dispersed $Pt/Al_2O_3$ catalysts [Corolleur et al., 1972]. The ring opening of methylcyclopentane ($3\text{-}^{13}C$) (formed from the 2-methylpentane($5\text{-}^{13}C$) reaction) yielding n-hexane ($2\text{-}^{13}C$) and n-hexane ($3\text{-}^{13}C$) of equal amounts is expected. The discrepancy in these amounts for $PtSb/Al_2O_3$ is probably due to a sample of low concentration in n-hexane.

The selectivities for the breakage of the two secondary-secondary and one secondary-tertiary carbon bond in the methylcyclopentane intermediate have not been

obtained in this work due to the experimental difficulties in transferring all the C6 hydrocarbon components into the NMR tube.

2. Reaction of Benzene and Deuterium

The reaction of benzene with deuterium can be divided into an exchange reaction and an addition reaction to form deuterated benzene and cyclohexane, respectively. Studies were carried out at 110 and 250°C on $Pt/Al_2O_3$, $PtTe/Al_2O_3$, and $PtSb/Al_2O_3$ catalysts. The exchange rates were too fast to obtain quantitative kinetic data. Mass transfer limitations probably prevailed under the reaction conditions. The results using various catalysts were therefore compared only qualitatively by examining the distribution of deuterated benzene and cyclohexane at similar conversions.

The deuterium distribution of the reactant, benzene, and the product, cyclohexane, were determined by GC-MS. After the correction of the spectra for the natural abundance of $^{13}C$ and mass fragmentation, other calculations were performed. First, defining $d_i$ as the fraction of total benzene or cyclohexane with i deuterium atoms, the average deuterium content, $\phi$, of each hydrocarbon molecule was calculated

$$\phi = \sum_{i=0}^{n} i d_i$$

where n = 6 for benzene and 12 for cyclohexane. As equilibrium is approached, $\phi_e/n$ must equal the fraction of deuterium present in the initial reaction mixture. Therefore, since the initial reaction mixture consists of 440 torr $D_2$ and 25 torr benzene,

$$(\phi_e) = \left(\frac{D}{D+H}\right)n$$

$$= \left(\frac{(440)(2)}{(440)(2)+(25)(6)}\right)n$$

$$= 0.85n$$

As mentioned previously, single exchange and multiple exchange may occur simultaneously on the metal surface. If only single exchange is operable, the deuterium distribution, before equilibrium is reached, should be given by the binomial distribution calculated at the measured $\phi$. On the other hand, any deviations imply the existence of multiple exchange.

The binomial distribution function is defined as:

$$d_{i,n,\phi} = \binom{n}{i}\phi^i(1-\phi)^{n-i}$$

$$\binom{n}{i} = \frac{n!}{i!(n-i)!}$$

where i = 0 to n.

**a. Deuterium Addition Reaction**

The deuterium distribution of the cyclohexane product using a series of catalysts at 110 and 250°C are given in Figures III-13 to III-16. The average deuterium content of cyclohexane, $\phi$, the conversion of benzene to cyclohexane, A, and the levels of deuteration calculated by the binomial distribution function are also provided. No major differences in the levels of deuteration in cyclohexane are observed among the different catalysts at the same temperature. In addition, the average deuterium contents are approximately constant, ≈10-11 at 250°C and ≈9-10 at 110°C, and seem to be unrelated to how much benzene has been reacted (30-70% conversion). Notice that the value of $\phi$ at 250°C (≈10.5) is similar to the relative deuterium content in the reaction mixture, $\phi_e$ or (0.85)(12). Furthermore, the levels of deuteration also resemble those of the binomial distribution. These results indicate that the reaction is very near equilibrium. However, at 110°C, deviation of the deuteration distribution from the binomial distribution function is observed. A Chi-Square test has been performed and can be found in Appendix E.

**b. Benzene Exchange Reaction**

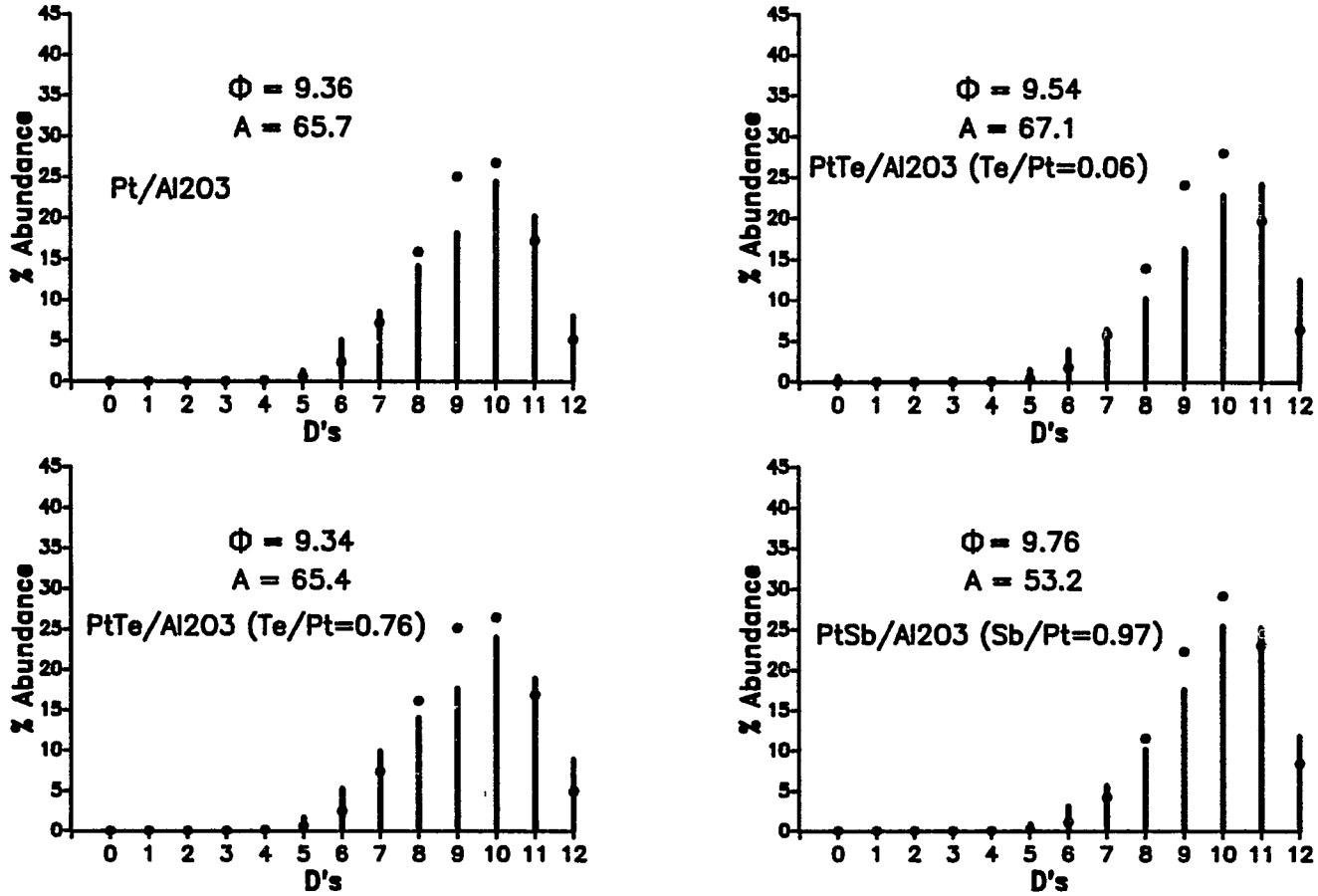


Figure III–13. Deuterium Distribution in Cyclohexane from the Reaction of Benzene and Deuterium at 110°C.
Φ : Average Deuterium Content in Cyclohexane
A : % Conversion of Benzene to Cyclohexane
• : Value Calculated by Binomial Distribution Function

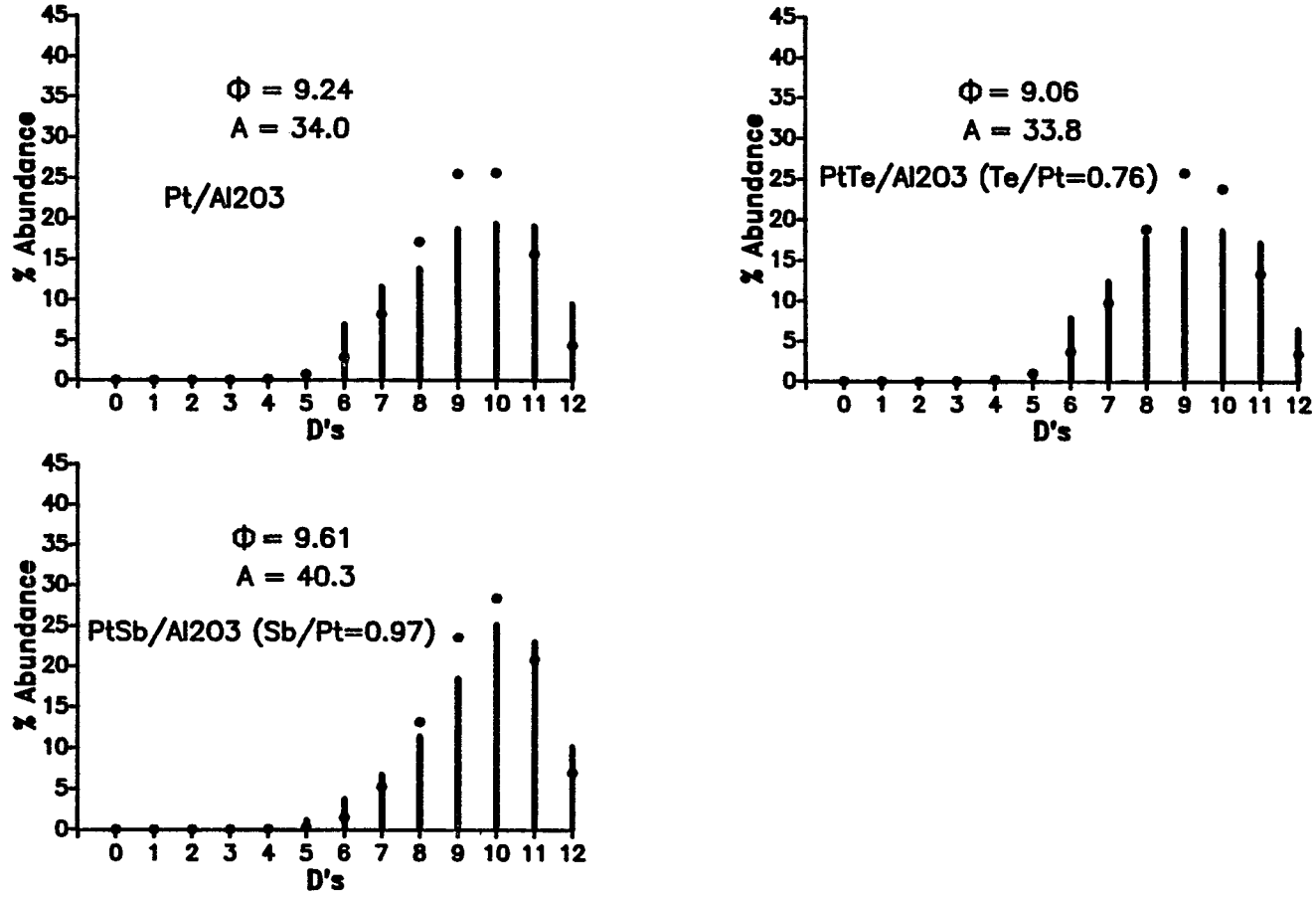


Figure III–14. Deuterium Distribution in Cyclohexane from the Reaction of Benzene and Deuterium at 110°C.
Φ : Average Deuterium Content in Cyclohexane
A : % Conversion of Benzene to Cyclohexane
• : Value Calculated by Binomial Distribution Function

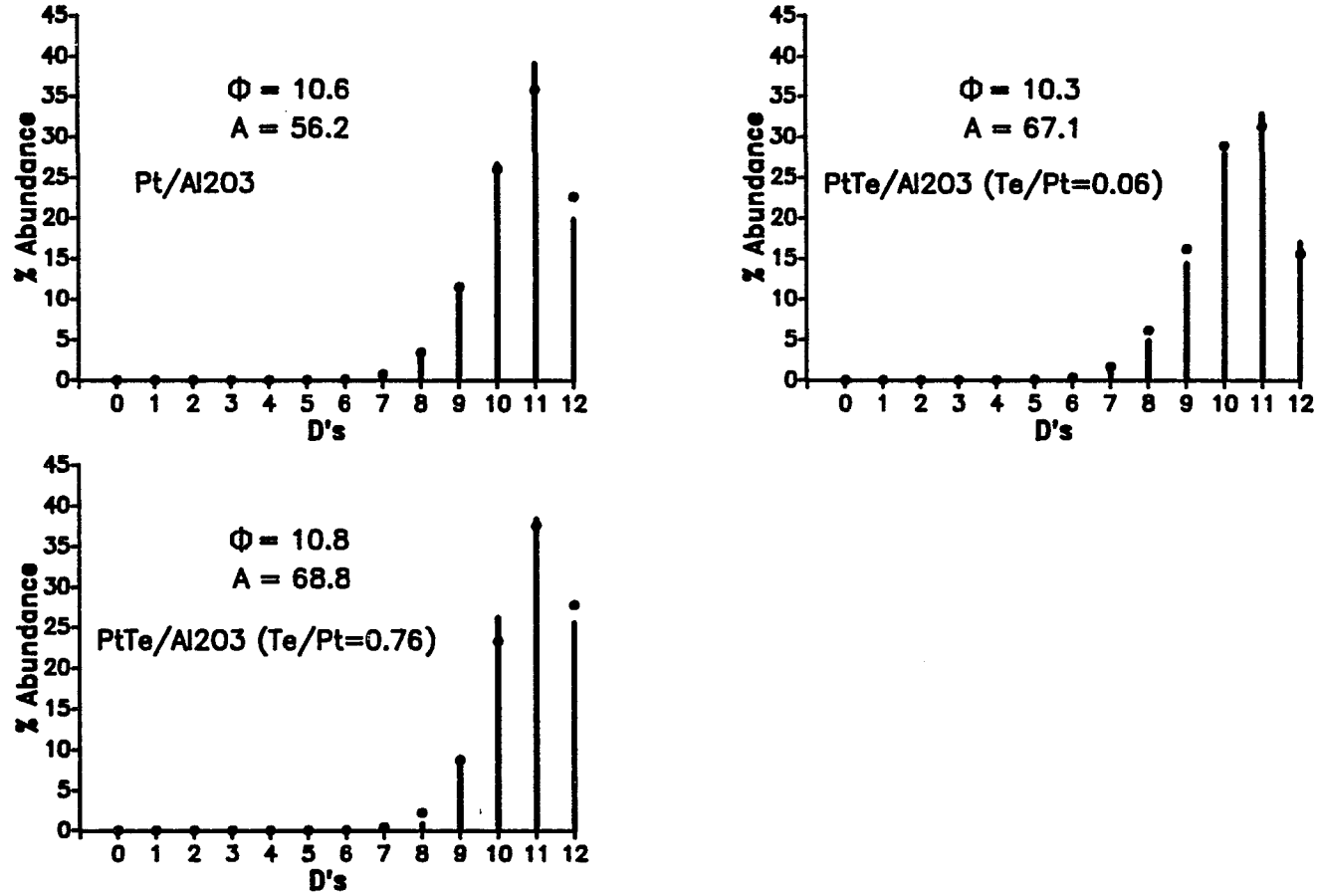


Figure III–15. Deuterium Distribution in Cyclohexane from the Reaction of Benzene and Deuterium at 250°C.
Φ : Average Deuterium Content in Cyclohexane
A : % Conversion of Benzene to Cyclohexane
• : Value Calculated by Binomial Distribution Function

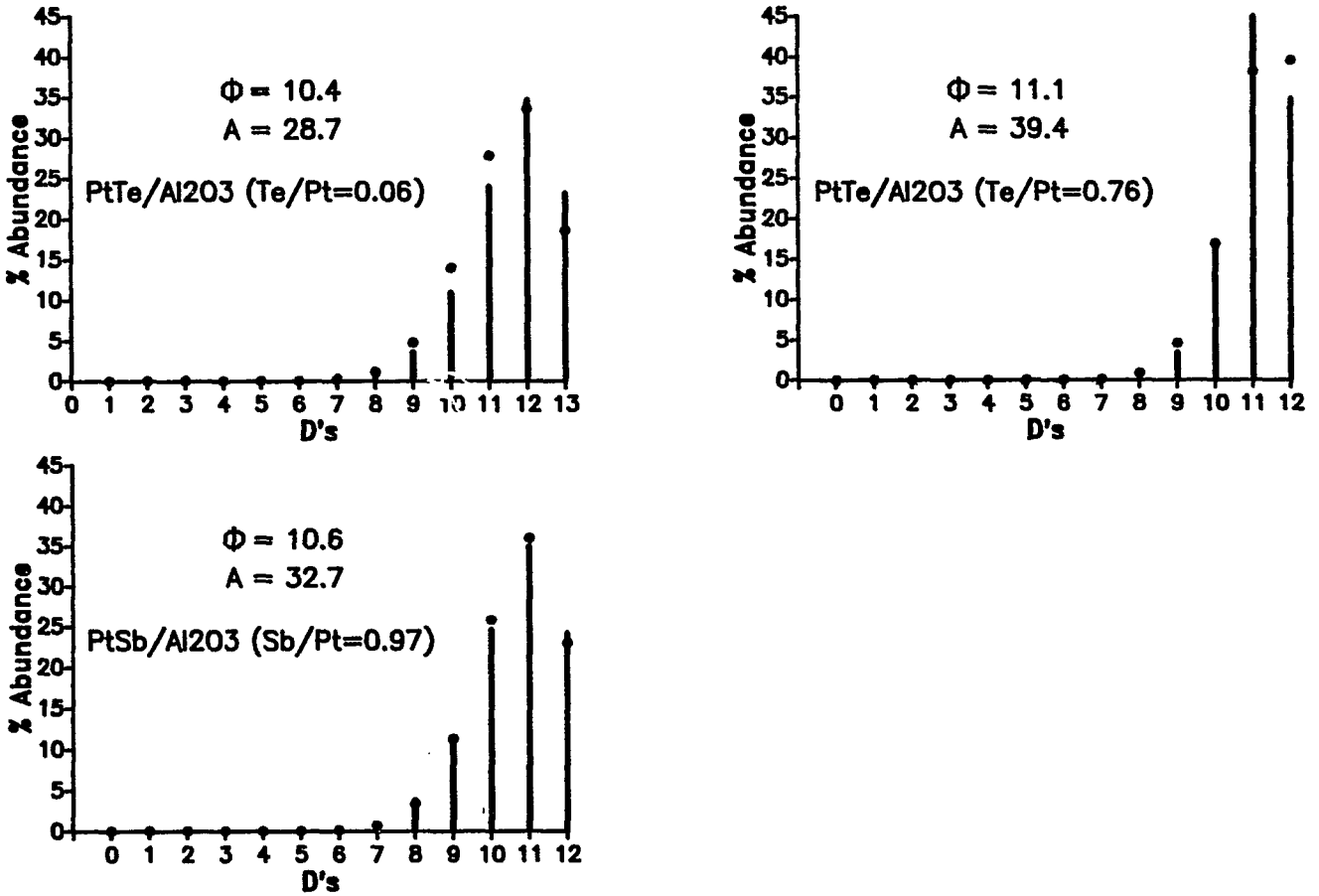


Figure III–16. Deuterium Distribution in Cyclohexane from the Reaction of Benzene and Deuterium at 250°C.
Φ : Average Deuterium Content in Cyclohexane
A : % Conversion of Benzene to Cyclohexane
• : Value Calculated by Binomial Distribution Function

Data for the exchange reaction of benzene on $PtTe/Al_2O_3$ (Te/Pt=0.06), $PtTe/Al_2O_3$ (Te/Pt=0.76), and $PtSb/Al_2O_3$ at comparable conversion are presented in Figures III-17 and III-18. Here X is defined as % of benzene converted to deuterated benzene (100%-%$d_0$). The exchange rate of benzene on $Pt/Al_2O_3$, at either 110 or 250°C, was so fast that comparable data were not obtainable. A clear divergence from the binomial distribution indicates that multiple exchange is important, while significant levels of $d_1$ indicate that single exchange is also important. The levels of deuteration in benzene are similar for all the catalysts tested at 250°C and the low Te-content $PtTe/Al_2O_3$ at 110°C. However, high Te-content $PtTe/Al_2O_3$ and $PtSb/Al_2O_3$ at 110°C exhibit lower levels of deuteration than does low Te-content $PtTe/Al_2O_3$.

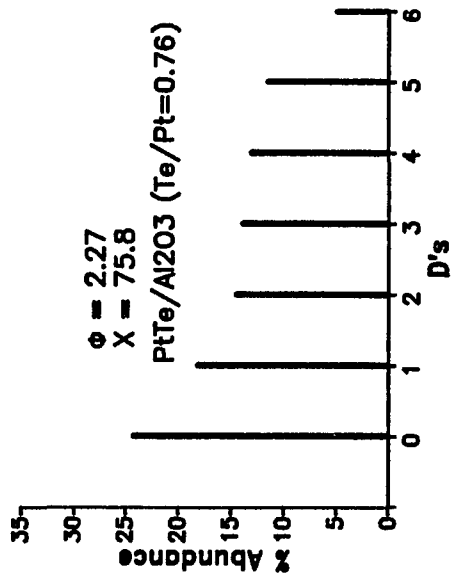


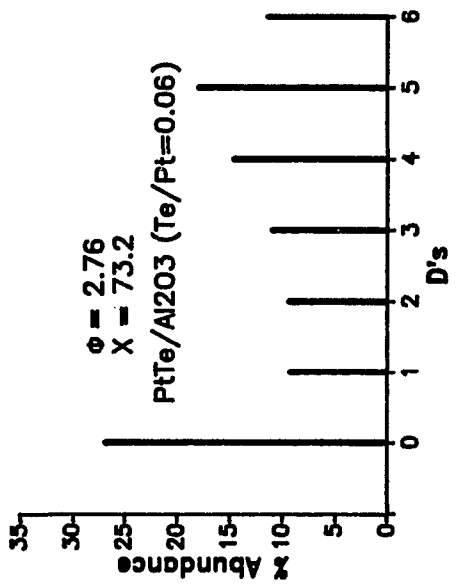


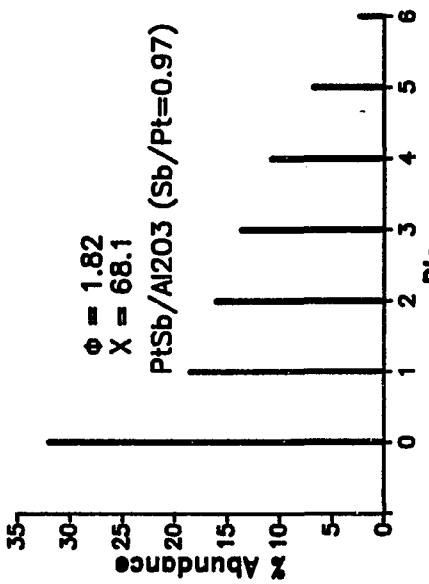


Figure III–17. Deuterium Distribution in Benzene from the Reaction of Benzene and Deuterium at 110°C.
Φ: Average Deuterium Content in Benzene
X: % of Benzene Exchanged

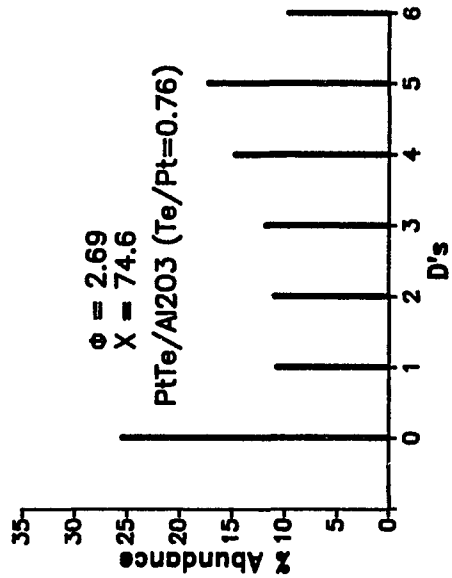


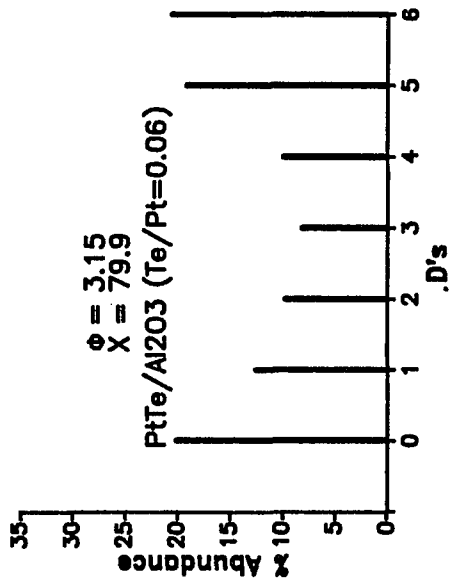


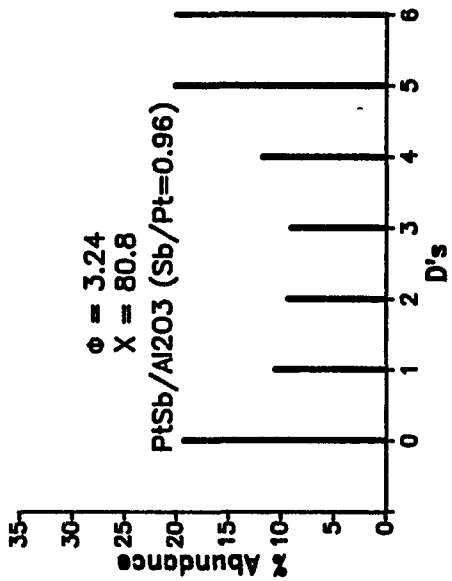


Figure III–18. Deuterium Distribution in Benzene from the Reaction of Benzene and Deuterium at 250°C.

Φ : Average Deuterium Content in Benzene
X : % of Benzene Exchanged

# IV. DISCUSSION

## A. Surface characterization

### 1. Chemisorption of Hydrogen and Carbon Monoxide

The inhibition of hydrogen and carbon monoxide adsorption when tellurium or antimony is added to the $Pt/Al_2O_3$ base catalyst is possibly caused by partial poisoning of platinum active sites. Catalyst poisoning can be considered a "geometric" effect and may be desirable since the rate of the hydrogenolysis reaction, which requires an ensemble of sites, is thereby diminished. It is also possible that the decrease is due to the surface enrichment of tellurium or antimony on the platinum crystallites. Tellurium and antimony have lower surface free energies than platinum if one estimates the surface free energy as one-quarter the component's heat of sublimation [Somorjai, 1972; Williams and Nason, 1974] and are therefore preferred on the surface in most cases. However, this enrichment hypothesis can be invoked only if the alloy crystallites formed are relatively large because macroscopic thermodynamic properties may not apply to very small crystallites particularly under non-inert gas environments [Williams and Dason, 1974]. A further possibility which may explain chemisorption inhibition is electronic modification of the platinum on

bonding with the second metal. This is possibly the main factor in the suppression of hydrogen adsorption on catalysts formed via vapor deposition of tellurium on $Pt/Al_2O_3$ because the small amount of tellurium deposited should not be able to block all of the platinum surface sites and the catalyst is still capable of adsorbing carbon monoxide. Notice that approximately 1/1 tellurium or antimony to platinum atomic ratio may be required to cover all the platinum atoms because the atomic radius of platinum, tellurium, and antimony are approximately equal. However, experiments using the isotopic dilution method indicated no electronic interactions between the accessible platinum and antimony and therefore, it is unlikely that electronic effects alter chemisorption in this system.

**2. Fourier Transform Infrared Spectroscopy**

The results from the isotopic dilution experiments clearly show the relative importance of geometric and electronic effects on low-Te content $PtTe/Al_2O_3$ and $PtSb/Al_2O_3$. Electron donation from tellurium outer orbitals to platinum d-orbitals can be concluded, while the observation of no electronic effect for $PtSb/Al_2O_3$ needs further clarification. As discussed previously, partial poisoning can be considered a geometric effect.

However, this does not preclude electronic interaction between platinum and antimony. On the contrary, partial poisoning may be caused by excess electron donation from the antimony to the platinum d orbitals to form a completely inactive platinum and antimony compound. Such "excess electronic effect" can appear as a geometric effect since the poisoned platinum atoms may simply dilute the unpoisoned platinum atoms.

It is appropriate to discuss also the observation of intensity transfer from the low band frequency ($^{12}CO$) to the high band frequency ($^{13}CO$) in isotopic dilution experiments. Intensity transfer occurs because of the different dipole moments associated with various $^{12}CO$-$^{13}CO$ band frequency modes. Toolenaar et al. [1983] have reported that "$^{13}CO$ contributes to the resulting dipole moment of the in-phase $^{12}CO$-$^{13}CO$ vibrations at the $^{12}CO$-like frequency, while $^{12}CO$ diminishes the resulting dipole moment of the $^{12}CO$-$^{13}CO$ out-of-phase vibrations at the $^{13}CO$-like frequency". A similar explanation has been used by Decius [1955] and Persson and Ryberg [1980, 1981]. The relative intensities of the two bands were a function of the distance between the chemisorbed CO molecules ($^{12}CO$ and $^{13}CO$) with the high frequecy band becoming relatively more intense as the intermolecular

distance was decreased. The reduction of intensity transfer by alloying is therefore realized since alloying increases the intermolecular distance between chemisorbed $^{12}CO$ and $^{13}CO$.

## B. Kinetic Studies

### 1. Vapor Deposited $PtTe/Al_2O_3$

It is evident that $PtTe/Al_2O_3$ catalysts prepared by the vapor deposition method differ from catalysts prepared by the coimpregnation method, as proved by differences in their stabilities and capacities for hydrogen adsorption. The instability of vapor-deposited catalysts prevented us from performing spectroscopic studies and also from obtaining absolute isomerization and cracking activities to correlate with tellurium content. Nevertheless, the modified catalysts displayed higher selectivity for isomerization than $Pt/Al_2O_3$.

The results obtained for the vapor-deposited $PtTe/Al_2O_3$ catalysts suggest that the unusual behavior of these catalysts is possibly due to the incorporation of carbonaceous deposits in the PtTe system since the most selective catalysts were formed only when n-hexane was added to the carrier gas used for tellurium deposition. There is no direct evidence of carbon participation in

the formation of an active species, but consider the incorporation of Te into the platinum crystallites of the highly dispersed monometallic $Pt/Al_2O_3$ catalyst. As the vaporization of tellurium begins, less than 1% of the catalyst surface is occupied by the platinum metal. A legitimate question arises as to whether the vaporized tellurium molecules can "see" and alloy with the platinum clusters on the alumina surface. Weak physical adsorption of tellurium molecules could explain the instability of tellurium in these catalysts. Possibly, the catalyst just consists of individual islands of platinum and tellurium clusters, and is indifferent to the presence of hydrogen or helium. However, changes occur on the surface of the catalyst when it is in contact with a stream containing n-hexane. Carbonaceous deposits, byproducts of hydrogenolysis reactions, may act as a linkage between tellurium and platinum, or may block the passage of tellurium in and out of the pores. Therefore, the catalyst system might be some form of Pt-Te-C, although the role of carbon in this catalyst and the details of the formation are highly speculative.

The influence of C-deposits on the operation of reforming catalysts has been noted by several researchers. Lang et al. [1972] showed that the rate of

dehydrocyclization of n-heptanes as well as the selectivies for isomerization and hydrogenolysis in the reactions of n-heptanes are dependent upon the ordering of the carbonaceous layer. In an investigation of ethylene hydrogenation on a Pt(111) surface, Weinberg et al. [1974] concluded that the carbonaceous layer is the catalytic site. Similar conclusions were also reached by Gardner and Hansen [1970] using a tungsten-stepped surface. Völter et al. [1981], in studying $PtSn/Al_2O_3$ and $PtPb/Al_2O_3$ catalysts, also pointed out that both C-deposits and the second metal are responsible for modified selectivies and activities of platinum sites.

**2. Coimpregnated $PtTe/Al_2O_3$ and $PtSb/Al_2O_3$**

Although coimpregnated $PtTe/Al_2O_3$ shows similar selectivity behavior to vapor-deposited $PtTe/Al_2O_3$, the formation of a stable PtTe cluster in the coimpregnated materials which is somehow different from that of vapor-deposited $PtTe/Al_2O_3$ is indicated by the differences in their stabilities and capacities for hydrogen adsorption. In addition, relatively stable alloys of platinum and tellurium on coimpregnated $PtTe/Al_2O_3$ must have been formed before the reaction experiments. Otherwise, a film of tellurium would have been visually observed on the downstream cold wall of the glass reactor

during the activation period and reaction experiments. Note that our experiments showed that elemental tellurium is not strongly adsorbed on $Al_2O_3$ at 400°C.

The kinetic results for the coimpregnated catalysts can be explained as follows. The increase in selectivity for isomerization and concurrent decrease in hydrocracking yield can result from either an increase in isomerization activity or a decrease in hydrocracking activity. $PtTe/Al_2O_3$ with low Te content falls into the former category; the isomerization activity increases while the cracking activity is about the same as $Pt/Al_2O_3$. The increase in isomerization activity is possibly caused by electron donation from tellurium as determined by the $^{12}CO$ stretching frequency. High-content tellurium catalysts and all $PtSb/Al_2O_3$ fall into the latter category, for which geometric effects appear to predominate. Alloying of platinum with tellurium or antimony dilutes the active platinum surface such that the ensemble size is reduced. Hydrocracking reactions typically take place on larger platinum ensembles than does isomerization; hydrocracking rates are therefore diminished. Dehydrogenation reactions are typically similar to isomerization reactions with respect to their sensitivity to electronic effects and insensitivity to

geometric effects. This assertion is borne out by the results of Table III-8.

A hypothesis is proposed to explain the relative importance of electronic and geometric effects for $PtTe/Al_2O_3$ with various tellurium concentrations. The phase diagram of the Pt-Te system [Gimpl et al., 1963] shows that phase separation of PtTe and $PtTe_2$ may occur when the tellurium concentration is between 50 to 67 at.%. $PtTe_2$ has an electrical resistivity of $3.85 \times 10^{-5}$ ohm-cm at 25°C, which is higher than that of PtTe and Pt, $2.07 \times 10^{-5}$ and $1.0 \times 10^{-5}$ ohm-cm respectively. Consequently, it is possible that the observation of an electronic effect at low tellurium content is due to the formation of a PtTe phase, in which platinum is chemically modified but more active for hydrogenation and isomerization. However, at high concentrations of tellurium (Te/Pt $\geq$ 0.26), $PtTe_2$ may be present as the larger fraction of the surface. It is doubtful that $PtTe_2$, with an electrical resistivity approaching that of tellurium or antimony, can possess much catalytic activity. Phase separation into active and inactive Pt/Te alloys can be considered as poisoning of platinum by tellurium and could be similar to a geometric effect for which the platinum surface is diluted into smaller ensembles. Barbier et

al. [1986] also used the dilution effect to account for the decrease in the rate of coking or hydrogenolysis reactions when $Pt/Al_2O_3$, $Ir/Al_2O_3$ or $PtIr/Al_2O_3$ catalysts was partially poisoned by sulfur, although they did not exclude other possibilities.

Electronic effects were not observed on any $PtSb/Al_2O_3$ catalyst, although it should be noted that the Sb/Pt ratios in all cases exceeded ≈0.10 and it is possible that lower ratios may include electronic effects as in the $PtTe/Al_2O_3$. The modifications in selectivity and activity for $PtSb/Al_2O_3$ resemble those of $PtTe/Al_2O_3$ with high tellurium content. Similar arguments presented previously for high-Te content $PtTe/Al_2O_3$ may therefore be rationalized for $PtSb/Al_2O_3$.

Another notable, though less significant, effect of alloying is the roughly constant yield to benzene, compared to $Pt/Al_2O_3$. Isomerization and aromatization reactions generally proceed through a common cyclic intermediate, adsorbed methylcyclopentane, when acidic supports are used. This has also been shown to be true for certain alloy systems [Coq and Figueras, 1984; O'Cinneide and Gault, 1975]. A number of investigators [Thoang et al., 1984; Eberly, 1979; Brignac and Swan, 1984; Völter et al., 1981; Davis et al., 1976] have found

that alloying with Sb, Bi, Te, Sn and Pb improves the yield to aromatics. The discrepancy between our results and their work may be an effect of the relatively non-acidic support used here, as it is generally believed that ring expansion from a five-member to a six-member ring requires the independent action of the metal and acidic centers of reforming catalysts [Sinfelt, 1964; Parera et al., 1986]. In fact, direct six-member ring closure, which occurs on the metal surface without involving acidic centers, is favored for metal catalysts on nonacidic supports [Davis, 1976; Dautzenberg and Platteeuw, 1970]. Because hydrogenolysis of methylcyclopentane to form 2-methylpentane and 3-methylpentane can occur on metal (platinum) sites [Barron et al., 1966; Corolleur et al., 1972], it is not surprising that metal alloy catalysts on nonacidic supports display higher yields to isomerized rather than aromatized products. In addition, it seems that direct six-member ring closure is not affected by the addition of post-transition metal elements, as indicated by the roughly constant yield to benzene.

## C. Mechanistic Studies of Isomerization and Hydrogenation Reaction

### 1. Carbon-13 Tracer Experiments

The role of tellurium and antimony in $PtTe/Al_2O_3$ and $PtSb/Al_2O_3$ has been discussed in the previous sections and briefly, the addition of a small amount of tellurium to $Pt/Al_2O_3$ modifies the electronic structure of platinum, whereas $PtTe/Al_2O_3$ of high tellurium content and $PtSb/Al_2O_3$ exhibit only geometric effects. Thus the elucidation of electronic and geometric effects on skeletal isomerization proceeds by the investigation of $PtTe/Al_2O_3$ (Te/Pt=0.06) and $PtSb/Al_2O_3$ (Sb/Pt=0.97). It is not possible to postulate another mechanism based on our limited amount of data. Instead, the results are explained using the various proposed mechanisms available in the literature.

Earlier exploratory studies on platinum catalyzed isomerization emphasized mainly the dependence on the metal particle size and the results were therefore explained more or less on the basis of geometrical crystallographic considerations. Examples of these are the work done by Corolleur et al. [1972], O'Cinneide and Gault [1975], and Diaz et al. [1983]. These authors compared poorly dispersed $Pt/Al_2O_3$ (loaded with at least 10 wt% Pt and comprised of large metal crystallites) with alloy catalysts such as $PtRu/Al_2O_3$ and $PtAu/Al_2O_3$, or with highly dispersed $Pt/Al_2O_3$ (0.2 wt% Pt). In this

work, the $Pt/Al_2O_3$ catalysts employed are already highly dispersed. The relative contributions of cyclic and bond shift mechanisms for the conversion of 2-methylpentane to 3-methylpentane and n-hexane obtained on our catalysts are also in good agreement with those reported in the literature for a highly dispersed $Pt/Al_2O_3$ catalyst [Corolleur et al., 1972; O'Cinneide and Gault, 1975]. These results indicate that the $Pt/Al_2O_3$ catalysts we prepared are comparable with highly dispersed $Pt/Al_2O_3$ (0.2 wt% Pt) catalysts prepared by other investigators.

The Pt function in $PtTe/Al_2O_3$ (Te/Pt=0.06) should remain highly dispersed since the small amount of tellurium only causes an electronic modification. For $PtSb/Al_2O_3$ (Sb/Pt=0.97) catalysts, the platinum surface area has probably been greatly reduced by the antimony. The isotopic dilution experiments also show a decrease in dipole-dipole coupling, which indicate that the mutual distance between active platinum sites has been increased, and these centers probably appear as isolated atoms. Many isomerization mechanisms requiring single or multiple contiguous platinum sites have been proposed to explain platinum catalyzed skeletal isomerization. A single site mechanism is more appropriate in our systems since platinum centers are well dispersed. This is also

consistant with our observations which indicates that the rate of isomerization is insensitive to geometric effects.

Reactive species with one and two platinum site(s) for $C_5$-cyclic isomerization have been discussed by Gault [1981] (see Figure I-8). According to Gault, a selective cyclic mechanism, which predominates in catalysts with large platinum crystallites, does not allow interconversion between 2-methylpentane and n-hexane. Hence, a nonselective cyclic mechanism, which occurs only on highly dispersed catalysts (as in our catalysts), must be responsible for the formation of n-hexane from 2-methylpentane in our studies. 3-methylpentane probably accompanies n-hexane through non-selective cyclic pathways though some may be formed through a selective cyclic pathway which may operate in parallel if there is a distribution of surface sites.

Of the four basic bond shift mechanisms, reviewed by Gault [1981] (Figure I-7), the Anderson-Avery and Muller-Gault mechanisms are less likely to be operative in our systems since they require a larger number of platinum atoms for the isomerization to occur. Although the Garin-Gault mechanism requires only a single platinum site, it involves carbon-carbon bond breaking/making and

a concurrent increase in hydrocracking products associated with an increase in bond shift mechanism after alloying should have been observed if the Garin-Gault mechanism is operative. However, after the addition of tellurium or antimony to $Pt/Al_2O_3$, no or insignificant increase in hydrocracking selectivity was observed. On the other hand, the isomerization mechanism of Rooney-Samman would not require an increase in hydrocracking activity concurrent with an increase in bond shift and therefore is more likely to be the predominant mechanism in both the tellurium and antimony systems.

According to the Rooney-Samman mechanism, the isomerization of 2-methylpentane to 3-methylpentane and n-hexane via bond shift can be depicted as

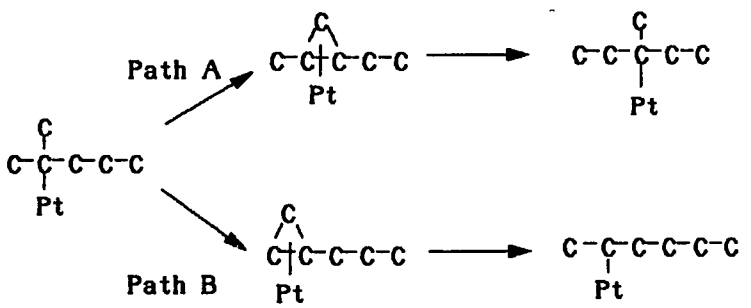


The carbonium-ion-like transient species in path A is probably much more stable than that in path B based on

thermodynamic viewpoints and the criteria for the stability of carbonium ions. Therefore, the yield to 3-methylpentane should be higher, in agreement with our findings. Catalysts with large platinum crystallites generally favor propyl shift over methyl shift in the formation of n-hexane from 2-methylpentane [O'Cinneide and Gault, 1975]. In these systems, the Anderson-Avery mechanism and the Muller-Gault mechanism may be more important in promoting isomerization via bond shift. Note that the Rooney-Samman mechanism can only promote methyl shift isomerization. We have observed a small amount of propyl shift over $Pt/Al_2O_3$ at 340°C and this activity is destroyed by addition of antimony, again indicating platinum dilution effects. Diaz et al. [1983] also found that methyl shift is more favorable than propyl shift when alloying $Pt/Al_2O_3$ with ruthenium. No methyl shift has been observed in the formation of n-hexane from 2-methylpentane, indicating that path B in the Rooney-Samman mechanism is insignificant under our reaction conditions. Path A of the Rooney-Samman mechanism is clearly preferred over the cyclic mechanism in the isomerization of 2-methylpentane to 3-methylpentane when tellurium or antimony modifiers are added to $Pt/Al_2O_3$.

With these observations concerning cyclic and bond shift mechanisms in hand, the fundamental question is why the addition of tellurium or antimony to platinum increases the relative contribution of the bond shift mechanism (Table III-14). The effect of tellurium on the bond strength of the chemisorbed species with the platinum sites is manifest. For the Rooney-Samman mechanism, the transient species is stabilized by lowering the energy of the antibonding orbital associated with one of the three-carbon-center orbitals in the transient species by interaction with the platinum d-orbitals [McKervey, et al., 1973]. The platinum d-orbital is in turn modified by electronic donation from tellurium to platinum as observed in the isotopic dilution experiments. Thus, we expect the observed electronic interaction to alter the rate of the isomerization reaction proceeding according to the Rooney-Samman mechanism. The non-selective cyclic mechanism does not depend on a similar intermediate and therefore, tellurium electronic interactions will not affect its rate to the same extent. A change in selectivity is therefore observed.

Since the nonselective cyclic mechanism and the Rooney-Samman bond shift mechanism require only single

platinum atoms, the increase of the latter by alloying of platinum with antimony can hardly be explained by geometric (surface dilution) effects. However, if our $Pt/Al_2O_3$ catalysts contain some relatively large platinum crystallites which form 3-methylpentane via the selective cyclic mechanism, these sites could be destroyed by surface dilution resulting in a relative increase in the rate of bond shift. Another possibility is that a highly diluted Pt surface indeed favors the Rooney-Samman mechanism as other investigators have suggested [Van Schaik et al., 1975], although a detailed explanation is not known.

**2. Reaction of Benzene and Deuterium**

Deuterium levels near equilibrium in cyclohexane on all catalysts clearly show that carbon-hydrogen bond breaking/making is extremely fast compared to reactions such as hydrogenolysis and isomerization which require carbon-carbon bond breaking/making. This reaction is so rapid that diffusional effects probably mask the surface reaction and no useful kinetic data may be extracted. Only slight differences in deuterium levels and deuterium distribution have been detected and given that diffusional effects are probably in effect, no other firm conclusions may be drawn.

# V. Conclusions and Recommendations

## A. Conclusions

Bimetallic reforming catalysts have played an important role in petroleum refinery processes over the last two decades. Tellurium and antimony are potential modifiers which, when alloyed with platinum, may be useful in improving liquid yields or ultimate octane numbers in catalytic reforming operations. $PtTe/Al_2O_3$, prepared by vapor deposition of elemental tellurium onto $Pt/Al_2O_3$ and coimpregnation of platinum and tellurium onto $Al_2O_3$, and $PtSb/Al_2O_3$, also prepared by coimpregnation, were characterized using various methods and the results were compared with $Pt/Al_2O_3$. The conclusions can be summarized as follows.

1. The addition of tellurium or antimony to platinum supported on nonacidic alumina decreases the overall catalytic activity, but increases the isomerization selectivity and reduces the selectivity to hydrocracking products.

2. Alloy formation on vapor-deposited $PtTe/Al_2O_3$ may require carbonaceous deposits to achieve an enhancement in selectivity. The resulting alloy system behaves differently from coimpregnated $PtTe/Al_2O_3$. Vapor-deposited $PtTe/Al_2O_3$, compared to coimpregnated $Pt/Al_2O_3$,

showed no or insignificant adsorption capacity for hydrogen and tellurium was relatively unstable on the catalytic surface during reaction runs.

3. For coimpregnated catalysts, electronic effects are recognizable in samples of low tellurium content and geometric effects are recognizable in all others. An electronic effect caused by electron donation from tellurium to platinum increases the specific activities of isomerization and dehydrogenation reactions for catalysts of low Te/Pt ratio (0.06). A geometric effect, which may arise from partial poisoning of the platinum surface by added tellurium or antimony, decreases the specific activity of the hydrocracking reaction, and is the dominant effect when the post-transition metal/Pt ratio exceeds ≈0.1. Although their modes of action differ, both effects result in improved selectivity to desired products. The kinetic data are in agreement with results obtained using FTIR and the isotopic dilution method.

4. Isomerization reactions of n-hexane proceed through a five-member ring compound, adsorbed methylcyclopentane. The ring expansion of the five-member to a six-member ring cannot occur to an appreciable extent because of a relatively non-acidic support. Direct

six-member ring closure is probably responsible for the formation of benzene and this mechanism is not affected by the addition of post-transition elements.

5. Isomerization reactions of 2-methylpentane (2-$^{13}$C) and 2-methylpentane (5-$^{13}$C) show that cyclic and bond shift mechanisms can well describe the isomerization reactions of 2-methylpentane to 3-methylpentane and n-hexane. n-Hexane is formed primarily by a $C_6$ cyclic mechanism on the highly diluted platinum surface. Cyclic and bond shift mechanisms are both responsible for the formation of 3-methylpentane, while the latter mechanism becomes more favorable after the addition of tellurium or antimony to $Pt/Al_2O_3$. The mechanism of isomerization is best described by the Rooney-Samman mechanism for bond shift and a non-selective $C_6$ ring opening for the cyclic mechanism.

6. The results from the reaction of benzene and deuterium at 110°C and 300°C indicate a very fast reversible surface addition reaction (deuteration) and rapid single and multiple exchange of deuterium with benzene.

## B. Recommendations

1. Since this research has focused on the catalytic effects of tellurium or antimony on the platinum function alone, the effects of chlorine, which is generally added to enhance the acidity of the support in commercial reforming catalysts, on the catalytic behavior of the modified catalysts should be examined.

2. This work indicates that the addition of tellurium or antimony to $Pt/Al_2O_3$ suppresses hydrogenolysis reactions. Since $PtRe/Al_2O_3$ and $PtIr/Al_2O_3$ are used industrially and these materials promote hydrogenolysis, a study of the effects of tellurium and antimony on these alloy systems may be warranted.

3. The long term activity (stability) of the modified catalysts cannot be easily determined in the recirculation batch reactor. A continuous flow reactor together with catalyst carbon content analysis should be employed in order to obtain this information.

4. Commercial reforming reactions are usually operated at relatively high pressures of 34 to 50 atm and at temperatures of 480 to 500°C. Catalysts under these reaction conditions should be studied in order to evaluate their practical use as reforming catalysts.

5. Structural information related to the alloy formation, such as metal crystallite size and the

oxidation state of the metal components, should be obtained using surface sensitive spectroscopies.

6. The investigation of other post-transition elements may provide a generalized theory on the effects of these modifiers on reforming catalysts.

## Literature Cited

Adams, Johnson, Wilcox, "Laboratory Experiments in Org. Chemistry", Sixth Edition, 1970. pp. 192-194.

Adkins, S. R., and Davis, B. H., J. Catal. 89, 371 (1984).

Anderson, J. R., and Kemball, C., Adv. Catal, 9, 51 (1957).

Anderson, J. R., and Baker, B. G., (a) Nature (London), 187, 937 (1960); (b) Proc. R. Soc. London, Ser. A, 271, 402 (1963).

Anderson, J. R., and Avery, N. R., J. Catal. 5, 446 (1966).

Apesteguia, C. R., Brema, C. E., Garetto, T. F., Borgna, A., and Parera, J. M., J. Catal. 89, 52 (1984).

Bacaud, R., and Bussière, P., J. Catal. 69, 399 (1981).

Barbier, J., and Marecot, P., J. Catal. 102, 21 (1986).

Barron, Y., Cornet, D., Maire, G., and Gault, F.G., J.Catal. 2, 152 (1963).

Barron, Y., Maire, G., Muller, J. M., and Gault, F.G., J. Catal. 5, 428 (1966).

Bastein, A. G. T. M., Toolenaar, F. J. C. M., and Ponec, V., J. Catal. 90, 88 (1984).

Benesi, H. A., Curtis, R. M., and Studer, H. P., J. Catal. 10, 328 (1968).

Biloen, P., Dautzenberg, F. M., and Sachtler, W. M. H. J. Catal. 50, 77 (1977).

Biloen, P., Helle, J. N., Verbeek, H., Dautzenberg, F. M., and Sachtler, W. M. H., J. Catal. 63, 112 (1980).

Bird, R. B., Stewart, W. E., and Lightfoot, E. N. "Transport Phenomena", Wiley, New York (1960), p. 510-511.

Blakely, D. W., and Somorjai, G. A., J. Catal. 42, 181 (1976).

Brignac, D. G., Swan, G. A., U.S. Patent 4,485,188 (1984).

Carter, J. L., McVicker, G. B., Weissman, W., Kmak, W. S., and Sinfelt, J. H., Appl. Catal. 3, 327 (1982).

Castro, A., Scalza, O., Benvenuto, E., Baronetti, G., and Parera, J., Catal. 69, 222 (1981).

Chambellan, A., Dartigues, J. M., Corolleur, C., and Gault, F. G., Nouv. J. Chim. 1, 1 (1977).

Christoffel, E. G., and Paál, Z., J. Catal. 73, 30 (1982).

Coq, B., and Figueras, F., J. Catal. 85, 197 (1984).

Corolleur, C., corolleur, S., and Gault, F. G., J. Catal. 24, 385 (1972).

Coughlin, R. W., Hasan, A., and Kawakami, K., J. Catal. 88, 163 (1984).

Dartigues, J. M., Chambellan, A., and Gault, F. G., J. Am. Chem. Soc., 98, 856 (1976).

Dautzenberg, F. M., and Platteeuw, J. C., J. Catal., 19, 41 (1970).

Dautzenberg, F. M., and Platteeuw, J. C., J.Catal., 24, 364 (1972).

Davis, B. H., and Venuto, P. B., J. Catal. 15, 363 (1969).

Davis, B. H., J. Catal. 42, 376 (1976).

Davis, B. H., Westfall, G. A., Watkins, J., and Pezzanite, J., J. Catal. 42, 247 (1976).

Decius, J. C., J. Chem. Phys. 23, 1290 (1955).

Dejongste, H. C., Kuijers, K. J., and Ponec, V.,"Proceedings, 6th International Congress on Catalysis, London, 1976, " p.915.

Diaz, G., Garin, F., Maire, G., J. Catal. 82, 13-25 (1983).

Dietz, W. A., J. Gas. Chrom. 5, 68 (1967).

Dorling, T. A., Burlace, C. J., and Moss, R. L., J. Catal. 12, 207 (1968).

Dorling, T. A., Lynch, B. W. J., and Moss, R. L., J. Catal. 20, 190 (1971).

Eberly, P. E., Jr., U.S. Patent, 4,169,785 (1979) and 4,149,991 (1979).

Farkas, A., and Farkas, L., Trans. Faraday Soc. 35, 906 (1939).

Freel, J., J. Catal., 25, 149 (1972).

Gardner, N. C., and Hansen, R. S., J. Phys. Chem. 74, 3298 (1970).

Garin, F., and Gault, F. G., J. Am. Chem. Soc., 97:16, 4466 (1975).

Gault, F. G., Advan. in Catal. 33, 1 (1981).

Gil'debrand, E. I., Int. Chem. Eng., 6, 449 (1966).

Gimpl, M. L., Nelson, C. E., and Fuschillo, N., Trans. Amer. Soc. Metal 56, 209 (1963).

Goldwasser, J., Arenas, B., Bolivar, C., Castro, G., Bodriguez, A., Fleitas, A., and Giron, J., Catal. 100, 75 (1986).

Haensel, V., U.S. Patents 2,479,109 and 2,479,110 (1949).

Hammaker, R. M., Francis, S. A., and Eischens, R. P., Spectrochimica Acta, Vol. 21, 1295 (1965).

Horiuti, J., and Polanyi, M., Nature 132, 819, 931 (1933).

Hosten, L. H., and Froment, G. F., Ind. Eng. Chem. Prod. Res. Dev. 10, 280 (1971).

Kazanskii, B. A., Fadeev, V. S., and Gostunskaya, I. V., Izv. Akad. Nauk SSSR, Ser. Khim. 677 (1971).

Kemball, C., Advan. Catal. 11, 223 (1959).

Kirlin, P. S., Strohmeier, B. R., and Gates, B. C., J. Catal. 98, 308-316 (1986).

Kluksdahl, H. E., U.S. Patent 3,415,737 (1968).

Lang , B., Joyner, R. W., and Somorjai, G. A., J. Catal. 27, 405 (1972].

Lanh, H. D., Thoang, H. S., Lieske, H., and Völter, J., Applied Catalysis, 11, 195 (1984).

Ledoux, P., Hsia, Y. S., and Kovenklioglu, S., J. Catal. 98, 367 (1986).

Lester, G. R., J. Catal. 13, 187 (1969).

Lieske, H., and Völter, J., J. Catal. 90, 96 (1984).

Maurel, R., Leclercq, G., and Barbier, J., J. Catal. 37, 324 (1975).

Mc Kervey, M. A., Rooney, J. J., Samman, N. G., J. Catal. 30, 330 (1973).

Mills, G. A., Heinemann, H., Milliken, T. H., and Oblad, A. G., Ind. Eng. Chem., 45, 134 (1953).

Muller, A. C., Engelhard, P. A., and Weisang, J. E., J. Catal. 56, 65 (1979).

Muller, J. M., and Gault, F. G., Bull. Soc. Chim. Fr. 416 (1970).

Muller, J. M., and Gault, F. G., Proc. Int. Congr. Catal. 4th, 1968 Paper No. 15 (1971).

Muller, J. M., and Gault, F. G., J. Catal. 24, 361 (1972).

O'Cinneide, A., and Gault, F. G., J. Catal. 37, 311 (1975).

Palazov, A., Bonev, Ch., Kadinov, G., Shopov, D., Lietz, G., and Völter J., J. Catal. 71, 1-8 (1981).

Parera, J. M., Beltramini, J. N., Querini, C. A., Martinelli, E. E., Churin, E. J., Aloe, P. E., and Figoli, N. S., J. Catal. 99, 39 (1986).

Persson, B. N. J., and Ryberg, R., Solid State Commun. 36, 613 (1980); Persson, B. N. J., and Ryberg, R. Phys. Rev. B 24, 6954 (1981).

Ponec, V., and Sachtler, M. W. H., J. Catal. 24, 250 (1972).

Rooney, J. J., J. Catal. 2, 52 (1963).

Rooney, J. J., and Webb, G., J. Catal. 3, 488 (1964).

Sachtler, W. M. H., J. Mol. Catal. 25, 1 (1984).

Sexton, B. A., Hughes, A. E., and Foger, K., J. Catal. 88, 466 (1984).

Sinfelt, J. H., Advan. Chem. Eng. 5, 37 (1964).

Sinfelt, J. H., Carter, J. L., and Yates, D. J. C., J. Catal. 24, 283 (1972).

Sinfelt, J. H., Advan. in Catal. 23, 91 (1973).

Soma-Noto, Y., and Sachtler, W. M. H., J. Catal., 32, 315 (1974).

Somorjai, G. A., in "Principles of Surface Chemistry", pp. 56-64, Prentice-Hall, 1972.

Spenadel, L., and Boudart, M., J. Phys. Chem. 64, 204 (1960).

Stoop, F., Toolenaar, F. J. C. M., and Ponec, V., J. Catal. 73, 50 (1982).

Taylor, T.I., "Catalysis" (P.H. Emmett, ed. ), Vol. V. Reinhold, New Yourk, 1957.

The Sadtler standard Spectra, 100 MHz $^{13}$C-NMR, Sadtler Research Laboratories (1969-).

Thoang, H. S., Lanh. H. D., Völter, S., "Proceedings, 8th International Congress on Catalysis, Berlin, 1984, " p.II-509.

Toolenaar, F. J. C. M., Stoop, F., and Ponec, V., J. Catal. 82, 1 (1983).

Van Schaik , J. R. H., Dessing, R. P., and Ponec, V., J. Catal. 38, 273 (1975).

Völter, J., Lietz, G., Uhlemann, M., and Hermann, M., J. Catal. 68, 42 (1981)

Voorhies, A., and Bryant, P. A., AIChE J. 14, 832 (1968).

Weinberg, W. H., Deans, H. A., and Merrill, R. P., Surf. Sci. 41, 312 (1974).

Williams, F. L., and Nason, D., Surf. Sci. 45, 377 (1974).

## Appendix A. Dead Volume Determination in the Volumetric Adsorption Apparatus

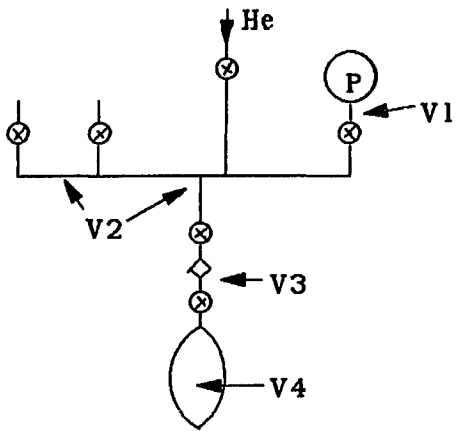


wt. of test tube + $H_2O$ : 57.6383g
wt. of test tube : 46.0309g

wt. of $H_2O$ : 11.6274g

Temp ($H_2O$) : 25°C
Density ($H_2O$) : 0.99708

Vol. of test tube, $V_4$ = 11.6274/0.99708
= 11.66 cc

He expansion : $P_1V_1 = P_2(V_1+V_2)$

| | P (torr) | $V_2/V_1$ |
|---|---|---|
| $87.06V_1 = 64.52\ (V_1+V_2)$ | 87.06 ⟶ 64.52 | 0.3493 |
| $64.52V_1 = 47.78\ (V_1+V_2)$ | 64.52 ⟶ 47.78 | 0.3504 |
| $47.78V_1 = 35.36\ (V_1+V_2)$ | 47.78 ⟶ 35.36 | 0.3512 |
| $35.36V_1 = 26.15\ (V_1+V_2)$ | 35.36 ⟶ 26.15 | 0.3525 |
| $26.15V_1 = 19.33\ (V_1+V_2)$ | 26.15 ⟶ 19.33 | 0.3529 |
| $19.33V_1 = 14.28\ (V_1+V_2)$ | 19.33 ⟶ 14.28 | 0.3533 |
| $14.28V_1 = 10.55\ (V_1+V_2)$ | 14.28 ⟶ 10.55 | 0.3536 |
| $10.55V_1 = 7.79\ (V_1+V_2)$ | 10.55 ⟶ 7.79 | 0.3543 |
| $7.69V_1 = 5.75\ (V_1+V_2)$ | 7.79 ⟶ 5.75 | 0.3548 |

He expansion : $P_1V_1 = P_2(V_1+V_2) = P_3(V_1+V_2+V_3)$

$55.23V_1 = 40.88(V_1+V_2) = 33.32(V_1+V_2+V_3) \longrightarrow 0.8708V_2$
$40.49V_1 = 29.95(V_1+V_2) = 29.95(V_1+V_2+V_3) \longrightarrow 0.8705V_2$

$\longrightarrow V_3 = 0.871V_1$

$P_1(V_1+V_2+V_3) = P_2(V_1+V_2+V_3+V_4)$

$27.06(V_1+V_2+V_3) = 15.87(V_1+V_2+V_3+11.66)$

$V_1 = 9.99$ cc
$\longrightarrow V_2 = 3.53$ cc
$V_3 = 3.07$ cc

$21.13(V_1+V_2+V_3) = 12.39(V_1+V_2+V_3+11.66)$

$V_1 = 9.97$ cc
$\longrightarrow V_2 = 3.52$ cc
$V_3 = 3.06$ cc

$45.54(V_1+V_2+V_3) = 26.73(V_1+V_2+V_3+11.66)$

$V_1 = 10.04$ cc
$\longrightarrow V_2 = 3.53$ cc
$V_3 = 3.07$ cc

The average of $V_2 = 3.53$ cc

$V_1$ was then calculated as a function of pressure. Since the pressure gauge is a diaphragm type, we expect slight expansion at higher pressures.

| P (torr) | $V_1$ (cc) |
|---|---|
| 87.06 —> 64.52 | 10.11 |
| 64.52 —> 47.78 | 10.07 |
| 47.78 —> 35.36 | 10.05 |
| 35.36 —> 26.15 | 10.01 |
| 26.15 —> 19.33 | 10.00 |
| 19.33 —> 14.28 | 9.99 |
| 14.28 —> 10.55 | 9.98 |
| 10.55 —> 7.79 | 9.96 |
| 7.79 —> 5.75 | 9.95 |

## Appendix B.
## Calculation of Effectiveness Factor

Data:

| | |
|---|---|
| Reactor Volume, $V_R$ | : 580 cc |
| Catalyst Wt., $Pt/Al_2O_3$ | : 0.02 g |
| Particle SizE | : 0.063 cm (average of 20-40 mesh particles) |
| Void Volume, $V_g$ | : 0.71 cc/g |
| Surface Area, $S_g$ | : 215 $m^2/g$ |
| Bulk Density | : 0.577g/cc |
| Initial Rate, n-$C_6$ at 400°C | : $1.41 \times 10^{-7}$ mols/s |
| Initial Rate, Cy-$C_6$ at 300°C | : $5.77 \times 10^{-7}$ mols/s |
| Initial Condition | : 25 torr hydrocarbon, 440 torr $H_2$, 335 torr He |

According to Weisz-Prater Criterion

$$\frac{(r_v)_{obs} L^2}{D_e C_s^s} = \Phi = \eta \phi^2$$

where $r_v$ = observed reaction rate
$L$ = characteristic particle size
= R/3 for a spherical catalyst pellet
$R$ = Radius of the pellet
$D_e$ = effective diffusivity
$C_s^s$ = surface concentration
$\eta$ = effective factor
$\phi$ = Thiele modulus

if $\Phi << 1$, there are no pore diffusion limitations

1. n-$C_6$ reaction

Surface composition of n-hexane:

$$C_s^s = \frac{P}{RT} = 1.345 \times 10^{-6} \frac{mols}{cm^3}$$

The observed rate:

$$r_v = \frac{r_0}{V_{pellet}}$$

$$V_{pellet} = \frac{0.02}{0.577} = 0.0347 cm^3$$

$$r_v = \frac{1.41 \times 10^{-7}}{0.0347}$$

$$= 4.063 \times 10^{-6} \frac{mols}{cm^3 s}$$

Assuming a spherical catalyst pellet of ratius R

$$L = \frac{(0.063)/2}{3} = 0.015 cm$$

The pore radius

$$\bar{r} = \frac{2V_g}{S_g} = 6.6 \times 10^{-9} cm$$

In order to calculate the effective diffusivity, the bulk diffusivity was first approximated by the Chapman-Enskog equation,

$$D_{A,B} = \frac{0.001858\left[T^3\left(\frac{1}{M_A} + \frac{1}{M_B}\right)\right]^{1/2}}{P\sigma_{AB}^2 \Omega_D}$$

where $D_{A,B}$ [=] $cm^2 sec^{-1}$, T [=] K, $M_1$ & $M_2$ [=] molecular weights, P [=] atm, $\sigma_{AB}$ = collision integral [=] Å, and $\Omega_D$ is a dimensionless function of T and the Lennard-Jones parameters $\sigma_{AB}$ and $\varepsilon_{AB}$.

In using this equation, the physical properties of B were defined as the average of those for $H_2$ and He.

T = 673K
$M_A$ = 86, $M_B$ = 3
P = 1 atm
$\sigma_{AB}$ = 4.305
$\Omega_D$ = 0.78

$$D_{A,B} = \frac{0.001858\left[673^3\left(\frac{1}{86} + \frac{1}{3}\right)\right]^{1/2}}{(1)(4.305)^2(0.78)}$$

$$= 1.318 cm^2/s$$

The Knudson diffusivity

$$D_K = 9.7 \times 10^3 \bar{r} \sqrt{\frac{T}{A}}$$

in which r is the average pore radius

$$\bar{r} = \frac{2V_g}{S_g} = 6.6 \times 10^{-7} cm$$

$$D_K = 9.7 \times 10^3 (6.6 \times 10^{-7}) \sqrt{\frac{673}{86}}$$

$$= 0.0179 cm^2/s$$

The effective diffusivity was then estimated

$$D_e = \left( \frac{1}{D_{AB}} + \frac{1}{D_K} \right)^{-1} \left( \frac{\epsilon_g}{\tau} \right)$$

where $\tau$ is the tortuosity factor and was assumed to be equal to 3

$$D_e = \left( \frac{1}{(1.318)} + \frac{1}{(0.0179)} \right)^{-1} \left( \frac{0.7}{3} \right)$$

$$= 4.12 \times 10^{-3} cm^2/s$$

From the magnitudes of the diffusion coefficients, it is evident that the majority of the mass transport will occur by Knudsen diffusion.
Substitution of the forgoing values into Eqn A.1 gives

$$\Phi = \frac{(4.063 \times 10^{-6})(0.0105)^2}{(4.12 \times 10^{-3})(1.345 \times 10^{-6})}$$

$$= 0.081$$

Since

$$\Phi = \eta \phi^2 = \left( \frac{\tanh \phi}{\phi} \right) \phi^2$$

$$= (\tanh \phi) \phi$$

$$= 0.081$$

$$\phi = 0.289$$

The effectiveness factor for $Pt/Al_2O_3$ for $n\text{-}C_6$ reaction at 400°C

$$\eta = \frac{\tanh\phi}{\phi}$$

$$= \frac{0.281}{0.289}$$

$$= 0.973$$

$$\cong 1$$

**2. For cyclohexane reaction at 300°C:**
**The observed rate,**

$$r_v = \frac{5.77 \times 10^{-7}}{0.0347}$$

$$= 1.663 \times 10^{-5} \frac{mols}{cm^3 s}$$

**The binary bulk diffusivity was found to be**

$$D_{A,B} = \frac{0.001858\left[573^3\left(\frac{1}{84}+\frac{1}{3}\right)\right]^{1/2}}{(1)(4.396)^2(0.78)}$$

$$= 0.993 cm^2/s$$

**The Knudsen diffusivity**

$$D_K = 9.7 \times 10^3 (6.6 \times 10^{-7}) \sqrt{\frac{573}{84}}$$

$$= 0.0167 cm^2/s$$

**The effective diffusivity**

$$D_e = \left(\frac{1}{0.993} + \frac{1}{0.0167}\right)^{-1} \left(\frac{0.7}{3}\right)$$

$$= 3.832 \times 10^{-3} cm^2/s$$

$$\Phi = \frac{(1.663 \times 10^{-5})(0.0105)^2}{(3.832 \times 10^{-3})(1.345 \times 10^{-6})}$$

$$= 0.356$$

$$= (\tanh\phi)\phi$$

$\phi = 0.634$

**The effective factor for $Pt/Al_2O_3$ for cyclohexane reaction at 300°C**

$$\eta = \frac{0.561}{0.634}$$

$$\cong 0.88$$

Appendix C. Product Distribution Data at 30% Conversion of n-Hexane.

1. $PtTe/Al_2O_3$ (Vapor Deposition, Te/Pt = 0.37, Carrier Gas = He) [a]catalyst at 400°C.

| | [b]1st | 2nd | 3rd | 4th | 5th |
|---|---|---|---|---|---|
| [c]Time | 77 | 96 | 105 | 101 | 115 |
| C1 | 0.44 | 0.17 | ≈0.00 | 0.14 | 0.22 |
| C2 | 0.77 | 0.60 | 0.59 | 0.55 | 0.54 |
| C3 | 1.78 | 1.25 | 1.09 | 0.97 | 0.90 |
| i-C4 | ≈0.00 | 0.20 | 0.35 | 0.35 | 0.37 |
| n-C4 | 1.47 | 0.97 | 0.80 | 0.70 | 0.69 |
| i-C5 | 0.16 | ≈0.00 | ≈0.00 | 0.21 | 0.28 |
| n-C5 | 2.00 | 0.65 | 0.57 | 0.47 | 0.52 |
| 2-MP | 8.92 | 12.20 | 12.21 | 11.73 | 12.41 |
| 3-MP | 5.25 | 6.60 | 7.59 | 7.97 | 7.19 |
| MCP | 7.00 | 6.01 | 5.30 | 5.26 | 5.58 |
| Benzene | 2.21 | 2.39 | 1.55 | 1.44 | 1.30 |
| % Conv | 30.0 | 30.0 | 30.0 | 30.0 | 30.0 |

[a] Catalyst, 0.1 g, 0.7 wt% Pt.

[b] Test number.

[c] Time to reach 30% conversion, min.

2. $PtTe/Al_2O_3$ (Vapor Deposition, Te/Pt = 0.24, Carrier Gas = He) [a]catalyst at 400°C.

| | [b]1st | 2nd | 3rd | 4th |
|---|---|---|---|---|
| [c]Time | 110 | 95 | 77 | 97 |
| C1 | 0.51 | 0.20 | 0.16 | 0.24 |
| C2 | 0.82 | 0.72 | 0.64 | 0.99 |
| C3 | 1.55 | 1.51 | 1.40 | 1.30 |
| i-C4 | ≈0.00 | ≈0.00 | ≈0.00 | ≈0.00 |
| n-C4 | 1.42 | 1.25 | 1.16 | 1.03 |
| i-C5 | 0.13 | ≈0.00 | ≈0.00 | ≈0.00 |
| n-C5 | 1.87 | 1.33 | 0.94 | 0.99 |
| 2-MP | 11.16 | 10.61 | 12.01 | 12.50 |
| 3-MP | 6.49 | 6.28 | 7.11 | 7.20 |
| MCP | 3.40 | 4.82 | 4.50 | 3.80 |
| Benzene | 2.72 | 3.28 | 2.10 | 2.00 |
| % Conv | 30.0 | 30.0 | 30.0 | 30.0 |

[a] Catalyst, 0.1 g, 0.7 wt% Pt.

[b] Test number.

[c] Time to reach 30% conversion, min.

3. $PtTe/Al_2O_3$ (Vapor Deposition, Te/Pt = 0.38, Carrier Gas = $H_2$) [a]catalyst at 400°C.

| | [b]1st | 2nd | 3rd | 4th |
|---|---|---|---|---|
| [c]Time | 38 | 143 | 107 | 140 |
| C1 | 0.43 | 0.18 | 0.17 | 0.10 |
| C2 | 0.94 | 0.60 | 0.81 | 0.88 |
| C3 | 3.03 | 1.37 | 1.51 | 1.76 |
| i-C4 | ≈0.00 | 0.27 | 0.44 | 0.50 |
| n-C4 | 1.65 | 0.93 | 1.02 | 1.25 |
| i-C5 | ≈0.00 | 0.26 | ≈0.00 | ≈0.00 |
| n-C5 | 2.04 | 0.59 | 0.75 | 0.69 |
| 2-MP | 6.95 | 9.43 | 9.22 | 9.54 |
| 3-MP | 4.17 | 6.36 | 5.48 | 5.66 |
| MCP | 6.33 | 7.74 | 7.93 | 7.50 |
| Benzene | 4.38 | 2.26 | 2.68 | 2.12 |
| % Conv | 30.0 | 30.0 | 30.0 | 30.0 |

[a] Catalyst, 0.1 g, 0.7 wt% Pt.

[b] Test number.

[c] Time to reach 30% conversion, min.

4. $PtTe/Al_2O_3$ (Vapor Deposition, Te/Pt = 0.40, Carrier Gas = [d]Re) [a]catalyst at 400°C.

| | [b]1st | 2nd | 3rd |
|---|---|---|---|
| [c]Time | 325 | 375 | 365 |
| C1 | ≈0.00 | ≈0.00 | ≈0.00 |
| C2 | 0.59 | 0.53 | 0.66 |
| C3 | 0.95 | 0.98 | 0.98 |
| i-C4 | 0.49 | 0.50 | 0.60 |
| n-C4 | 0.61 | 0.65 | 0.66 |
| i-C5 | ≈0.00 | ≈0.00 | ≈0.00 |
| n-C5 | 0.36 | 0.44 | 0.48 |
| 2-MP | 11.62 | 11.55 | 11.45 |
| 3-MP | 6.87 | 6.55 | 6.68 |
| MCP | 6.62 | 6.29 | 6.80 |
| Benzene | 1.87 | 2.51 | 1.70 |
| % Conv | 30.0 | 30.0 | 30.0 |

[a] Catalyst, 0.1 g, 0.7 wt% Pt.

[b] Test number.

[c] Time to reach 30% conversion, min.

[d] A "reforming" gas mixture consisting of 25 torr n-hexane, 440 torr $H_2$, and He to 800 torr.

5. $PtTe/Al_2O_3$ (Vapor Deposition, Te/Pt = 0.14, Carrier Gas = [d]Re) [a]catalyst at 400°C.

| | [b]1st | 2nd | 3rd | 4th | 5th |
|---|---|---|---|---|---|
| [c]Time | 350 | 340 | 376 | 285 | 280 |
| C1 | 0.09 | 0.18 | 0.16 | 0.18 | 0.23 |
| C2 | 0.42 | 0.53 | 0.59 | 0.67 | 0.74 |
| C3 | 1.20 | 1.05 | 1.85 | 2.25 | 2.21 |
| i-C4 | ≈0.00 | ≈0.00 | ≈0.00 | ≈0.00 | ≈0.00 |
| n-C4 | 0.70 | 0.97 | 1.20 | 1.26 | 1.38 |
| i-C5 | 0.12 | ≈0.00 | ≈0.00 | ≈0.00 | ≈0.00 |
| n-C5 | 0.45 | 0.70 | 0.70 | 0.84 | 1.04 |
| 2-MP | 13.79 | 11.56 | 11.17 | 9.24 | 9.17 |
| 3-MP | 8.11 | 7.52 | 7.53 | 6.33 | 6.13 |
| MCP | 3.90 | 5.53 | 5.42 | 6.76 | 6.85 |
| Benzene | 1.23 | 1.87 | 1.38 | 2.44 | 2.25 |
| % Conv | 30.0 | 30.0 | 30.0 | 30.0 | 30.0 |

[a] Catalyst, 0.1 g, 0.7 wt% Pt.

[b] Test number.

[c] Time to reach 30% conversion, min.

[d] A "reforming" gas mixture consisting of 25 torr n-hexane, 440 torr $H_2$, and He to 800 torr.

6. $PtTe/Al_2O_3$ Catalysts (Coimpregnation).

| Te/Pt | 0.00 | 0.06 | 0.23 | 0.76 | 1.2 |
|---|---|---|---|---|---|
| wt. cat. (mg) | 20 | 20 | 100 | 200 | 200 |
| [a] time | 43 | 40 | 39 | 51 | 80 |
| C1 | 0.88 | 0.52 | 0.57 | 0.75 | 0.52 |
| C2 | 1.25 | 0.58 | 0.71 | 0.97 | 1.37 |
| C3 | 2.78 | 1.65 | 1.82 | 1.63 | 1.89 |
| i-C4 | ≈0.00 | 0.09 | ≈0.00 | 0.34 | 1.17 |
| n-C4 | 2.30 | 1.15 | 1.36 | 1.19 | 1.40 |
| i-C5 | 0.22 | 0.28 | 0.23 | 0.24 | 0.59 |
| n-C5 | 3.56 | 2.04 | 2.08 | 1.94 | 1.47 |
| 2-MP | 4.60 | 7.38 | 6.98 | 7.87 | 6.98 |
| 3-MP | 2.62 | 4.23 | 4.23 | 4.66 | 4.31 |
| MCP | 6.0 | 6.6 | 6.8 | 6.4 | 6.3 |
| Benzene | 5.8 | 5.5 | 5.2 | 4.0 | 4.0 |
| % Conv. | 30.0 | 30.0 | 30.0 | 30.0 | 30.0 |

[a] Time to reach 30% conversion, min.

7. $PtSb/Al_2O_3$ catalysts (Coimpregnation).

| Te/Pt | 0.00 | 0.14 | 0.41 | 0.69 | 0.97 | 1.24 |
|---|---|---|---|---|---|---|
| wt. cat. (mg) | 20 | 50 | 50 | 50 | 50 | 50 |
| [a] time | 43 | 44 | 70 | 108 | 115 | 120 |
| C1 | 0.88 | 0.38 | 0.41 | 0.31 | 0.36 | 0.30 |
| C2 | 1.25 | 0.64 | 0.59 | 0.57 | 0.55 | 0.51 |
| C3 | 2.78 | 1.24 | 1.32 | 1.35 | 1.34 | 1.31 |
| i-C4 | ≈0.00 | ≈0.00 | 0.12 | ≈0.00 | ≈0.00 | ≈0.00 |
| n-C4 | 2.30 | 1.09 | 0.98 | 0.90 | 1.10 | 0.99 |
| i-C5 | 0.22 | ≈0.00 | 0.32 | 0.11 | 0.14 | 0.14 |
| n-C5 | 3.56 | 1.75 | 1.67 | 1.31 | 1.60 | 1.25 |
| 2-MP | 4.60 | 7.92 | 8.46 | 9.20 | 8.55 | 8.63 |
| 3-MP | 2.62 | 4.82 | 5.03 | 6.15 | 5.16 | 5.29 |
| MCP | 6.0 | 6.8 | 6.7 | 6.6 | 6.8 | 7.4 |
| Benzene | 5.8 | 5.3 | 4.4 | 3.5 | 4.4 | 4.2 |
| % Conv. | 30.0 | 30.0 | 30.0 | 30.0 | 30.0 | 30.0 |

[a] Time to reach 30% conversion, min.

## Appendix D. Raw Data for $^{13}C$-NMR Experiments.

### 1. 2-MP (2-$^{13}C$) Isomerization on $Pt/Al_2O_3$ at 290°C.

| Position (ppm) | Area |
|---|---|
| 14.26 | 0.39 |
| 14.34 | 0.56 |
| 20.51 | 1.01 |
| 22.24 | 0.64 |
| 22.73 | 1.78 |
| 22.94 | 1.21 |
| 27.40 | 1.33 |
| 27.43 | |
| 27.76 | |
| 28.09 | 100.00 |
| 28.13 | |
| 29.15 | 0.41 |
| 34.61 | 1.31 |
| 36.19 | 1.03 |
| 41.12 | 0.53 |
| 41.81 | 0.46 |

2. 2-MP (2-$^{13}$C) Isomerization on $Pt/Al_2O_3$ at 340°C.

| Position (ppm) | Area |
|---|---|
| 14.28<br>14.33 | 0.14 |
| 20.48 | 0.16 |
| 22.24 | 0.09 |
| 22.69 | 0.36 |
| 22.93 | 0.21 |
| 27.36<br>27.71 | 9.09 |
| 29.10 | 0.16 |
| 34.56 | 0.16 |
| 36.13 | 0.40 |
| 41.06 | 0.05 |
| 41.75 | 0.06 |

3. 2-MP (5-$^{13}$C) Isomerization on $Pt/Al_2O_3$ at 290°C.

| Position (ppm) | Area |
|---|---|
| 11.41 | 0.53 |
| 14.29<br>14.61 | 9.88 |
| 20.12 | 0.06 |
| 20.45 | 0.35 |
| 20.80 | 0.04 |
| 22.57 | 0.20 |
| 22.65 | 1.23 |
| 25.26 | 2.46 |
| 27.63<br>27.68 | 0.11 |
| 31.58 | 1.10 |
| 41.33 | 0.11 |

4. 2-MP (5-$^{13}$C) Isomerization on $Pt/Al_2O_3$ at 340°C .

| Position (ppm) | Area |
|---|---|
| 14.37 | 0.62 |
| 22.64 | 2.98 |
| 25.25 | 8.72 |
| 31.57 | 3.12 |

Spectrum of 2-MP and 3-MP fraction was not taken.

5. 2-MP (2-$^{13}$C) Isomerization on $PtTe/Al_2O_3$ at 290°C.

| Position (ppm) | Area |
|---|---|
| 14.29 | 0.97 |
| 14.33 | |
| 20.51 | 1.09 |
| 22.42 | 0.83 |
| 22.73 | 3.32 |
| 22.78 | |
| 27.46 | |
| 27.58 | |
| 27.61 | |
| 27.75 | 100.00 |
| 27.93 | |
| 28.05 | |
| 29.14 | 0.62 |
| 34.61 | 1.36 |
| 36.18 | 1.12 |
| 41.27 | 0.48 |
| 41.62 | 0.49 |

6. 2-MP (5-$^{13}$C) Isomerization on $PtTe/Al_2O_3$ at 290°C.

| Position (ppm) | Area |
|---|---|
| 11.43 | 0.34 |
| 14.32<br>14.62 | 10.86 |
| 20.15 | 0.06 |
| 20.48 | 0.26 |
| 20.84 | 0.04 |
| 22.61 | 0.21 |
| 22.67 | 2.93 |
| 25.29 | 3.28 |
| 27.68<br>27.74 | 0.10 |
| 31.60 | 2.61 |
| 41.39 | 0.11 |

7. 2-MP (2-$^{13}$C) Isomerization on $PtSb/Al_2O_3$ at 340°C.

| Position (ppm) | Area |
|---|---|
| 14.33 | 0.14 |
| 20.50 | 0.20 |
| 22.22 | 0.11 |
| 22.72 | 0.30 |
| 22.91 | 0.22 |
| 27.40<br>27.74 | 100.00 |
| 29.12 | 0.41 |
| 34.59 | 0.45 |
| 36.17 | 0.27 |
| 41.09<br>41.78 | 0.06<br>0.08 |

8. 2-MP (5-$^{13}$C) Isomerization on $PtSb/Al_2O_3$ at 340°C.

| Position (ppm) | Area |
|---|---|
| 22.64 | 1.20 |
| 25.25 | 6.72 |
| 31.57 | 0.80 |

Spectrum of 2-MP and 3-MP fraction was not taken.

## Appendix E: Chi Square Test on the Levels of Deuterium in Cyclohexane

| Catalysts | T(°C) | D.F[a] | $\chi^2$ | Prob. | [b]A(%) |
|---|---|---|---|---|---|
| $Pt/Al_2O_3$ | 110 | 7 | 8.865 | 0.263 | 65.7 |
| | 110 | 7 | 8.865 | 0.263 | 34.0 |
| $PtTe/Al_2O_3$ (Te/Pt=0.06) | 110 | 7 | 17.893 | 0.013 | 67.1 |
| $PtTe/Al_2O_3$ (Te/Pt=0.76) | 110 | 7 | 11.982 | 0.101 | 65.4 |
| | 110 | 7 | 12.497 | 0.086 | 33.8 |
| $PtSb/Al_2O_3$ (Sb/Pt=0.97) | 110 | 7 | 9.355 | 0.228 | 53.2 |
| | 110 | 7 | 9.797 | 0.2003 | 40.3 |
| $Pt/Al_2O_3$ | 250 | 5 | 0.887 | 0.971 | 56.2 |
| $PtTe/Al_2O_3$ (Te/Pt=0.06) | 250 | 5 | 0.755 | 0.980 | 67.1 |
| | 250 | 5 | 2.650 | 0.754 | 28.7 |
| $PtTe/Al_2O_3$ (Te/Pt=0.76) | 250 | 5 | 1.811 | 0.875 | 68.8 |
| | 250 | 5 | 2.979 | 0.703 | 39.4 |
| $PtSb/Al_2O_3$ | 250 | 5 | 0.310 | 0.998 | 32.7 |

[a] Only the frequencies with significant values were tested. 110°C: D6 to D12, 250°C: D8 to D12.

[b] % Conversion of Benzene to Cyclohexane.

## Vita

The author, Chi Hung Cheng was born in Hong Kong on May 23, 1958, son of Mr. and Mrs. Wah Shui Cheng. He received his high school diploma from Pui-Shing Middle School in December, 1977.

On August 22, 1978, he emmigrated to the United States with his parents and sisters and was admitted as a citizen on May 1, 1987. In August, 1979, he enrolled in Lousisiana State University Department of Chemical Engineering where he received his B.S degree in Chemical Engineering in December, 1983. He entered directly into the doctoral program in Chemical Engineering in January, 1984. His graduate research interests concern reforming catalysts under the tutelage of Dr. Geoffrey L. Price.

During his graduate work, the author was supported by an Exxon Fellowship.

The author is a member of Phi Kappa Phi, Tau Beta Pi, and Phi Lambda Upsilon.

The author is currently a candidate for the degree of Doctor of Philosophy in the Department of Chemical Engineering at Louisiana State University.

**DOCTORAL EXAMINATION AND DISSERTATION REPORT**

**Candidate:** Chi Hung Cheng

**Major Field:** Chemical Engineering

**Title of Dissertation:** The Investigation of $PtTe/Al_2O_3$ and $PtSb/Al_2O_3$ Bimetallic Reforming Catalysts

Approved:

Major Professor and Chairman

Dean of the Graduate School

EXAMINING COMMITTEE:

**Date of Examination:**

November 22, 1988